Design and synthesis of triplex metallohelices

By

Alan David Faulkner

A thesis submitted in partial fulfilment of the requirements of the degree of

Doctor of Philosophy in Chemistry

Department of Chemistry, University of Warwick

March 2014

Table of Contents

List of figures

Chapter 1

Chapter 2

Chapter 3

Chapter 4

List of schemes

Chapter 2

Chapter 3

List of tables

Chapter 3

Chapter 4

Acknowledgements

Firstly I would like to thank my supervisor Prof. Peter Scott for allowing me to work on this project as well as for his and valuable insights and guidance over the last few years. I would also like to thank all the members of the Scott group, both past and present, for their helpful advice and support in and around the lab, in particular Suzanne Chris and Becky for their help and involvement in my project. Finally I would like to thank Anna for her loving support and her much need proof reading skills.

Publications

The following publications have arisen from the work described in this thesis:

Chapter 2

Origins of stereoselectivity in optically pure phenylethaniminopyridine tris-chelates $M(NN')_3^{n+}$ (M = Mn, Fe, Co, Ni and Zn), Howson, Suzanne E., Allan, Laura E., N. Chmel, Nikola P., Clarkson, Guy J., Deeth, Robert J., Faulkner, Alan D., Simpson, Daniel H., Scott, Peter. *Dalton Trans*., 2011 **40**, 10415-10433. doi: 10.1039/C1DT10588D

Optically pure heterobimetallic helicates from self-assembly and click strategies. Howson, Suzanne E., Clarkson, Guy J., Faulkner, Alan D., Kaner, Rebecca A., Whitmore, Michael J., Scott, Peter. *Dalton Trans*. 2013, **42**, 14967-14981, doi: 10.1039/C3DT51725J

Chapters 3 and 4

Asymmetric peptidomimetic 'triplex' metallohelices with high and selective activity against cancer cells. Alan D Faulkner, Rebecca A Kaner, Qasem MA Abdallah, Guy Clarkson, David J Fox, Pratik Gurnani, Suzanne E. Howson,

Roger M Phillips, David I. Roper, Daniel H. Simpson, Peter Scott. *Nat. chem.*

Accepted *May 2014*

Declaration

This work performed in this thesis was carried out in the Department of Chemistry, University of Warwick between July 2009 and March 2014. Unless otherwise stated, it is the work of the author and has not been submitted in whole or in part for any other degree at this or any other university.

Summary

Chapter 1 introduces the concept of π-stacking. Different literature interpretations based on both model systems and theoretical observation are discussed.

Chapter 2 describes how π-stacking interactions in a series of $[Zn\mathbf{L}^{n}_{3}]^{2+}$ complexes are affected by the incorporation of ring substituents by focusing on the *fac*:*mer* selectivity of these systems. The stability of Fe(II) complexes to undergo further functionalization post complexation is also investigated, in particular their ability to undergo copper(I)-catalysed Huisgen 1,3-dipolar cycloaddition 'click' reactions.

Chapter 3 focuses on the use of inter-ligand π-stacking interactions in the formation of asymmetric, bimetallic coordination complexes that we have termed triplexes metallohelices. The selectivity of these systems has been investigated by computational means. The structure has been confirmed by both solution and solid state measurement. In addition the inherent stability of these complexes to functionalization, both pre and post complexation, is also discussed.

Chapter 4 focuses on the synthesis of water soluble variants of triplex metallohelices and their potential biological applications. In particular their anti-cancer properties are presented in detail.

Chapter 5 details the experimental procedures used to carry out the work in this thesis.

List of abbreviations

Most of the abbreviations and symbols used in this thesis are in common use within the scientific community. Non-standard abbreviations and symbols use in this work are given below:

CuAAC	Copper(I)-catalysed Huisgen 1,3-dipolar cycloaddation
HHH	Head-to-Head-to-Head
HHT	Head-to-Head-to-Tail
SCGE	Single cell gel electrophoresis
SSBs	Single strand breaks
ICL	Inter-strand crosslinking
DSBs	Double strand breaks
FACS	Fluorescent-activated cell sorting
MIC	Minimum inhibitory concentrations
MBC	Minimum bactericidal concentrations

List of ligands

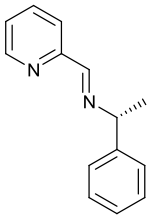

L[1]

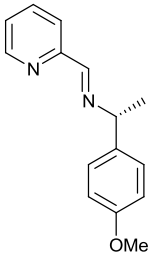

L[2]

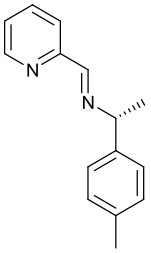

L[3]

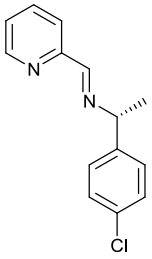

L[4]

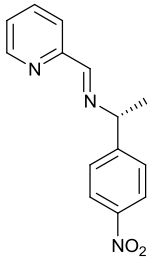

L[5]

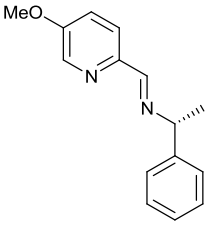

L[6]

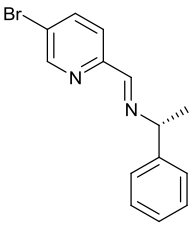

L[7]

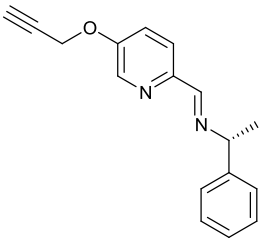

L[8]

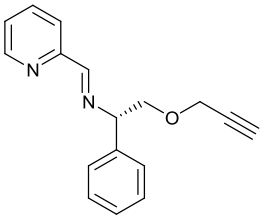

L[9]

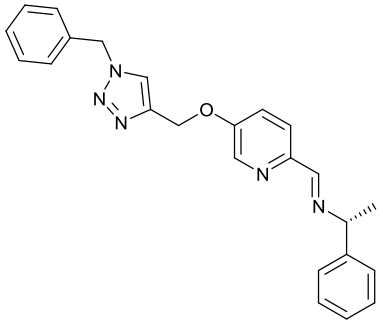

L[10]

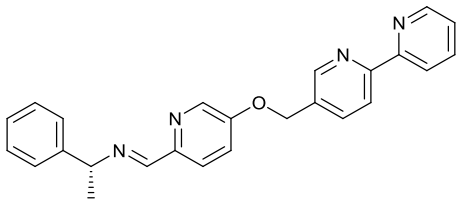

L[11]

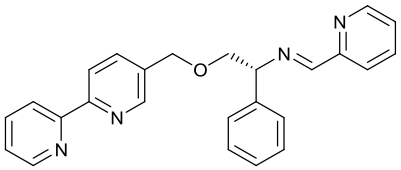

L[12]

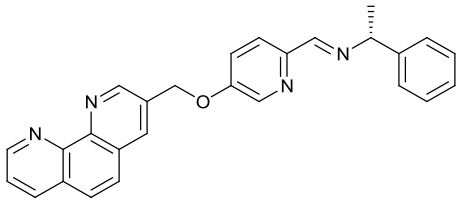

L[13]

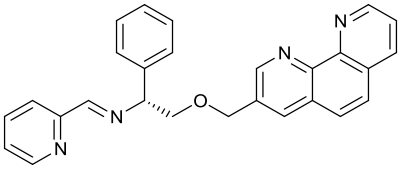

L[14]

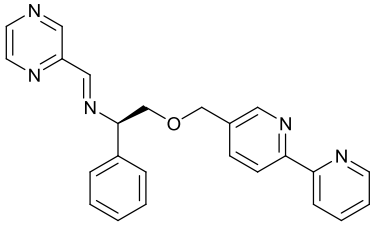

L[15]

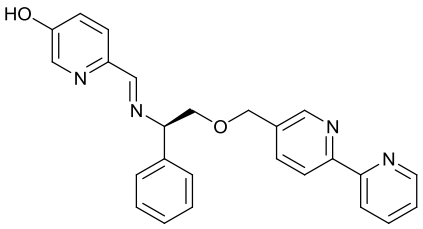

L[16]

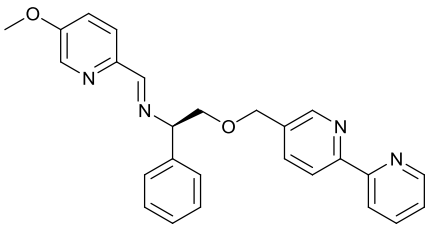

L[17]

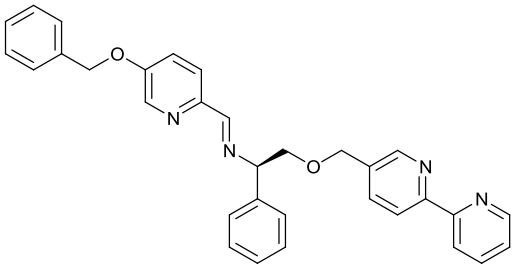

L[18]

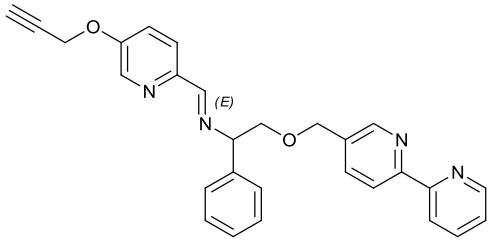

L[19]

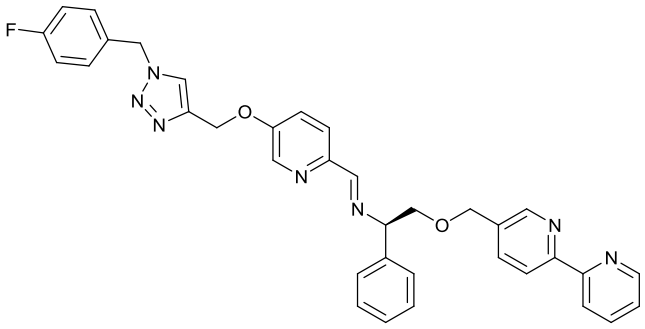

L[20]

Chapter 1

Introduction

1.1 π-stacking interactions

1.1.1 What is π-stacking?

The term π-stacking or π-π interaction is typically used to describe the favourable interaction between two or more aromatic groups. These interactions can be classified into one of three types based on their geometries; the parallel stacked or sandwich configuration (**a**, Figure 1.1), in which the two aromatic groups lie directly on top of each other, the edge-to-face T-stacked configuration (**b**, Figure 1.1), where one aromatic group is perpendicular to the other, and the parallel offset configuration (**c**, Figure 1.1), in which the two rings remain parallel to each other but unlike the sandwich configuration, the centres of the aromatic systems are separated laterally from each other.

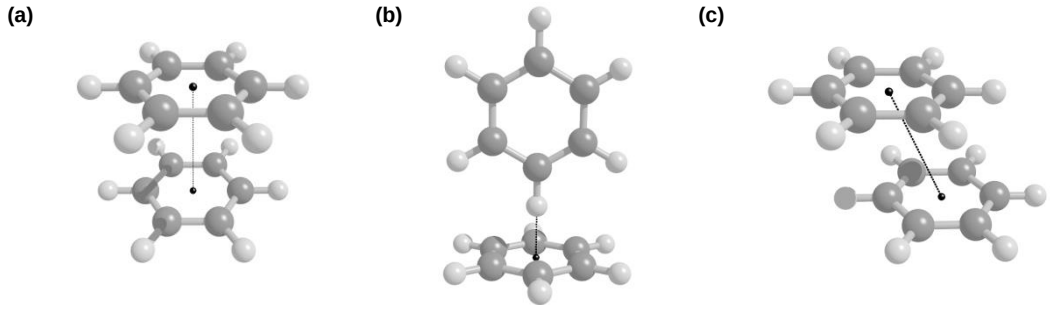

Figure 1.1 Types of π-stacking interactions: (a) Parallel stacked (Sandwich); (b) Edge-to-Face T-Stacked; Parallel offset (c).

Although variations in the geometries of theses prototypical systems are possible, e.g. eclipse vs staggered hydrogen atoms in the sandwich configuration, these perturbations are considered sufficiently small with respect to the overall energy of each configuration that they are generally not considered.[1]

1.1.2 Evidence of π-stacking.

π-Stacking interactions are regularly observed in the crystal structures of both small molecules and proteins[2-4] where it has been speculated that up to 60% of aromatic side chains participate in π-stacking interactions.[3] The sandwich configuration is however rarely observed, with both T-stacking and parallel offset interactions being the dominant configurations. Despite this the prototypical benzene dimer has proven difficult to study experimentally with binding energies in the gas phase being measured in the region of 1.6 ± 0.2 kcal mol^{-1} (Krause *et al.*[5]) to 2.4 ± 0.4 kcal mol^{-1} (Grover *et al.*[6]). Structural studies of these systems have also given rise to conflicting observations. Molecular beam experiments by Klemperer and co-workers indicated a T-stacked configuration[7, 8] with Arunan and Gutowsky later measuring the separation between the centres of

the two rings to be 4.96 Å.[9] However, both groups were unable to rule out the presence of either the sandwich or parallel offset configurations. Later work by Felker *et al.* using mass selected stimulated Raman spectroscopy indicated a low symmetry system, again consistent with a T-stacked configuration,[10] while multiphoton ionisation studies conducted by Schlag and co-workers suggested the presence of a more symmetric configuration *i.e.* a parallel stacked configuration.[11] These conflicting observations led Sherrill and co-workers to investigate the benzene dimer though high level theoretical calculations.[1, 12, 13] At the CCSD (T)/aug-cc-pVQZ level of theory both the T-stacked and parallel offset geometries were observed to be nearly isoenergetic with calculated binding energies being -2.74 and -2.78 kcal mol^{-1} respectively, while the sandwich configuration was found to represent a higher energy saddle point (-1.81 kcal mol^{-1}). For the T-stacked dimer the predicted intermolecular distance of 5.0 Å was also found to be in good agreement with the experimentally observed value of 4.96 Å,[9] while a vertical separation of 3.6 Å for a parallel configuration agrees well with that found in the crystal structures of many aromatic molecules of 3.3 – 3.6 Å.[14]

1.1.3 The quadrupole model.

While both experimental and theoretical studies of benzene dimers indicate the presence of an attractive interaction between aromatic rings, the origin of this interaction is debated in the literature.

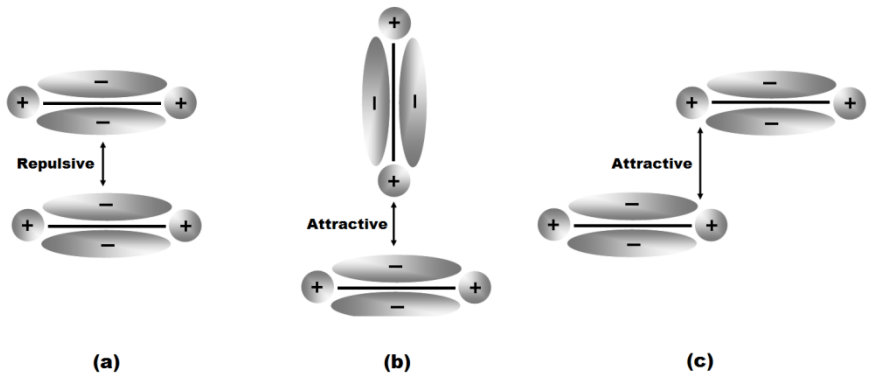

Figure 1.2 Quadrupole interactions in benzene dimers: (a) parallel stacked (Sandwiched); (b) Edge-to-Face T-Stacked; (c) Parallel offset.

The principal model based on quadrupole interactions, was put forward by Hunter and Sanders in 1990.[15] They argued that the presence of the electron-rich π system above and below the ring results in localised regions of negative charge on the faces, conversely an equal positive charge resides on the edge of the ring. In the absence of any polarising substituents, an attractive interaction is counterintuitive for the stacked configuration but favourable for both the T-stacked and parallel offset geometries (**b** and **c** in Figure 1.2). Extending this model further, Hunter and Sanders posited that the incorporation of either electron donating or withdrawing substituents into one or both of the benzene rings could act to modulate the magnitude of the quadrupole-quadrupole interactions *via* induction, thus allowing fine control over these systems.

Using this model and computation methods, Hunter initially investigated the interaction potential between two benzene rings as a function of horizontal displacement and their relative orientations, α (**a**, Figure 1.3). He observed that the resulting two dimensional plot (**b**, Figure 1.3), showed that variations of both the parallel offset and T-stacked orientations of the two benzene rings occurred

in regions of electrostatic attraction, while the parallel stacked configuration was observed to lie in a region of electrostatic repulsion as predicted by the model.

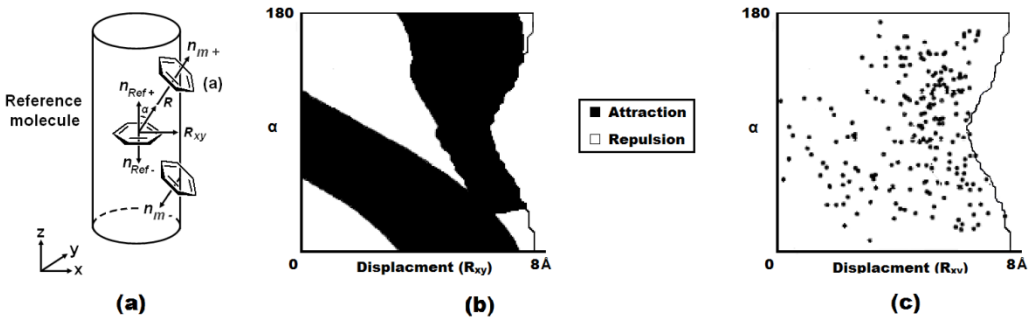

Figure 1.3 (a) Geometric parameters used in defining the position of one arene in relation to a reference molecule; (b) The Rxy, α dependence of the electrostatic interaction calculated using the quadrupole model. Redrawn from reference; (c) Scatter plot of the Rxy, α dependence of the experimentally observed geometries of Phe-Phe interactions in proteins.[2]

Furthermore Hunter observed that the predicted regions of favourable interactions correlated strongly with geometric orientations recorded in the protein databank between phenylalanine residues of protein structures (**b**, Figure 1.3).[2]

1.1.4 Direct experimental evidence for the quadrupole model.

Hunter noted that a key experimental difficulty in determining the cause of weak non-covalent interactions is that they tend to be swamped or heavily influenced by neighbouring interactions within the same molecule. As such they can only be measured as a perturbation of these stronger interactions.[16]

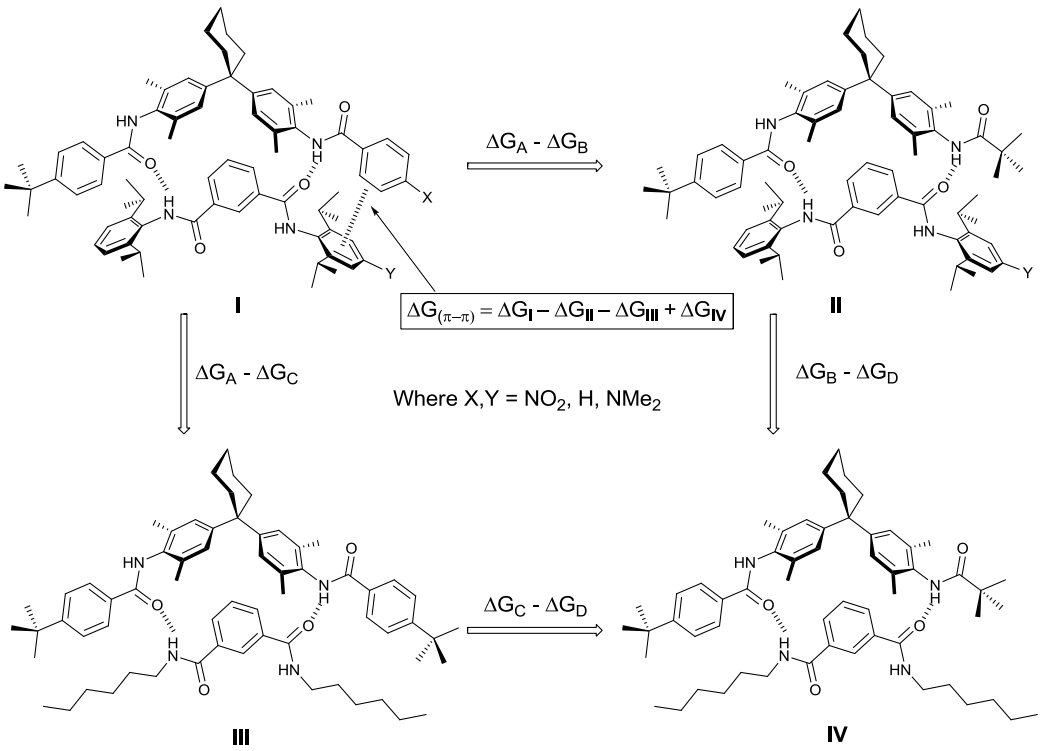

Figure 1.4 Double mutant cycle of molecular zipper complexes**.**

To counter this he proposed the use of a "double mutant cycle", a method which had been used previously to quantify side-chain-side-chain interactions in proteins,[17] to investigate a series of rigid molecular zipper complexes that are held together through a combination of hydrogen bonds and π-stacking interactions (Figure 1.4).[16, 18, 19] In these systems the magnitude of the terminal π-interaction in complex (**I)** could be estimated by removal of one of the interacting aryl groups generating compounds (**II)** and (**III)**. However this single mutation not only removes the interaction of interest but also other secondary interactions such as the one between the amide and the terminal aromatic rings, consequently the doubly mutated compound (**IV)** is needed to quantify the magnitude of these interactions. For each of the four compounds, association constants were calculated from ^{1}H NMR titrations in deuterated chloroform at 298 K. For compounds (**II)** – (**IV)** in which π-interactions are not possible, the

binding affinities were found to decrease indicating that π-interactions do contribute significantly to the stability of these systems.

$$\Delta G_{(\pi-\pi)} = \Delta G_I - \Delta G_{II} - \Delta G_{III} + \Delta G_{IV} \qquad \textbf{Equation 1.1}$$

Using Equation 1.1 it is possible to quantify the magnitude of the π-π interaction in compound (**I**). For systems in which X = Y = H (Figure 1.4) the attractive interaction between the terminal arenes was found to be 0.3 kcal mol^{-1}. Hunter went on extend these systems to include either electron donating or withdrawing groups in the X and Y positions.[18] It was found that the magnitude of interaction was sensitive to the nature of substituents with the value for $\Delta G_{(\pi\text{-}\pi)}$ varying from 0.2 kcal mol^{-1} repulsive, to -1.2 kcal mol^{-1} attractive. Plotting the resulting binding affinities for both X and Y substitutes against the σ_{para} Hammett parameters, Hunter was able to fit the results using the following function:-

$$\Delta\Delta G_{(para-x)}\ [kJ\ mol^{-1}] = 5.2\sigma_x\sigma_y - 1.9\sigma_x + 1.4\ \sigma_y - 1.5 \qquad \textbf{Equation 1.2}$$

The constant -1.5 in Equation 1.2 represents a weak attractive force between two aromatic rings in the absence of any substituents.[19] The cross term $5.2\sigma_x\sigma_y$ reflects the electrostatic interaction between the two global dipole moments across the two para-substituted rings, which is most favourable when the two groups are polarised in opposite directions. The remaining two terms reflect the local electrostatic interactions between the positively charged hydrogen atoms and the electronegative face of the ring.

$$\Delta\Delta G_{(meta-x)}\ [kJ\ mol^{-1}] = 2.5\sigma_x\sigma_y - 2.3\sigma_x + 1.5\ \sigma_y - 1.4$$ **Equation 1.3**

Hunter extended this approach to investigate the effect of substituents in the meta-position of each ring, once again plotting the resultant binding affinities against σ_{meta} Hammett parameters. Fitting of the resulting data indicates that the magnitude of the cross term was reduced by a half as shown in Equation 1.3. Hunter proposed that this results from the relative orientations of the dipole. In the para case the resultant dipole of the two rings is essentially parallel while in the meta case they are orientated 60˚ to each other as such the reduction in interaction energy of the system can be related by $\cos\theta$ (where θ is the relative angle between dipole moments). Hunter therefore proposed the following general Hammett equation for these molecular zipper systems:

$$\Delta\Delta G\ [kJ\ mol^{-1}] = (5.2\cos\theta)\sigma_x\sigma_y - 0.1\sigma_x + 1.5\ \sigma_y - 1.4$$ **Equation 1.4**

Due to the strong correlation between Hammett parameters and binding affinities in these systems, Hunter therefore proposed that the nature of the π-π interactions at the heart of these studies is primarily governed by electrostatic interactions. This conclusion agrees strongly with observations made by Cozzi *et al.* on a series of model π-stacking systems. Their initial studies focused on a series of substituted 1,8-diphenylnaphthalenes. In these systems the two phenyl rings adopt a parallel stacked configuration.[20, 21] During the rotation of a phenyl group by 180° this parallel stacked interaction is lost. As such, as the strength of the π-stacking interaction increases in these complexes so does the barrier of interconversion.

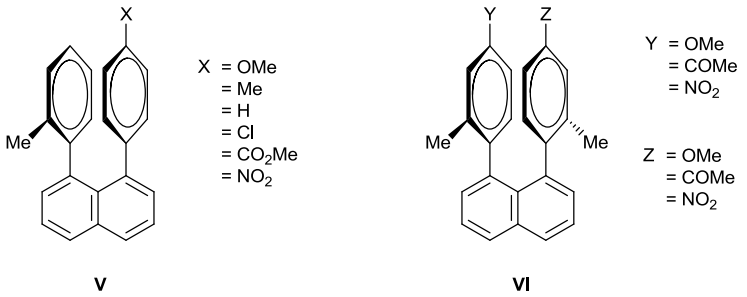

Figure 1.5 Model system based on substituted 1,8-diphenylnapthalenes employed by Cozzi *et al* to investigate π-stacking interactions

Room temperature ^{1}H NMR spectra of the series of compounds (**V**) (Figure 1.5), showed distinct signals for both the ortho- and meta- hydrogens on the phenyl rings, which on warming of the sample in DMSO were observed to coalesce allowing for the barrier to rotation to be determined. It was observed that the incorporation of an electron donating OMe substituent in position X in compound (**V**) (Figure 1.5), lead to a significantly lower barrier of interconversion (13.9 kcal mol^{-1}) than that observed for the electron withdrawing NO_2 substituent (17.3 kcal mol^{-1}).[20] Extending this study further, Cozzi investigated the incorporation of substituents into both phenyl rings in the series of compounds (**VI**) (Figure 1.5). Once again a linear correlation between donor properties of the substituent and barrier height was observed, with bis methoxy system being lowest in energy and the nitro/methylketone pair showing the largest barrier to rotation.[21]

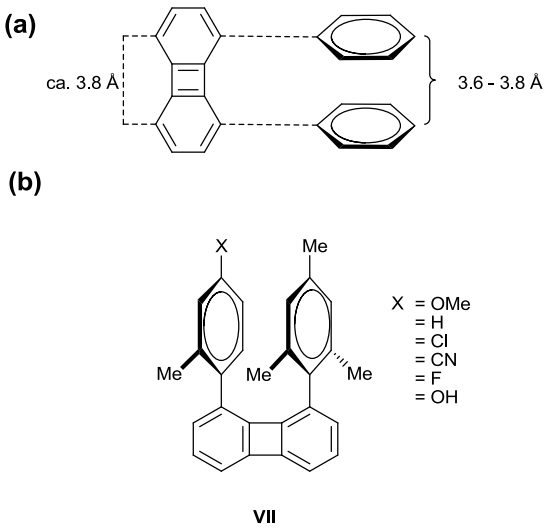

Figure 1.6 (a) comparison between the separation of phenyl ring in 1,8- diphenylbiphenylenes and observed separation of arenes in π-stacking interactions; (b) model systems based on substituted 1,8- diphenylbiphenylenes employed by Cozzi et al to investigate π-stacking interactions.

Cozzi has also investigated the use of 1,8-diphenylbiphenylenes which due to the greater separation of the phenyl groups than that observed in the 1,8-diphenylnaphthalenes more closely mimics the ideal separation of benzene ring in a stacked configuration (**a**, Figure 1.6). The interconversion between the stacked and non-stacked conformers for these systems was investigated using ^{1}H NMR. Following the same trend as the 1,8-diphenylnaphthalenes, an OMe substituent in the X position of the series of compounds (**VII**) (**b**, Figure 1.6) was found to result in a lower barrier to interconversion while a nitro substituent in the same position resulted in an increase in barrier height.

The observations of all three systems follow the predictions of Hunter and Sanders' quadrupole model; the incorporation of electron donating substituents such as an OMe group can be expected to destabilise the parallel π-stacking configuration while the contrasting electron withdrawing nitro group leads to the apparent stabilisation of this configuration. In an attempt to quantify

these observations, Cozzi and Siegel *et al.* proposed that the two arenes must be experiencing a through-space electrostatic interaction in agreement with the Hunter and Sanders' model,[15] as there was no evidence to say that conjugation played a significant role in these systems.[20, 22, 23]

1.1.5 Is the nature of π-stacking interactions the result of quadrupole interactions?

Wheeler and Houk[24] have investigated the nature of π-stacking interactions using a computational approach. They considered 24 substituted benzene-benzene and benzene-perfluorobenzene sandwich dimers at M05 2x/6-31+G(d) level of theory, in which the substituents ranged from strongly electron donating groups such as $NHCH_3$ (σ_m = -0.30) to strongly electron withdrawing groups e.g. NO_2 (σ_m = 0.71). They observed a liner correlation between the interaction energies of their substituted benzene dimer systems and the σ_m Hammet parameter. Furthermore, this trend was observed to be inverted for the C_6F_6-subsituted benzene systems. Both of these observations are consistent with predictions based upon the Hunter and Sanders model.[15] However it was also observed that *all* substituted systems resulted in an enhancement of the π-stacking interaction with respect to the unsubstituted system (Figure 1.7). Identical theoretical observations have also been made by Sherrill and co-workers,[1, 12] Lee *et al.* [25] and Grimme[26] for substituted benzene-benzene dimers. In addition, studies by Ringer *et al*. have shown that this enhancement of binding energy actually increases with the number of substituents on the aromatic system.[27]

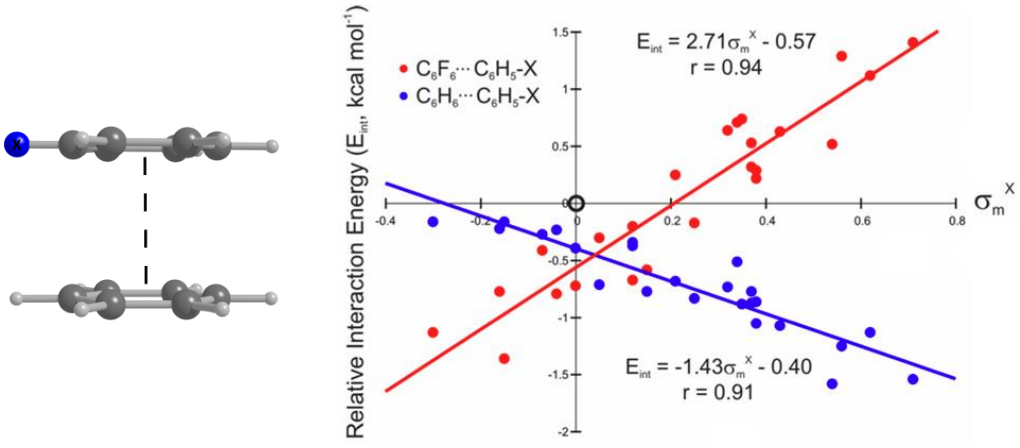

Figure 1.7 Interaction energy of substituted benzene dimers against the σ_m Hammet parameters, with the unsubstituted benzene dimer circled. Graph reproduced from reference.[24]

Investigating this effect further Wheeler and Houk[24] constructed a simple model in which one of the benzene rings is replaced with a simple hydrogen molecule, aligned such that the H—H_x bond is coincidental with the H—C bond of the benzene ring it replaced. Despite the crudeness of this model, an interaction potential between the benzene ring and hydrogen molecule is observed. Furthermore when the hydrogen (H_x, Figure 1.8) was substituted for the same range of electron donating or withdrawing groups used above, an identical trend between the interaction energies of the model systems and the σ_m Hammet parameters was observed as was seen previously for the substituted benzene dimer systems (Figure 1.7).

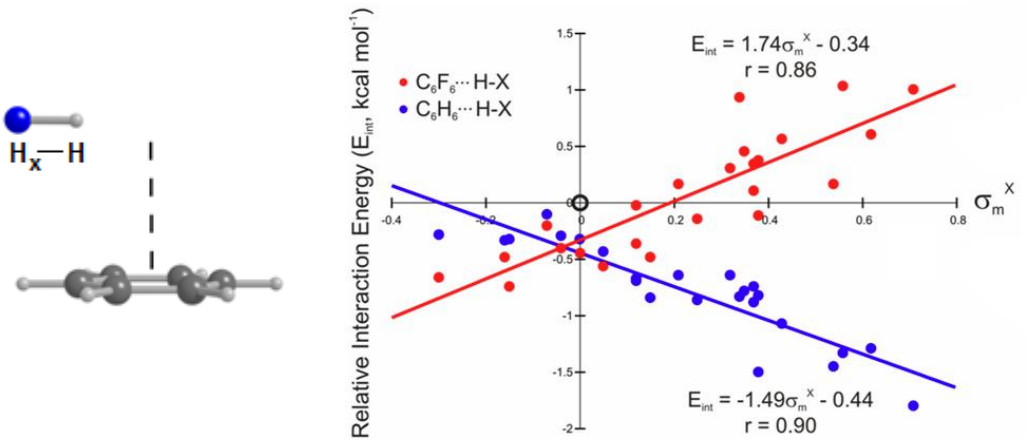

Figure 1.8 Left model H—H_X benzene dimers. Right the effect potential vs σ_m for these systems. Graph reproduced from reference.[24]

The interactions in these H—X/benzene systems clearly do not involve the π-system of the substituted benzene; the substituent effect observed for the benzene/substituted benzene dimers must instead arise from dispersive effects between the substituent and the unsubstituted ring. These interactions can be understood qualitatively in terms of interactions between the quadrupole moment of the unsubstituted benzene and the local dipoles introduced by the substituents. This is further supported by the observation that if the capping hydrogen atom in the model systems is replaced with a fluorine atom, the same trend is observed between interaction energy and the σ_m Hammet parameters.

1.1.6 The molecular torsion balance

Wilcox and co-workers have proposed a molecular torsion balance (**VIII**) (Figure 1.9), as a means to study the effects of substituents on π-stacking interactions by direct experimentation.[28, 29] In this system two conformers are possible, the folded conformer (Figure 1.9 left) which contains an edge-to-face T-stacking interaction and the unfolded conformer (Figure 1.9 right) in which no

such interaction is possible. These two conformational states are able to interconvert through slow rotation about the arene-arene bond at room temperature. As such the magnitude of the π-stacking interaction is reflected in the relative populations of the two states.

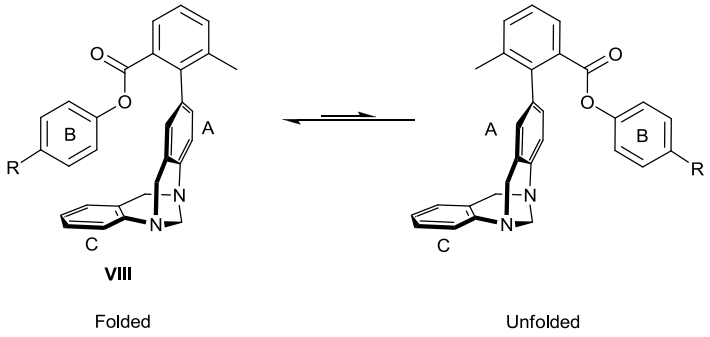

Figure 1.9 The molecular torsion balance

The effective population of the two states were determined by ^{1}H NMR spectroscopy at 298 K. For species where R = H the ratio between folded and unfolded conformers was found to be 3:2, indicating that the effective binding energy of the two arenes in this system is 0.24 kcal mol^{-1}, which is significantly lower than that found for the benzene dimer. The incorporation of electron withdrawing nitro and cyano substituents at the R position of compound (**VIII**), was found to increase preference for the folded conformation (3:1) as predicted by the Hunter and Sanders rules.[15] However the predicated destabilisation of the folded state with the incorporation of electron donating substituents in the same position was not observed. Interestingly, Wilcox observed a larger preference for the folded state when the phenyl ring B in compound (**VIII**) was replaced with either tert-butyl (4:1) or cyclohexane (7:3) groups.

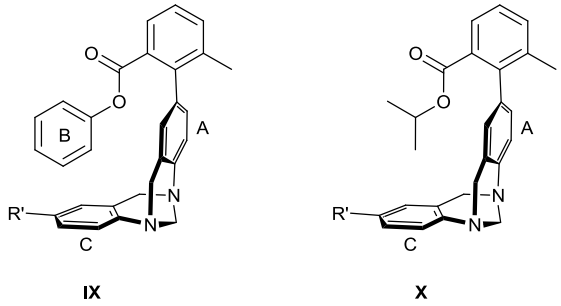

Figure 1.10 **S**ubstituted molecular torsion balances**.**

In order to study this effect further, Wilcox investigated the effect of electron donating and withdrawing groups at the R' position in two series of compounds (**IX**) and (**X**) (Figure 1.10).[29] For all substituents the barrier for interconversion was calculated to be 0.3 ± 0.1 and 0.5 ± 0.1 kcal mol^{-1} for the benzene series of compounds (**IX**), and the isopropyl substituted series (**X**) respectively. These small energies suggest that the dominating effect in these systems is not in fact electrostatics, as Hunter and Sanders propose, but rather due to London dispersion forces. Furthermore these studies also hint that the need for aromaticity may not in fact be required for π-stacking interactions.

There have been several criticisms of the fundamental assumptions made by the Wilcox torsion balance. While it is assumed that a preference for the folded state arises principally from the presence of π-π interactions, molecular mechanics studies conducted by Nakamura and Houk[30] have indicated that solvation effects actually lead to a stronger preference for the unfolded system than the folded one, suggesting that solvent acts to dampen out the effects of substituents in these systems. Furthermore *ab initio* and DFT calculations by Ribas *et al*.[31] indicate that the backbone of the torsion balance could play a non-innocent role in conformation energetics.

1.1.7 Is aromaticity required for π-stacking?

The molecular torsion balance, despite criticism, suggests that saturated alkyl groups can also participate in the π-stacking like interactions. These interactions were investigated further by Grimme using computational methods.[26] For small aromatic systems, consisting of one or two rings, the interaction energies of the T-stacked and parallel offset geometries was observed to be broadly similar to that of parallel offset saturated systems. As the number of rings was increased both the T-stacked aromatic and parallel saturated dimers showed a similar increase in interaction energies. In contrast, a much larger increase was observed for the parallel offset aromatic dimers. Grimme argues that π-stacking of small aromatic systems, i.e. those comprising two aromatic rings, is dominated by dispersive effects.

Bloom and Wheeler have also investigated the need for aromatic systems in stacking interactions using computational methods.[32] They first considered the sandwich dimers of benzene with the unsubstituted rings of 2-methylnaphthalene (**XI**) and 2-methyl-2,3-dihydronaphthalene (**XII**) (Figure 1.11). With the latter providing a means of decreasing the degree of aromaticity that is present in compound (**XI**) while retaining the same number of π electrons.

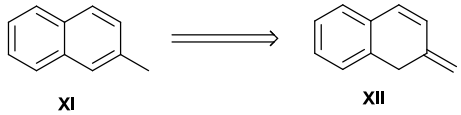

Figure 1.11 Molecular system used to quantify the effect of aromatic π delocalisation on stacking interactions: 2-methylnaphthalene (**XI**) and 2-methyl-2,3-dihydronaphthalene (**XII**)

As such, compounds (**XI**) and (**XII**) can be used to quantify the effects of aromaticity on stacking interactions. It was observed that the stacking of benzene with the non-aromatic, 2-methylene-2,3-dihydronaphthalene system (**XII**) was more favourable across a range of intermolecular distances.

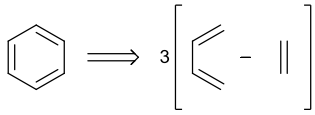

Figure 1.12 The homodesmotic dissection of benzene

Taking this idea further, they also investigated the homodesmotic dissection of benzene as depicted in Figure 1.12 as an alternative means to quantify the effect of aromaticity on stacking interactions. Comparing the CCSD(T) interaction energies of the sandwiched stack benzene dimer and the interaction energies of the benzene and dissected benzene dimer they found that the dissected benzene dimer was lower in energy by 0.31 kcal mol^{-1}. This preference for the dissected benzene dimer was found to increase to 1.0 kcal mol^{-1} for the parallel offset configuration; an increase of nearly 40% of the total interaction energy. Based on these observations, Bloom and Wheeler concluded that aromaticity is not the defining feature of 'aromatic interactions' and that, instead, dispersive interactions between the components of the system dominate this type of interaction.

1.1.8 Do N-heterocyclic rings participate in π-stacking?

Benzene dimers make ideal model systems to investigate π-stacking interactions, however *N*-heterocyclic systems are abundant in both biological systems and synthetic compounds,[4, 33, 34] where their presence is usually attributed to being

key to both structure and function of the compound. The incorporation of a nitrogen atom into the aromatic ring results in both a lowering of the overall molecular symmetry and the presence of a permanent dipole, giving rise to multiple configurations for each of the parallel stacked, parallel displaced and T-stacked geometries. Consequently, the majority of *N*-heterocyclic π-stacking studies that have been conducted have been theoretical in nature.[35-42] Sherrill[36] observed that for benzene-pyridine dimer systems dipole-induced-dipole interactions had relatively little impact on the orientation of the two aromatic groups, however these systems were found to be roughly 0.5 kcal mol^{-1} more stable than the benzene-benzene dimers.[36] In contrast the pyridine-pyridine systems were found to be highly influenced by dipole interactions, preferring orientations in which the dipoles were aligned anti-parallel to each other. In these preferred orientations, the pyridine dimers were found to be bound up to 1.0 kcal mol^{-1} more strongly than the corresponding benzene dimers. These observations strongly suggest an electrostatic type interaction between the two aromatic systems consistent with Hunter and Sanders description of π-stacking interactions.[43] In particular the dependence of the interaction energy on dipole orientation qualitatively agrees with Hunter's conclusions made for his double mutant cycles.[18]

1.1.9 Model *N*-heterocyclic systems

Experimental studies on model *N*-heterocyclic systems are rare due to the synthetic challenge of preparing model systems. Despite this, Gellman[44] and Gung[45] have both demonstrated an enhanced preference for π-stacking

interactions for systems that contain an *N*-heterocyclic system when compared to the equivalent system containing a phenyl group. Furthermore Dougherty[46] and Walters[18] have demonstrated separately that the orientation and inclusion of *N*-heterocyclic rings has a profound effect on cationic π-stacking interactions. Recently Shimitzu and co-workers made use of compound (**XIII**) (Figure 1.13) as a molecular torsion balance to further investigate the effects of *N*-heterocyclic systems on π-stacking.[47] The restricted rotation around a C_{aryl}–N_{imide} single bond resulted in an equilibrium between the two conformations in solution.

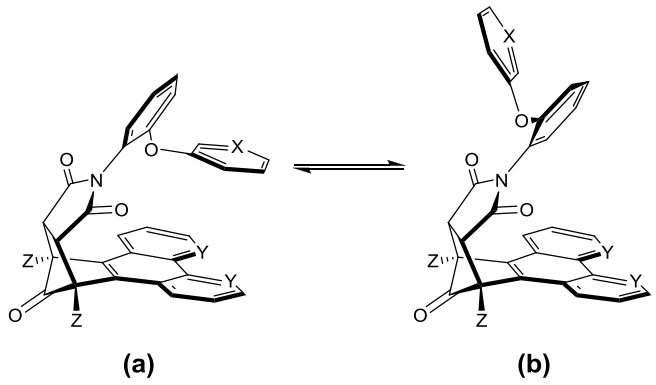

	X	Y	Z
XIII	CH	CH	Ph
XIV	N	CH	Ph
XV	CH	N	Me
XVI	N^+H	CH	Ph
XVII	CH	N^+H	Me
XVIII	N^+Me	CH	Ph
XIX	CH	N^+Me	Me

Figure 1.13 N-heterocyclic torsion balances.

In the closed conformation (**a**, Figure 1.13), the rigid bicyclic framework forces the aromatic surfaces into an offset parallel π-stacking geometry. While in the open conformation (**b**, Figure 1.13), these two surfaces are held apart. The relative strengths of the intramolecular π-stacking interactions in the N-heterocyclic molecular balances were assessed via ^{1}H NMR spectra at 23 °C in DMSO-d^6. It was observed that the neutral, *N*-heterocyclic containing compounds (**XIV**) and (**XVI**) (Figure 1.13), displayed π-stacking interactions that were respectively 0.4 and 0.5 kcal mol^{-1} more stable than those seen for the non-heterocyclic compound (**XIII**); agreeing with Sherrill's theoretical

observations.[36] An enhancement of the π-stacking interactions was also observed for cationic, *N*-heterocyclic compounds (**XVII**)-(**XIX**) (Figure 1.13), and was attributed to the greater electrostatic attraction arising from the cationic nitrogen ring and the π-cloud of the opposing aromatic surface.[47]

In order to determine the effect on solvent polarity on these systems, this analysis was repeated in both $CDCl_3$ and CD_3CN. In both cases a similar trend was observed with the cationic systems binding most strongly, and neutral systems binding more strongly than the non-*N*-heterocyclic systems. Finally, in addition to solution state analysis, Shimitzu characterised the *N*-heterocyclic molecular torsion balances by X-ray crystallography. All but one of the *N*-heterocyclic molecular balances were found to crystallise in the closed configuration, this was attributed to preference for these systems to favour the parallel offset *N*-heterocyclic π-stacking interaction. Only compound (**XV**) was observed to crystallise in the open state, supporting the solution studies which indicated that this compound contains the weakest π-stacking interaction of the *N*-heterocyclic systems. In contrast, the non-heterocyclic π-stacking balance (**XIII**) was consistently found to crystallize in the open conformation.

1.1.10 Summary

Although the exact nature of π-stacking interactions in both biological and synthetic complexes has proven difficult to study conclusively, both theoretical and experimental investigation of model systems has shown that an attractive interaction between two aromatic rings does exist. While the magnitude of this interaction appears to vary between systems and methods of investigation it is generally expected to lie in the region of 1-3 kcal mol^{-1} for benzene-benzene

systems. For most practical applications however one or both of the aromatic groups generally contain substituent groups, in addition to the presence of heteroatoms within the aromatic ring or cationic groups. This leads to an enhancement of the π-stacking interaction. As such, complexes containing π-stacking regions within their structure can be expected to experience an additional contribution to overall stability. Control over this interaction therefore becomes of particular interest in several areas of chemistry.

1.2 **π-stacking in helicate formation**

Although it has since been established that the first synthetic helix was formed by Stratton and Busch in 1958,[48] it is Lehn who is generally accredited with introducing the phrase '*helicate*' to supramolecular chemistry in order to describe a series of double-helical structures in which two molecular strands are wrapped around two or three Cu(I) ions.[49] Typically ligands designed to form helicates comprise two pairs of bidentate coordinating groups A and B connected *via* some linker i.e. **AB**–**BA**. Such ligands have C_2 or C_{2v} symmetry. Should the linker be sufficiently short or rigid, then the helicates of the two metal centres (*i.e.* Δ or Λ) may be mechanically coupled, so, for example, formation of a Δ configuration at the first metal induces Δ configuration at the second (Figure 1.14). Homochiral systems (*i.e.* Δ,Δ or Λ,Λ) are thus produced preferentially by this process of helication.[50] The overall sense of helicity of the system is denoted using the chirality descriptors *P* ("plus", right-handed helix, corresponding to Δ) and *M* ("minus", left-handed, Λ). In less conformationally restrained ligand systems,

where the configurations of the metal centres may vary more independently, the achiral *mesocate* (*i.e.* Δ,Λ) is also formed (Figure 1.14).

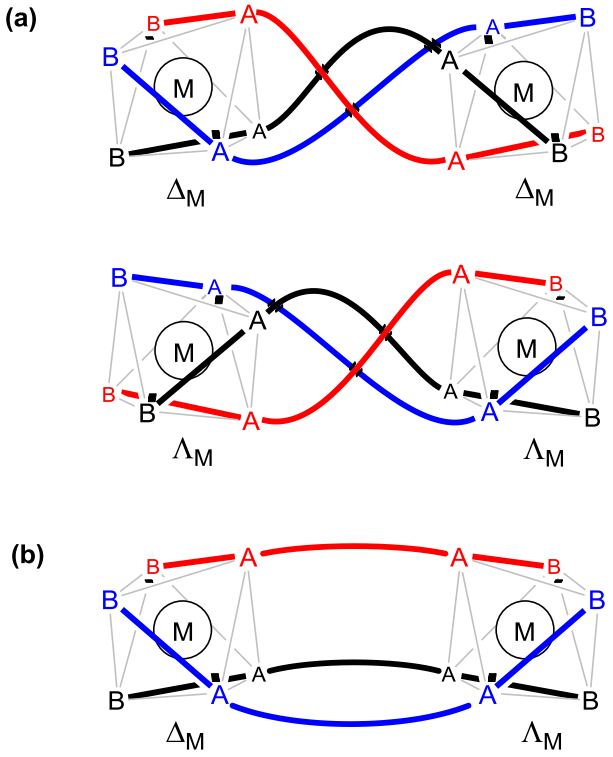

Figure 1.14 Schematic representations of (a) the two enantiomers of a bimetallic triple-stranded helicate and the mesocate (b). Each species contains two ocatahedral metals M connected by three ligands B-A—A-B.

The principal drawback to this approach is that, for most applications (e.g. in biological chemistry), a racemic mixture of *P* and *M* helicates is still formed which then requires separation through traditional methods such as crystallisation[51, 52] and chromatography,[53-56] after which racemisation may commonly occur.[52, 55] One solution to this problem is to include a stereogenic centre in the bridging unit, which induces a twist in the bridge itself through steric hindrance.[57-60] While this may give rise to the preferential formation of single enantiomers, the need for specific rigid ligands severely limits the synthetic flexibility of the system.

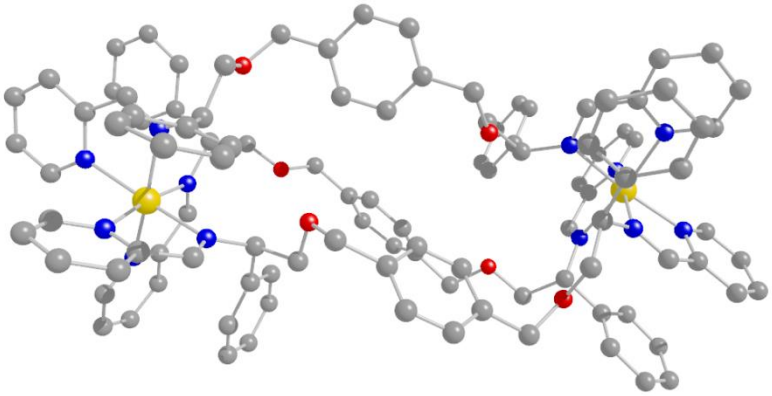

Figure 1.15 An optically pure D_3 bimetallic flexicate.

Recently a new more flexible approach to the formation of optically pure helicates has been pioneered by Scott and co-workers. Previously they had shown that a series of monometallic octahedral self-assembling *tris*-chelate systems, displayed an unprecedented level of *fac* selectivity due to the presence of three sets of concurrent sets of π-stacking interactions.[61] By connecting two of these thermodynamically stable monometallic units through a variety of organic linkers, they were able to synthesis a range of optically pure, functionally more diverse and water soluble bimetallic systems, which they have termed *flexicates* (Figure 1.15).[62] This advancement in helicate formation makes *flexicates* ideally suited for biological applications such as chemotherapeutics.

1.3 **Helicates as chemotherapeutics**

The World Health Organization defines cancer as *"the rapid creation of abnormal cells that grow beyond their usual boundaries, and which can then invade adjoining parts of the body and spread to other organs*".[63] It has been estimated that by 2030 there will be 21.4 million new cases diagnosed every year,[64] The naturally occurring protein p53 has been shown to be an effective anticancer agent through its control over a cell cycle check point which induces programed cell death (apoptosis) in response to DNA damage.[65] It has been established that the inheritance of faulty p53 proteins is associated with both increased susceptibility[66] and the early onset of several different cancers, including breast carcinomas, sarcomas, brain tumours and adrenal cortical carcinomas.[67] Deactivation of this protein through mutation is observed in half of all cancer cases,[68-72] and is linked to an increased likelihood of cancer cells evading normal restrictions against excessive cell growth.[73] The majority of these mutations have been observed to occur in the core DNA binding region of the protein.[74] This 200-amino acid portion of p53 folds into a compact structural domain, comprising of a loop-sheet-helix motif, in which the α-helix component is observed to bind in the major grove, as shown in Figure 1.16.[74]

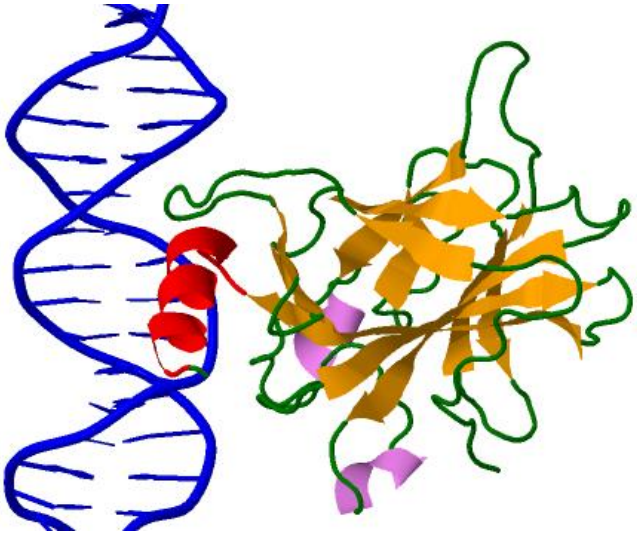

Figure 1.16 Schematic ribbon drawing of the core DNA binding component of p53, with the principle binding α-helix shown in red (obtained from the protein data bank, reference 1TUP). Only one of the three core domain molecules present in the crystal structure is shown

Wang and co-workers have demonstrated that the human host defence cathelicidin protien LL-37 (a) in Figure 1.17, displays both antimicrobial and anticancer properties.[75] The active unit, in like that in p53, is also a short amphipathlic α-helix.

Attemtps have been made to develop synthetic α-helix motifs as potential drug candiates,[76-79] however a combination of their challanging synthesis and their liability to proteases results in poor pharmacokinetics[78] has lead to the development of peptidomimetic systems.[80-84] These have recently been further supplemented by several helical assembles synthesied using a coordination chemistry approach.[55, 62, 85, 86]

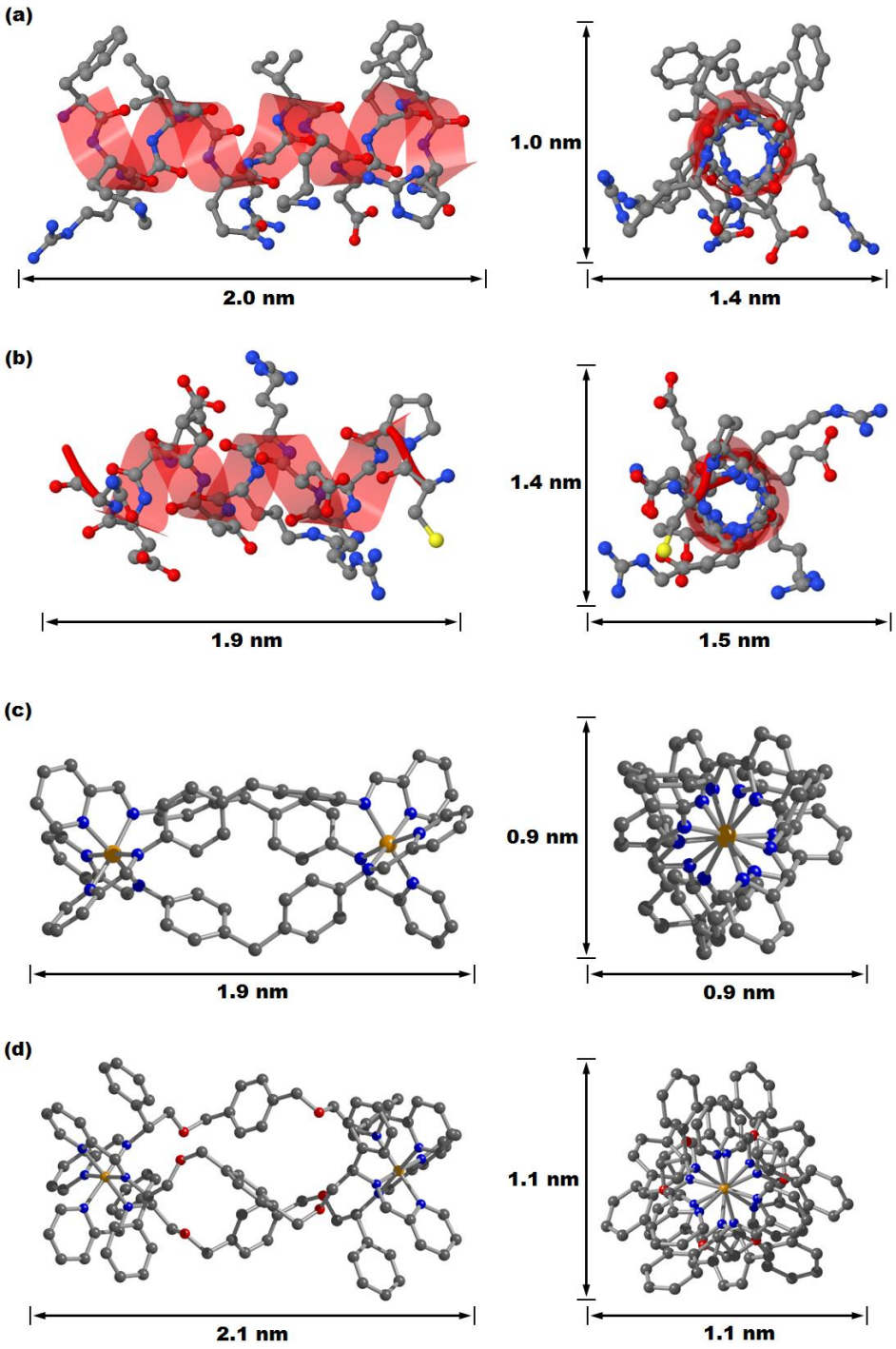

Figure 1.17 Comparsion of the dimesions of (a) The core strucutre of the antimicrobial and anticancer region of the human cathelicidin protien LL-37, (b) The principal α-helix component of P53 involed in DNA binding, (c), Hannon's bimetallic iron(II) cylinder,[85] (d) Scott and co-workers flexicate system.[62] Dimensions are estimated at the maximal distaces as determined from the crystal strucutres in each case. Hydrogen atoms have been removed for clarity.

Hannon and co-workers has focused on a bimetallic iron(II) cylinder approximately the same size as both the central located DNA binding α-helix of p53 and core structure of LL-37 (Figure 1.17). They have been observed to undergo binding in the major groove of DNA,[87] and have been shown to display cytotoxic activity towards a range of cancer cells lines.[85] In addition these bimetallic iron(II) cylinders have also been shown to be modestly active as antimicrobial agents against *Bacillus subtilis* (MIC = 32 mg/ml) and *Escherichia coli* (MIC = 64.7 mg/ml).[88] More recently, Scott and co-workers demonstrated that their water stable bimetallic flexicate systems[62] which are also of similar size to both LL-37 and the binding α-helix of p53 (Figure 1.17), are active on the nanomolar range against a range of cancer cell lines, noticeably HCT116 $p53^{+/+}$ (human colon carcinoma).[89] Furthermore, flexicate systems have been shown to exhibit higher antimicrobial activity against both Gram-negative bacterium *E. coli* (MC4100) and Gram-positive bacterium methicillin-resistance *S. aureus* (MRSA252).[62]

Both of these approaches allow for arguably simpler synthesis, especially on larger scales than are possible with peptidomimetic systems, however they are not without their own drawbacks. Hannon's systems require the separation of enantiomers post-complexation through the use of cellulose.[53-55] The stability of these complexes to racemization and decomposition post separation with prolonged exposure to aqueous media has, to the best of our knowledge, not been reported. Such drawbacks are not experienced by flexicate systems, however their highly symmetrical (D_3) design is still a step away from the structural complexity of asymmetric of α-helices.

1.4 **Conclusions**

The aim of this thesis is to further investigate the use of π-stacking interactions through both experimental and theoretical studies as a synthetic tool for use in coordination chemistry. By utilising these interactions, it will be demonstrated that it is possible to induce the formation of C_1 symmetric, bimetallic compounds through self-assembly which we have chosen to call *Triplex metallohelicates*. These compounds can be readily functionalised and exhibit remarkable stability in water, making them ideally suitable for biological applications. In particular, their activity against a range of cancer cell lines and surprising lack of antimicrobial activity will be discussed.

1.5 **References**

1. M. O. Sinnokrot and C. D. Sherrill, *J. Phys. Chem. A*, 2006, **110**, 10656-10668.
2. C. A. Hunter, J. Singh and J. M. Thornton, *J. Mol. Biol.*, 1991, **218**, 837-846.
3. S. Burley and G. Petsko, *Science*, 1985, **229**, 23-28.
4. C. Janiak, *Dalton Trans.*, 2000, 3885-3896.
5. H. Krause, B. Ernstberger and H. J. Neusser, *Chem. Phys. Lett.*, 1991, **184**, 411-417.
6. J. R. Grover, E. A. Walters and E. T. Hui, *J. Phys. Chem.*, 1987, **91**, 3233-3237.
7. J. M. Steed, T. A. Dixon and W. Klemperer, *J. Chem. Phys.*, 1979, **70**, 4940-4946.
8. K. C. Janda, J. C. Hemminger, J. S. Winn, S. E. Novick, S. J. Harris and W. Klemperer, *J. Chem. Phys.*, 1975, **63**, 1419-1421.
9. E. Arunan and H. S. Gutowsky, *J. Chem. Phys.*, 1993, **98**, 4294-4296.
10. P. M. Felker, P. M. Maxton and M. W. Schaeffer, *Chem. Rev.*, 1994, **94**, 1787-1805.
11. K. O. Bornsen, H. L. Selzle and E. W. Schlag, *J. Chem. Phys.*, 1986, **85**, 1726-1732.
12. M. O. Sinnokrot and C. D. Sherrill, *J. Phys. Chem. A*, 2004, **108**, 10200-10207.
13. M. O. Sinnokrot, E. F. Valeev and C. D. Sherrill, *J. Am. Chem. Soc.*, 2002, **124**, 10887-10893.
14. T. Dahl, *Acta Chem. Scand.*, 1994, **48**, 95-106.
15. C. A. Hunter and J. K. M. Sanders, *J. Am. Chem. Soc.*, 1990, **112**, 5525-5534.
16. H. Adams, F. J. Carver, C. A. Hunter, J. C. Morales and E. M. Seward, *Angew. Chem. Int. Ed.*, 1996, **35**, 1542-1544.
17. L. Serrano, M. Bycroft and A. R. Fersht, *J. Mol. Biol.*, 1991, **218**, 465-475.
18. F. J. Carver, C. A. Hunter, F. J. Carver and E. M. Seward, *Chem. Commun.*, 1998, 775-776.
19. F. J. Carver, C. A. Hunter, D. J. Livingstone, J. F. McCabe and E. M. Seward, *Chem. Eur. J.*, 2002, **8**, 2847-2859.
20. F. Cozzi, M. Cinquini, R. Annunziata, T. Dwyer and J. S. Siegel, *J. Am. Chem. Soc.*, 1992, **114**, 5729-5733.
21. F. Cozzi, M. Cinquini, R. Annuziata and J. S. Siegel, *J. Am. Chem. Soc.*, 1993, **115**, 5330-5331.
22. M. Oki, H. Iwamura and G. Yamamoto, *Bull. Chem. Soc. Jpn.*, 1971, **44**, 262-265.
23. M. Oki and G. Yamamoto, *Bull. Chem. Soc. Jpn.*, 1971, **44**, 266-270.
24. S. E. Wheeler and K. N. Houk, *J. Am. Chem. Soc.*, 2008, **130**, 10854-10855.
25. E. C. Lee, D. Kim, P. Jurečka, P. Tarakeshwar, P. Hobza and K. S. Kim, *J. Phys. Chem. A*, 2007, **111**, 3446-3457.
26. S. Grimme, *Angew. Chem. Int. Ed. Engl.*, 2008, **47**, 3430-3434.
27. A. L. Ringer, M. O. Sinnokrot, R. P. Lively and C. D. Sherrill, *Chem. Eur. J.*, 2006, **12**, 3821-3828.

28. S. Paliwal, S. Geib and C. S. Wilcox, *J. Am. Chem. Soc.*, 1994, **116**, 4497-4498.
29. E.-i. Kim, S. Paliwal and C. S. Wilcox, *J. Am. Chem. Soc.*, 1998, **120**, 11192-11193.
30. K. Nakamura and K. N. Houk, *Org. Lett.*, 1999, **1**, 2049-2051.
31. J. Ribas, E. Cubero, F. J. Luque and M. Orozco, *J. Org. Chem.*, 2002, **67**, 7057-7065.
32. J. W. Bloom and S. E. Wheeler, *Angew. Chem. Int. Ed. Engl.*, 2011, **50**, 7847-7849.
33. S. Yamada, *Org. Biomol. Chem.*, 2007, **5**, 2903-2912.
34. S. Yamada and J. S. Fossey, *Org. Biomol. Chem.*, 2011, **9**, 7275-7281.
35. W. Wang and P. Hobza, *ChemPhysChem*, 2008, **9**, 1003-1009.
36. E. G. Hohenstein and C. D. Sherrill, *J. Phys. Chem. A*, 2009, **113**, 878-886.
37. P. Mignon, S. Loverix, F. De Proft and P. Geerlings, *J. Phys. Chem. A*, 2004, **108**, 6038-6044.
38. B. K. Mishra and N. Sathyamurthy, *J. Phys. Chem. A*, 2004, **109**, 6-8.
39. Q. A. Smith, M. S. Gordon and L. V. Slipchenko, *J. Phys. Chem. A*, 2011, **115**, 4598-4609.
40. S. Tsuzuki, M. Mikami and S. Yamada, *J. Am. Chem. Soc.*, 2007, **129**, 8656-8662.
41. D. B. Ninković, J. M. Andrić and S. D. Zarić, *ChemPhysChem*, 2013, **14**, 237-243.
42. S. Karthikeyan and S. Nagase, *J. Phys. Chem. A*, 2012, **116**, 1694-1700.
43. C. A. Hunter and J. K. M. Sanders, *J. Am. Chem. Soc.*, 1990, **112**, 5525.
44. S. L. McKay, B. Haptonstall and S. H. Gellman, *J. Am. Chem. Soc.*, 2001, **123**, 1244-1245.
45. B. W. Gung, F. Wekesa and C. L. Barnes, *J. Org. Chem.*, 2008, **73**, 1803-1808.
46. P. C. Kearney, L. S. Mizoue, R. A. Kumpf, J. E. Forman, A. McCurdy and D. A. Dougherty, *J. Am. Chem. Soc.*, 1993, **115**, 9907-9919.
47. P. Li, C. Zhao, M. D. Smith and K. D. Shimizu, *J. Org. Chem.*, 2013, **78**, 5303-5313.
48. W. J. Stratton and D. H. Busch, *J. Am. Chem. Soc.*, 1958, **80**, 1286-1289.
49. J. M. Lehn, A. Rigault, J. Siegel, J. Harrowfield, B. Chevrier and D. Moras, *Proc. Natl. Acad. Sci.*, 1987, **84**, 2565-2569.
50. M. Albrecht, *Chem. Eur. J.*, 2000, **6**, 3485-3489.
51. R. Krämer, J.-M. Lehn, A. De Cian and J. Fischer, *Angew. Chem. Int. Ed.*, 1993, **32**, 703-706.
52. G. Baum, E. C. Constable, D. Fenske, C. E. Housecroft and T. Kulke, *Chemistry - A European Journal*, 1999, **5**, 1862-1873.
53. M. J. Hannon, I. Meistermann, C. J. Isaac, C. Blomme, J. R. Aldrich-Wright and A. Rodger, *Chem. Commun.*, 2001, 1078-1079.
54. J. M. C. A. Kerckhoffs, J. C. Peberdy, I. Meistermann, L. J. Childs, C. J. Isaac, C. R. Pearmund, V. Reudegger, S. Khalid, N. W. Alcock, M. J. Hannon and A. Rodger, *Dalton Trans.*, 2007, 734-742.
55. J. C. Peberdy, J. Malina, S. Khalid, M. J. Hannon and A. Rodger, *J. Inorg. Biochem.*, 2007, **101**, 1937-1945.
56. N. C. Fletcher, R. T. Brown and A. P. Doherty, *Inorg. Chem.*, 2006, **45**, 6132-6134.

57. E. J. Enemark and T. D. P. Stack, *Angew. Chem. Int. Ed.*, 1995, **34**, 996-998.
58. U. Kiehne and L. U. A, *Org. Lett.*, 2007, **9**, 5333-5336.
59. S. G. Telfer, R. Kuroda and T. Sato, *Chemical communications*, 2003, 1064-1065.
60. J. Hamblin, L. J. Childs, N. W. Alcock and M. J. Hannon, *J. Chem. Soc., Dalton Trans.*, 2002, 164-169.
61. S. E. Howson, L. E. N. Allan, N. P. Chmel, G. J. Clarkson, R. J. Deeth, A. D. Faulkner, D. H. Simpson and P. Scott, *Dalton Trans.*, 2011, **40**, 10416-10433.
62. S. E. Howson, A. Bolhuis, V. Brabec, G. J. Clarkson, J. Malina, A. Rodger and P. Scott, *Nat Chem*, 2012, **4**, 31-36.
63. W. H. Organisation, *Cancer Fact sheet No. 297*, http://www.who.int/mediacentre/factsheets/fs297/en/, Accessed 11th March, 2014.
64. A. Jemal, F. Bray, M. M. Center, J. Ferlay, E. Ward and D. Forman, *CA: A Cancer Journal for Clinicians*, 2011, **61**, 69-90.
65. M. B. Kastan, Q. Zhan, W. S. El-Deiry, F. Carrier, T. Jacks, W. V. Walsh, B. S. Plunkett, B. Vogelstein and A. J. Fornace, *Cell*, 1992, **71**, 587-597.
66. C. Whibley, P. D. P. Pharoah and M. Hollstein, *Nat. Rev. Cancer*, 2009, **9**, 95-107.
67. M. Olivier, D. E. Goldgar, N. Sodha, H. Ohgaki, P. Kleihues, P. Hainaut and R. A. Eeles, *Cancer Res.*, 2003, **63**, 6643-6650.
68. P. A. J. Muller, K. H. Vousden and J. C. Norman, *The Journal of Cell Biology*, 2011, **192**, 209-218.
69. N. Rivlin, R. Brosh, M. Oren and V. Rotter, *Genes & Cancer*, 2011, **2**, 466-474.
70. J. M. Nigro, S. J. Baker, A. C. Preisinger, J. M. Jessup, R. Hosteller, K. Cleary, S. H. Signer, N. Davidson, S. Baylin, P. Devilee, T. Glover, F. S. Collins, A. Weslon, R. Modali, C. C. Harris and B. Vogelstein, *Nature*, 1989, **342**, 705-708.
71. A. Eldar, H. Rozenberg, Y. Diskin-Posner, R. Rohs and Z. Shakked, *Nucleic Acids Res.*, 2013, **41**, 8748-8759.
72. R. S. Warren, C. E. Atreya, D. Niedzwiecki, V. K. Weinberg, D. B. Donner, R. J. Mayer, R. M. Goldberg, C. C. Compton, M. B. Zuraek, C. Ye, L. B. Saltz and M. M. Bertagnolli, *Clinical Cancer Research*, 2013, **19**, 5777-5787.
73. L. Hartwell, *Cell*, 1992, **71**, 543-546.
74. Y. Cho, S. Gorina, P. Jeffrey and N. Pavletich, *Science*, 1994, **265**, 346-355.
75. X. Li, Y. Li, H. Han, D. W. Miller and G. Wang, *J. Am. Chem. Soc.*, 2006, **128**, 5776-5785.
76. A. Tossi, L. Sandri and A. Giangaspero, *Peptide Science*, 2000, **55**, 4-30.
77. M. Zasloff, *Nature*, 2002, **415**, 389-395.
78. R. E. W. Hancock and H.-G. Sahl, *Nat Biotech*, 2006, **24**, 1551-1557.
79. Y. Huang, J. Huang and Y. Chen, *Protein Cell*, 2010, **1**, 143-152.
80. J. M. Davis, L. K. Tsou and A. D. Hamilton, *Chem. Soc. Rev.*, 2007, **36**, 326-334.
81. A. Grauer and B. König, *Eur. J. Org. Chem.*, 2009, **2009**, 5099-5111.

82. V. Haridas, *Eur. J. Org. Chem.*, 2009, **2009**, 5112-5128.
83. C. G. Cummings and A. D. Hamilton, *Curr. Opin. Chem. Biol.*, 2010, **14**, 341-346.
84. A. L. Boyle and D. N. Woolfson, *Chem. Soc. Rev.*, 2011, **40**, 4295-4306.
85. A. C. G. Hotze, N. J. Hodges, R. E. Hayden, C. Sanchez-Cano, C. Paines, N. Male, M.-K. Tse, C. M. Bunce, J. K. Chipman and M. J. Hannon, *Chem. Biol.*, 2008, **15**, 1258-1267.
86. A. D. Richards, A. Rodger, M. J. Hannon and A. Bolhuis, *Int.l J. Antimicrob. Agents*, 2009, **33**, 469-472.
87. M. J. Hannon, V. Moreno, M. J. Prieto, E. Moldrheim, E. Sletten, I. Meistermann, C. J. Isaac, K. J. Sanders and A. Rodger, *Angew. Chem. Int. Ed.*, 2001, **40**, 879-884.
88. A. D. Richards, A. Rodger, M. J. Hannon and A. Bolhuis, *International journal of antimicrobial agents*, 2009, **33**, 469-472.
89. V. Brabec, S. E. Howson, R. A. Kaner, R. M. Lord, J. Malina, R. M. Phillips, Q. M. A. Abdallah, P. C. McGowan, A. Rodger and P. Scott, *Chemical Science*, 2013.

Chapter 2

Functionalisation of monometallic complexes

2.1 **Introduction**

The synthesis of optically pure complexes has been of interest since the early days of coordination chemistry beginning with Werner's resolution of as proof of the theory of "coordination".[1] Recently the first highly diastereoselective synthesis of a coordination complex was achieved.[2]

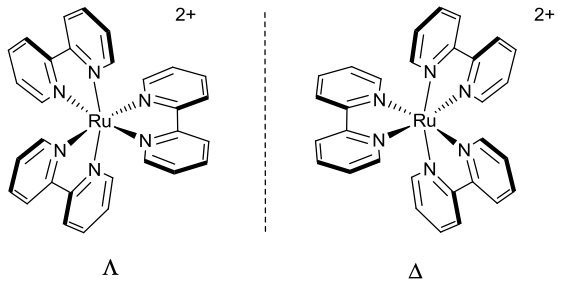

Figure 2.1 The two enantiomers of $[Ru(bipy)_3]^{2+}$.

Tris-chelate octahedral complexes with symmetrical (**A-A**) type ligands, *e.g.* $[Ru(bpy)_3]^{2+}$ are generally formed as racemic mixtures of the Δ and Λ enantiomers (Figure 2.1).[1] For more chemically diverse unsymmetrical (**A-B)** ligands such as monosubstituted bipyridines,[3, 4] additional geometric *fac* and *mer* configurations are introduced resulting in four isomers: *fac*-Δ, *mer*-Δ, *fac*-Λ and *mer*-Λ. Excluding any additional steric or electronic effects, a statistical 1:3 *fac*:*mer* ratio is observed. For many applications such as anion recognition,[5, 6] molecular sensors,[7, 8] supramolecular chemistry,[9, 10] DNA targeting,[11, 12] protein probes[13] and cancer therapy,[14] single isomers are required. While it is possible to resolve these systems through various techniques for inert metals,[15-22] such as ruthenium, these approaches are typically low yielding.[23] For more labile systems, such approaches are further hindered by racemisation.[24]

In order to overcome the issues of resolution, several stereoselective synthetic strategies have been developed. These consist of either the use of temporary chiral auxiliaries, which favour the formation of one enantiomer,[25, 26] or the use of multidentate ligands to pre-organise the configuration at the metal centre.[3, 27-31] These approaches are not without their drawbacks, typically resulting in relatively lengthy and inflexible syntheses which are often restricted to inert metals, thereby introducing a problem of kinetic rather than thermodynamic stereoselection. For more labile metals, complete thermodynamic control of the diastereoselection had not been achieved until recently, whereby iron(II) complexes with simple optically pure diimine ligands (Scheme 2.1) were shown in our laboratories to result in optically and stereochemically pure *fac* isomers with *d.r.* > 200:1.[32, 33] This unprecedented level of selectivity can be attributed in part to the presence of secondary π-

stacking interactions between the benzyl group of one $\mathbf{L}^1$ type ligand and the pyridine imine of the adjacent ligand.

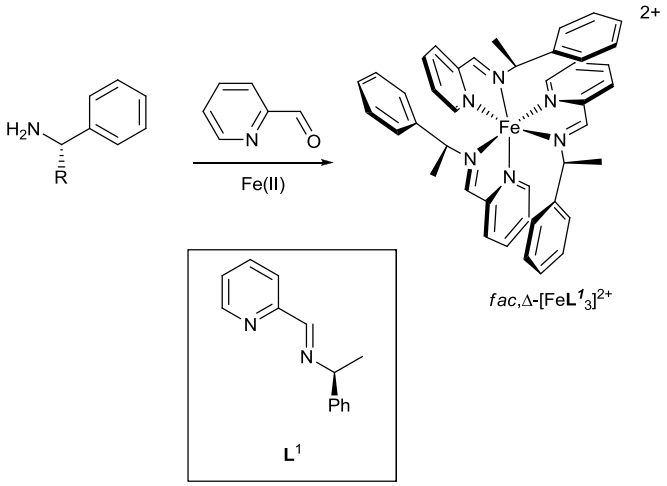

Scheme 2.1 Diasteroselective synthesis of *fac*,Δ-[Fe$\mathbf{L}^1_3$]$^{2+}$ using chiral Schiff base ligands.

In this chapter the nature of the π-stacking interactions observed in complexes related to *fac*,Δ-[Fe$\mathbf{L}^1_3$][ClO_4]$_2$ will be investigated further. In particular how these interactions are influenced by the introduction of electron donating or withdrawing substituents and the effect this has on the *fac*:*mer* ratios of analogous Zinc (II) complexes. The unusual stability imparted on the *fac*,Δ-[Fe$\mathbf{L}^1_3$][ClO_4]$_2$ complexes from these π-stacking interactions will also be investigated. In particular their suitability to undergo further CuAAC 'click' reactions post complexation will be demonstrated.

The work presented in this chapter is part of a collaborative study into the nature and functionalisation of optically pure monometallic systems and forms part of two papers.[34, 35]

2.2 **Substituent effects on selectivity in Zn(II) systems.**

As part of a larger study into the origins of selectivity in a series of optically pure *tris*-chelate $[ML_3]^{2+}$ compounds[34] it was observed that $[Zn\mathbf{L}^{\mathbf{1}}_3]^2$ complexes exhibit poorer *fac:mer* selectively than the corresponding $[Fe\mathbf{L}^{\mathbf{1}}_3]^{2+}$ systems. Single crystal XRD studies revealed that the pyridine-phenyl centroid-centroid distance was significantly elongated in the zinc complexes. As this distance is considered as the best description of π-stacking interactions, this increase in separation suggests a weakening in the strength of this interaction.[34]

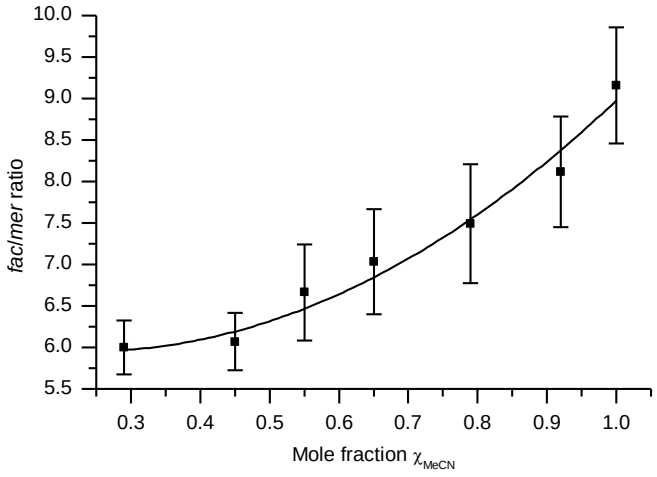

Figure 2.2 How the *fac*:*mer* selectivity varies with solvent polarity (mole fraction of acetonitrile) for $[Zn\mathbf{L}^{\mathbf{1}}_3][ClO_4]_2$. Reproduced form reference.[34]

It was found that the *fac*:*mer* ratio of $[Zn\mathbf{L}^{\mathbf{1}}_3][ClO_4]_2$ varied according to solvent polarity from a theoretical extrapolated ratio of 5.8:1 in a pure DCM solution with a polarity index of 3.1, to a 9:1 *fac*:*mer* ratio in pure acetonitrile at a polarity index of 5.8 (Figure 2.2).[34] This is likely to result from the combination of the hydrophobic effect preferentially stabilising the *fac* isomer due to the greater

number of hydrophobic π-stacking interactions present and the more polar *fac* isomer favouring the more polar solvent systems.

Both solid state measurements and solution studies indicate the important role played by π-stacking interactions in the overall selectivity for the *fac* isomer in these systems. As such, an increase in the magnitude of this interaction may lead to greater selectivity of these complexes. The majority of studies on π-stacking interactions are confined to model organic systems as discussed in Chapter 1, but the effects of metal coordination can be expected to be highly influential. The donation of electron density from the nitrogen atoms in the ligand to the metal centre can be expected to lower the overall electron density on the ring thus favouring inter-ligand π-stacking interactions.[36] Despite the dominance of this interaction, this model suggests that the magnitude of π-stacking interactions can be further influenced through the incorporation of additional substituents into either of the aromatic groups involved in the interaction. We were therefore interested in ascertaining if the incorporation of additional substituents in to the aromatic components of the ligand would allow the selectivity for *fac* vs. *mer* formation of a series of Zn(II) systems to be further improved.

2.2.1 Incorporation of substituents in the phenyl group.

A range of commercially available chiral α-methylbenzylamines subsituted in the 4-position, provide a facile way to incorporate either electron donating or withdrawing substituents into the amine component of the ligand. The desired substituted complexes $[Zn\mathbf{L}^{n}_{3}][ClO_4]_2$ (*n* = 2-5, Figure 2.3) were prepared in a one pot reaction between one equivalent of $Zn(ClO_4)_2 \cdot 6H_2O$ and three

equivalents of both the desired substituted chiral α-methylbenzylamine and pyridine aldehyde in acetonitrile to give pale yellow solutions. The dropwise addition of ethyl acetate resulted in the precipitation of white microcrystalline solids in all cases.

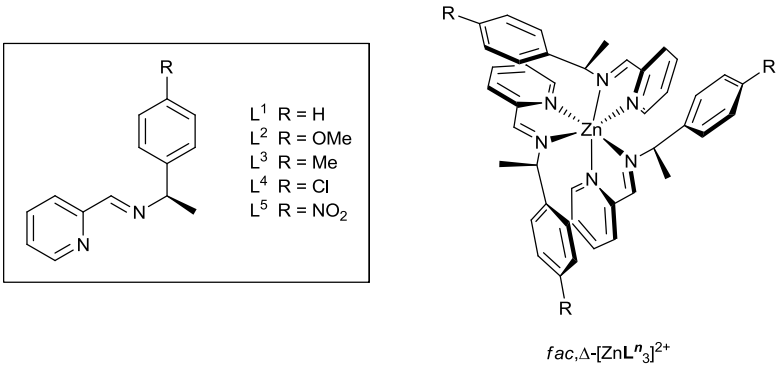

Figure 2.3 Benzyl substituted complexes of $[Zn\mathbf{L}^{n}_{3}][ClO_4]_2$ (n = 1-5).

Single crystals suitable for X-ray diffraction studies were obtained for complexes $[Zn\mathbf{L}^{n}_{3}][ClO_4]_2$ (n = 2, 3, 5) through slow vapour diffusion of ethyl acetate into acetonitrile solutions. Unfortunately single crystals of $[Zn\mathbf{L}^{4}_{3}][ClO_4]_2$ were not obtained. The selectivity of these systems arises from a combination of intermolecular interactions. The *R* chiral centre in ligand $\mathbf{L}^{2}$ results in a transfer of chirality from the ligand to the metal centre *via* steric interaction between ligands causing the complex $[Zn\mathbf{L}^{2}_{3}][ClO_4]$ to preferentially form the Δ enantiomer. The formation of three sets of concurrent π-stacking interactions between the substituted phenyl ring and the pyridine aldehyde of the adjacent ligand results in the overall preference for the *fac* isomer. As such the substituted complex $[Zn\mathbf{L}^{2}_{3}][ClO_4]$ was observed to crystallise as the Δ-*fac* diastereomer (Figure 2.4).This configuration is analogous to those observed for the unsubstituted parent complex $[Zn\mathbf{L}^{1}_{3}][ClO_4]$ and that observed for complexes

$[Zn\mathbf{L}^{3}{}_{3}][ClO_4]$ and $[Zn\mathbf{L}^{5}{}_{3}][ClO_4]$. The pyridine-phenyl centroid-centroid distances give perhaps the best assessment of π-stacking interactions in these complexes.[34] For all substituted systems measured, this distance (**b** in Figure 2.5) was found to be slightly longer (ca 0.2 Å) than that of the parent $[Zn\mathbf{L}^{1}{}_{3}][ClO_4]_2$ complex suggesting a slight weakening in the π-stacking interactions in all cases.

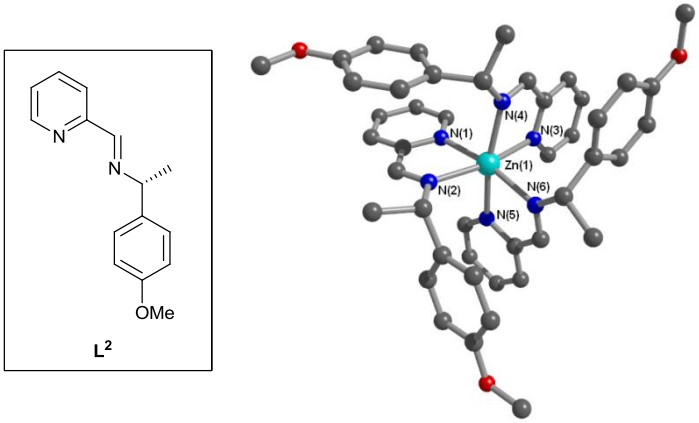

Figure 2.4 Crystal structure of $[Zn\mathbf{L}^{2}{}_{3}][ClO_4]_2$ hydrogen atoms. Solvent molecules and counter ions have been removed for clarity. Selected bond lengths (Å) and angles (°): Zn(1)-N(1) 2.187(9), Zn(2)-N(2) 2.179(2), Zn(1)-N(3) 2.187(9), Zn(2)-N(4) 2.179(2), Zn(1)-N(5) 2.187(9), Zn(2)-N(6) 2.179(2), N(1)-Zn(1)-N(2) 77.1(2), N(3)-Zn(1)-N(4) 77.1(2), N(5)-Zn(1)-N(6) 77.1(2).

As expected the ^{1}H NMR spectra of each of the substituted complexes $[Zn\mathbf{L}^{n}{}_{3}][ClO_4]_2$ (n = 2-5) at 233 K shows the presence of two separate species. These can be readily identified by a single quartet (**a**, Figure 2.6) at ca 5.40 ppm corresponding to the three equivalent CH groups of the *fac* isomer and three separate quartets (**b**, Figure 2.6) in the region 4.45-5.30 ppm, one for each of the inequivalent CH protons of the *mer* isomer. The ^{1}H NMR spectra of the substituted complexes $[Zn\mathbf{L}^{n}{}_{3}]^{2+}$ (where n = 3-5) all show an increased preference for the *fac* isomer compared to the parent $[Zn\mathbf{L}^{1}{}_{3}]^{2+}$ complex (Figure 2.5). While an increase in selectivity is predicted by the Hunter-Sanders model,[37] for ligand systems containing electron withdrawing groups, a similar increase in

selectivity is not expected for the $[Zn\mathbf{L}^{\mathbf{3}}{}_3]^{2+}$ complex due to the presence of the electron donating methyl group.

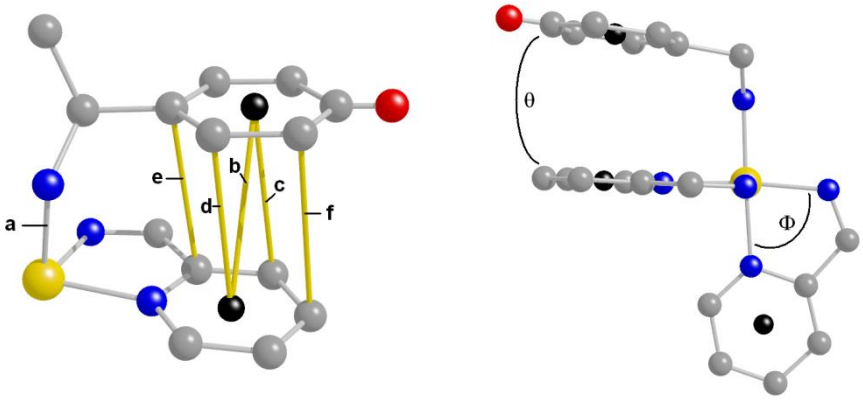

Parameter	Where R (Red sphere) =				
	MeO	**Me**	**H[a]**	**Cl**	**NO_2**
a	2.179	2.171	2.17	-	2.193
b	4.190	4.041	3.67-4.08	-	4.348
c	4.608	3.853	3.5-3.83	-	4.17
d	3.693	3.510	3.30-3.61	-	3.543
e	3.728	3.595	3.47-3.55	-	3.779
f	4.086	3.810	3.33-3.97	-	3.990
θ	8.54	8.18	3.58-14.12	-	16.53
Φ	77.12	76.70	77.08	-	76.66
fac:*mer*	8:1	17:1	8:1	11:1	17:1

[a] Bond lengths and angle are reproduced from reference.[32]

Figure 2.5 Selected structural measurements for π-stacking interaction in complexes $[Zn\mathbf{L}^{\boldsymbol{n}}{}_3]^{2+}$ (n = 1-5). *fac*:*mer* ratios determined from ^{1}H NMR spectroscopy at 233 K.

Further theoretical investigations into the nature of π-stacking interactions, conducted by Wheeler and Houk[38] and others,[39-42] have suggested that the strength of these interactions increases with the number of aromatic substituents. While this supports the increased preference for the *fac* isomer observed in the substituted complexes $[Zn\mathbf{L}^{\boldsymbol{n}}{}_3]^{2+}$ (where *n* = 3-5), the methoxy substituted $[Zn\mathbf{L}^{\mathbf{2}}{}_3]^{2+}$ complex does not follow this predicted trend, showing the same *fac*:*mer* ratios to the parent complex. Hunter previously highlighted the difficulty

in separating π-stacking interactions from other interactions within the same molecule.[43] As such it is likely that the observed *fac*:*mer* ratios in these complexes arise from a combination of influences rather than as a direct consequence of the strength of the π-stacking interaction.

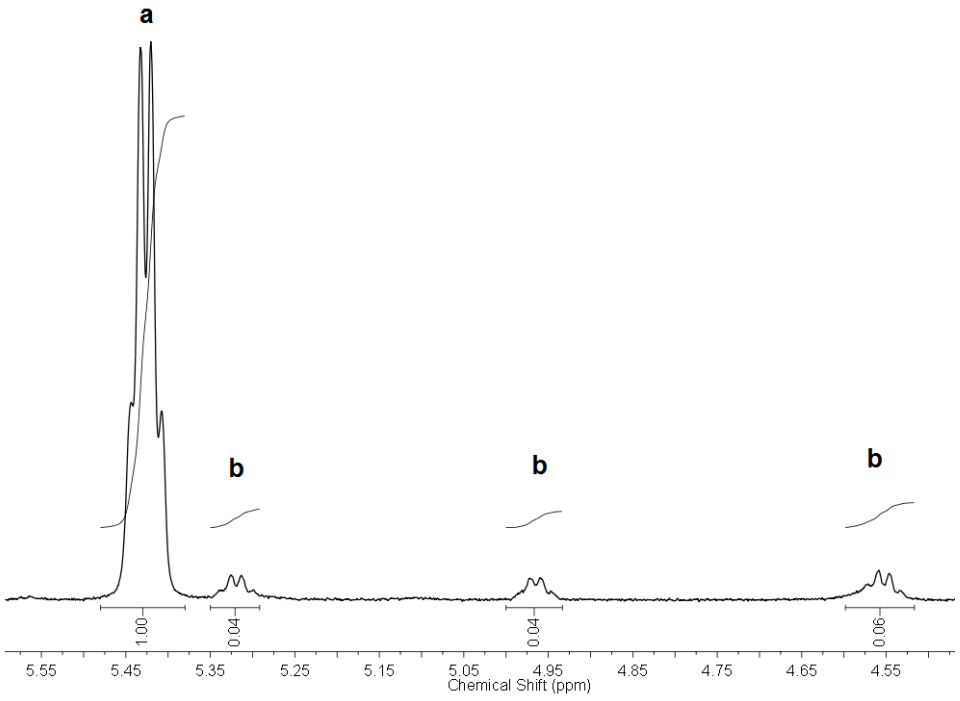

Figure 2.6 ^{1}H NMR spectrum of $[Zn\mathbf{L}^{2}_{3}][ClO_4]_2$ at 233 K in CDCN showing (a) The single quartet corresponding to the CH proton of the major *fac* isomer and (b) The three equivalent quartets of the minor *mer* isomer.

2.2.2 Incorporation of substituents into the pyridine aldehyde

The electron withdrawing 5-bromopicolinaldehyde is available commercially, while the recently published synthesis of 5-(hydroxy)picolinaldehyde (**IV** in Scheme 2.2),[44] offers an effective synthetic route to the incorporation of an electron donating methoxy substituent on the pyridine aldehyde.

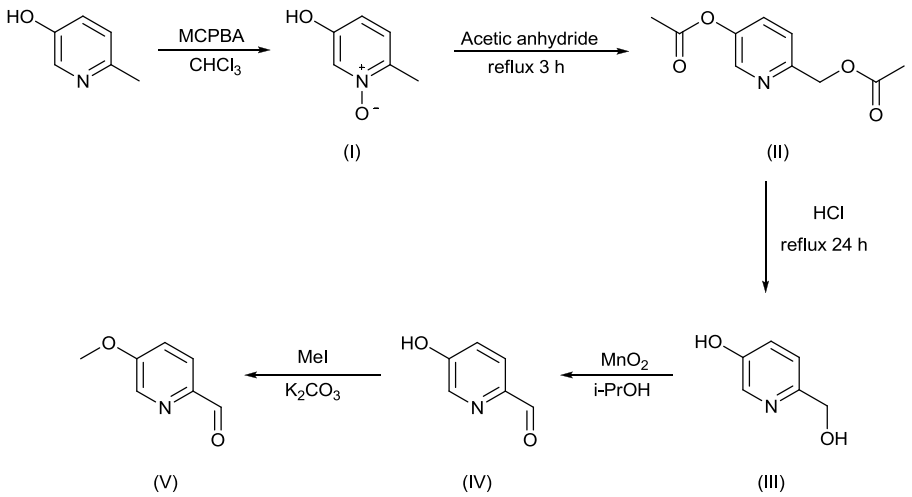

Scheme 2.2 Syntheses of 5-methoxypicolinaldehyde.

5-hydroxy-2-methylpyridine was oxidised with MCPBA to form 5-hydroxy-2-methylpyridine-1-oxide (I) in a 74 % yield. Refluxing in acetic anhydride for 3 h yielded 6-((acetyloxy)methyl)pyridin-3-yl acetate in near quantative yields. This was in turn hydrolysed to 6-(hydroxymethyl)pyridin-3-ol in 76 % yield. Finally oxidation of the alkanol with activated manganese (IV) oxide yielded 5-(hydroxy)picolinaldehyde (IV) in 45 % yield after recrystalisation from water. This could be further converted to the desired 5-(prop-2-ynyloxy)picolinaldehyde (V) in good yields (>70 %) by heating with two equivalents of potassium carbonate and an equimolar amount of methyl iodide in acetonitrile, prior to filtration through a silica plug.

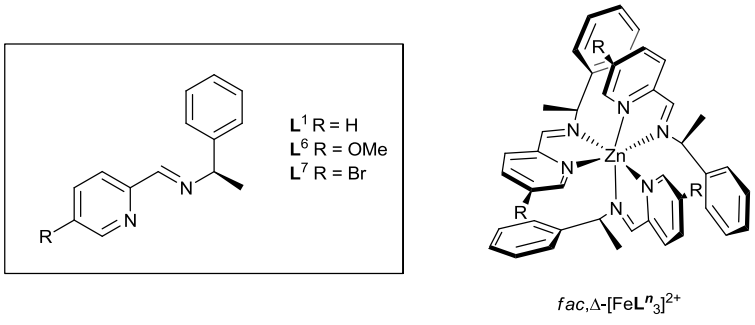

Figure 2.7 Substituted picolinaldehydes, complexes of $[Zn\mathbf{L}^{n}_{3}]^{2+}$ (n = 1, 6 & 7).

The desired substituted complexes $[Zn\mathbf{L}^{6}{}_{3}][ClO_4]_2$ and $[Zn\mathbf{L}^{7}{}_{3}][ClO_4]_2$ were then prepared in the standard one pot reaction. Single crystals suitable for X-ray diffraction studies were obtained through vapour diffusion of ethyl acetate into acetonitrile solutions for both $[Zn\mathbf{L}^{6}{}_{3}][ClO_4]_2$ and $[Zn\mathbf{L}^{7}{}_{3}][ClO_4]_2$.

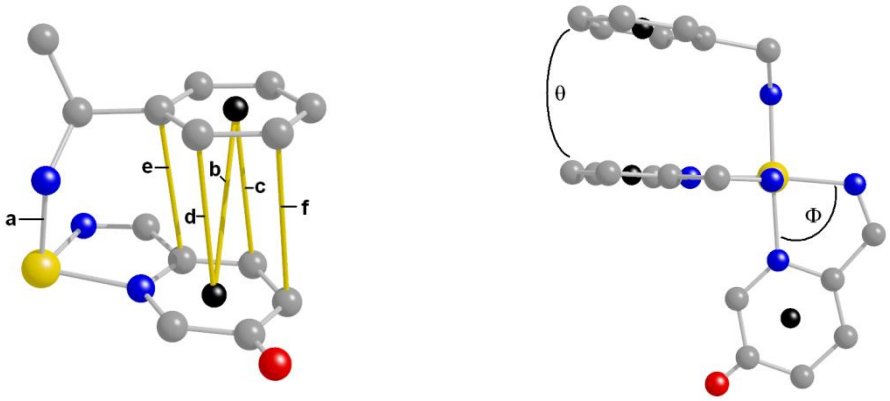

Parameter	Where R (Red sphere) =		
	MeO	H[a]	Br
a	2.16-2.17	2.17	2.16
b	3.70-3.81	3.67-4.08	3.60
c	3.49-3.58	3.5-3.83	3.41
d	3.39-3.41	3.30-3.61	3.37
e	3.39-3.46	3.47-3.55	3.36
f	3.51-3.68	3.33-3.97	3.39
θ	2.30-9.73	3.58-14.12	0.91
Φ	76.64-77.21	77.08	77.59
fac:*mer*	13:1	8:1	14:1

[a] Bond lengths and angles are reproduced from reference[32]

Figure 2.8 Selected structural measurements for π-stacking interaction in complexes of $[Zn\mathbf{L}^{n}{}_{3}]^{2+}$ (n = 1, 6 and 7). *fac:mer* ratios determined from ^{1}H NMR spectroscopy at 233 K.

The substituted complexes were again observed to crystallise as the *fac* isomer with three sets of concurrent π-stacking interactions between ligands. Unlike the previous substituted complexes $[Zn\mathbf{L}^{n}{}_{3}]^{2+}$ (where n = 2-5) the centroid-centroid distances measured for complexes $[Zn\mathbf{L}^{6}{}_{3}][ClO_4]_2$ and $[Zn\mathbf{L}^{7}{}_{3}][ClO_4]_2$ were the

same as those observed in the parent complex, $[Zn\mathbf{L}^1{}_3][ClO_4]_2$ (Figure 2.8). The ^{1}H NMR spectra of these complexes showed the presence of both *fac* and *mer* isomers, with each of the substituted complexes showing an increased preference for the *fac* isomer when compared to $[Zn\mathbf{L}^1{}_3][ClO_4]_2$ (Figure 2.8). This result is unexpected on the basis of the Hunter-Sanders' model,[37] and instead suggesting that the increase in aromatic substituents alone accounts for the enhancement in π-stacking as predicted by Wheeler and Houk.[38] Despite this it is again likely that metal coordination dominates these systems. This effect has been considered in greater detail in Chapter 3.

2.3 Functionalisation of monometallic iron(II) systems through CuAAC 'click' chemistry post complexation.[35]

The steroselectivity of formation of $[Fe\mathbf{L}^1{}_3][ClO_4]_2$ systems and their ability to tolerate the inclusion of functional groups into the ligand design creates an opportunity to conduct further chemical reactions post complexation. In particular we were interested in the potential for these complexes to undergo copper(I)-catalysed Huisgen 1,3-dipolar cycloaddition (CuAAC) 'click' reactions which despite being popular in synthetic, biological and materials chemistry, are relatively rare for pre-formed metal complexes. In the few examples that do exist, the metal is typically used to template the various reaction components in "gathering and threading" approaches in rotaxane and catenane formation.[45-53] Despite this, there are several examples in which inert metal systems such as those containing ruthenium, have proven suitable for 'click' type reactions.[54-60]

However, in cases where more labile metals are used, click reactions do not proceed cleanly with displacement of the metals by the Cu 'click' catalyst occurring either directly or via electron transfer.[56]

2.3.1 Route to 'clickable' monometallic systems.

In principle it is possible to incorporate alkyne groups into the ligand structure via either the chiral amine or the pyridine carboxaldehyde components of the ligand as shown in Figure 2.9. Previous members of this group,[61] have noted that the reaction between $[Fe\mathbf{L}^{8}_{3}][ClO_4]_2$ and benzyl azide in the presence triethylamine and one equivalent of CuI in dry MeCN results in the formation of a single species as shown by ^{1}H NMR. However microanalytical data of this sample indicates the presence of copper(I) iodide in a 1:1 ratio with the complex. It was subsequently confirmed by single crystal XRD that a copper(I) atom was coordinated in a trigonal planar geometry to the nitrogen atoms in position 3 of the triazole rings. Interestingly the sense of helicity of the Cu(I) centre was observed to be the opposite of that of the Fe(II) centre, i.e. $\Delta_{Fe}\Lambda_{Cu}$. As such, the resulting bimetallic species can be considered the first example of an optically pure heterohelicate. Despite the success of this approach as a route to C_3 symmetric heterohelicates the incorporation of copper(I) into the these systems is not ideal due to a decrease in the overall solubility of the complex. Attempts to remove the copper salt resulted in decomposition of the complex.[61]

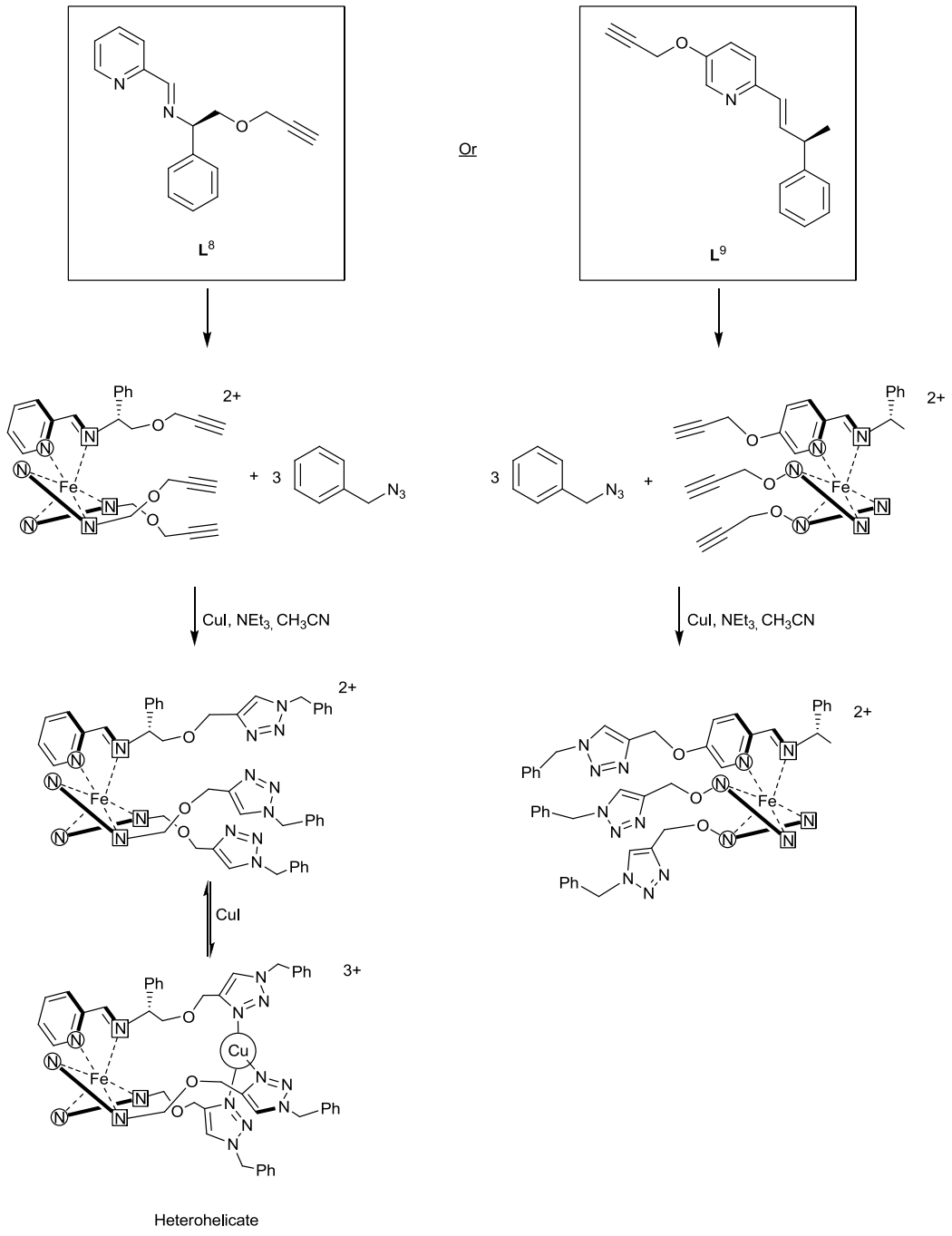

Figure 2.9 Two approaches for 'click' chemistry on monometallic complexes.

Consequently the incorporation of an alkyne group via the pyridine carboxaldehyde offers an alternative route to functionalise these complexes through 'click' chemistry. It has been shown previously that pyridinyl ether groups in this position are not sufficiently preorganised for binding of metal

atoms as the greater separation of the alkyne groups reduces the propensity to coordinate copper(I) during the 'click' reaction.[35]

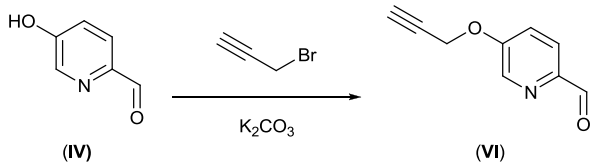

Scheme 2.3 Synthesis of 5-(prop-2-ynyloxy)picolinaldehyde.

5-(hydroxy)picolinaldehyde (**IV** Scheme 2.3), was converted to the desired 5-(prop-2-ynyloxy)picolinaldehyde (**VI**) in good yields (>70 %), by heating with two equivalents of potassium carbonate and an equimolar amount of propargyl bromide in acetonitrile, prior to filtration through a silica plug. The diastereomerically pure compound *fac*,Λ_{Fe},R_C-[Fe$\mathbf{L}^{\mathbf{9}}{}_3$][$ClO_4$]$_2$ was then prepared in a one pot reaction between one equivalent of Fe(ClO_4)$_2$·6H_2O and three equivalents of α-methylbenzylamine and 5-(prop-2-ynyloxy)picolinaldehyde in acetonitrile to give a purple solution. The dropwise addition of ethyl acetate resulted in the precipitation of a dark purple microcrystalline solid which was shown to be diastereomerically pure by ^{1}H NMR spectroscopy. Subsequently this alkyne compound was treated with benzyl azide in the presence of dry triethylamine and a catalytic amount of copper iodide (0.3 eq. per complex) in dry acetonitrile which again afforded a dark purple solid. However, ^{1}H NMR spectra of the resulting product indicated the presence of several species which could be identified as the starting material, [Fe$\mathbf{L}^{\mathbf{9}}{}_3$][$ClO_4$]$_2$ alongside several 'clicked' species [Fe$\mathbf{L}^{\mathbf{9}}{}_2\mathbf{L}^{\mathbf{10}}$][$ClO_4$]$_2$, [Fe$\mathbf{L}^{\mathbf{9}}\mathbf{L}^{\mathbf{10}}{}_2$][$ClO_4$]$_2$ and [Fe$\mathbf{L}^{\mathbf{10}}{}_3$][$ClO_4$]$_2$ (Figure 2.11). Increasing the amount of CuI in the reaction to one equivalent per Fe centre resulted in [Fe$\mathbf{L}^{\mathbf{10}}{}_3$][$ClO_4$]$_2$ being observed as the major product in the

reaction mix however traces of both $[Fe\mathbf{L}^{9}{}_{2}\mathbf{L}^{10}][ClO_4]_2$ and $[Fe\mathbf{L}^{9}\mathbf{L}^{10}{}_{2}][ClO_4]_2$ were still present. Ultimately three equivalents of CuI per Fe unit, or more, were required to obtain complete conversion to the desired $[Fe\mathbf{L}^{10}{}_{3}][ClO_4]_2$ 'clicked' species (Figure 2.11). Interestingly, complete conversion caused a change in the peak corresponding to the diastereotopic O–CH_2–triazole group in the ^{1}H NMR spectrum (g, Figure 2.11). The peak was observed to have widened to ca 0.25 ppm indicating the possible coordination Cu^+ in to the complex i.e. $[Fe\mathbf{L}^{10}{}_{3}Cu]^{3+}$. Despite this observation in the ^{1}H NMR spectrum, no peaks were observed for the Cu-bound species in mass spectrometry. Unfortunately attempts to recrystallize this species for analysis led to slow decomposition and formation of red paramagnetic products. This is likely to be due to the formation of a bis complex $[Fe\mathbf{L}^{10}{}_{2}]^{2+}$ (Figure 2.10) as a result of the chelate effect due to the resulting triazole containing ligand $\mathbf{L}^{10}$ being appropriately structured to coordinate in a tridentate fashion.

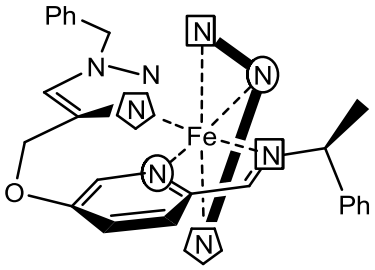

Figure 2.10 Proposed structure of $[Fe\mathbf{L}^{10}{}_{2}]^{2+}$.

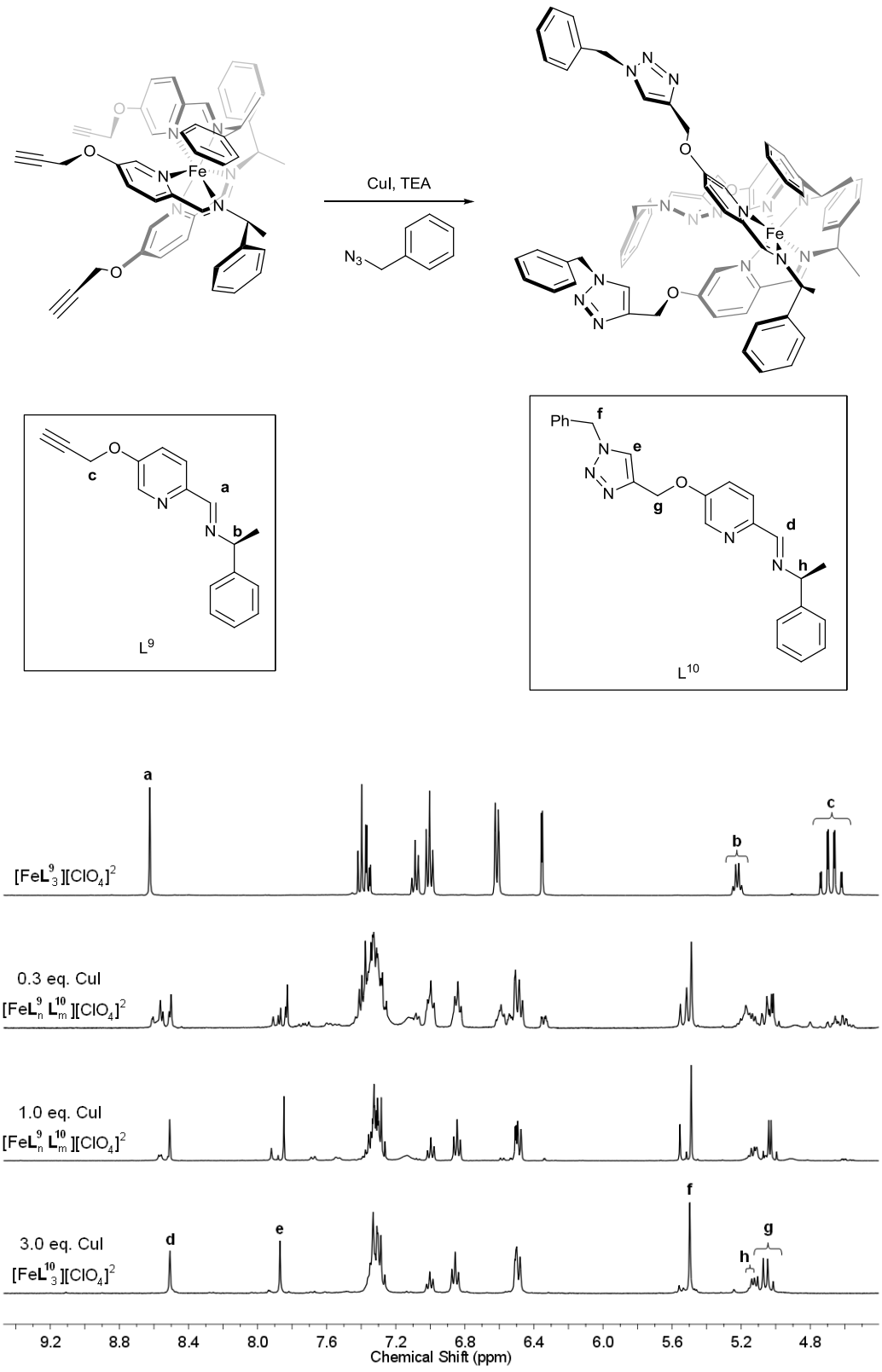

Figure 2.11 ^{1}H NMR spectra showing how conversion to the desired [Fe$\mathbf{L}^{10}_3$][ClO_4]$_2$ 'clicked' species depends on the equivalents of CuI used.

2.4 **Conclusions**

In this chapter, two separate approaches to the functionalization of optically pure monometallic complexes have been investigated. The first approach involves the incorporation of substituents into either the phenyl or pyridine aldehyde components of the ligand. It was observed that functional group in the 4-position have little impact on the inter ligand π-stacking interactions in the solid state, however investigation of the *fac*:*mer* ratios of theses complexes calculated in solution, suggests that these complexes do not follow the trend predicted by the Hunter and Sanders electrostatic model.[37] Hunter has previously noted the difficulty in identify π-stacking contributions to a system due to their tendency to be heavily influenced by neighbouring interactions within the same system.[43] We ourselves have noted that solvent effects also play a role in the selectivity of $[Zn\mathbf{L}^{\mathbf{1}}_3][BF_4]_2$ complexes.[34] As such the selectivity ratios determined for these systems are likely to result from a combination of factors and not simply from an electrostatic interaction between the phenyl and pyridine rings. What these studies do highlight however is that these systems are able to support a diverse range of substituents within the ligand design without loss of stereoselectivity. Furthermore, due to the structural similarity of these Zn(II) complexes with the highly stereoselective $[Fe\mathbf{L}_3]^{2+}$ systems,[34] this approach provides a route to functionalised stereoselective monometallic systems.

The second approach to functionalization of these $[M\mathbf{L}_3]^{2+}$ complexes focused on the ability to incorporate an alkyne group into the pyridine aldehyde component of the ligand, making them suitable to undergo further CuAAC 'click' reactions post complexation. It was observed that the resulting complex

$[Fe\mathbf{L}^{9}_{3}][ClO_4]_2$ underwent 'click' reactions without incorporating copper(I) into the overall structure. Unfortunately the resulting complex, $[Fe\mathbf{L}^{10}_{3}][ClO_4]_2$ was found to undergo decomposition as a result of the chelate effect. This approach however establishes a precedent for the functionalization of stereoselective systems post complexation.

2.5 **References**

1. A. Werner and A. Vilmos, *Z. Anorg. Allg. Chem.*, 1899, **21**, 145 - 158.
2. S. E. Howson, L. E. Allan, N. P. Chmel, G. J. Clarkson, R. van Gorkum and P. Scott, *Chem. Commun. (Camb.)*, 2009, 1727-1729.
3. N. C. Fletcher, M. Nieuwenhuyzen and S. Rainey, *J. Chem. Soc., Dalton Trans.*, 2001, 2641-2648.
4. A. Grabulosa, M. Beley and P. C. Gros, *Eur. J. Inorg. Chem.*, 2008, 1747-1751.
5. C. R. Rice, *Coord. Chem. Rev.*, 2006, **250**, 3190-3199.
6. P. A. Gale and R. Quesada, *Coord. Chem. Rev.*, 2006, **250**, 3219-3244.
7. M. H. Keefe, K. D. Benkstein and J. T. Hupp, *Coord. Chem. Rev.*, 2000, **205**, 201-228.
8. V. Balzani, A. Juris, M. Venturi, S. Campagna and S. Serroni, *Chem. Rev.*, 1996, **96**, 759-834.
9. F. R. Keene, *Coord. Chem. Rev.*, 1997, **166**, 121-159.
10. F. R. Keene, *Chem. Soc. Rev.*, 1998, **27**, 185-194.
11. K. E. Erkkila, D. T. Odom and J. K. Barton, *Chem. Rev.*, 1999, **99**, 2777-2796.
12. C. Metcalfe and J. A. Thomas, *Chem. Soc. Rev.*, 2003, **32**, 215-224.
13. K. K.-W. Lo, K. H.-K. Tsang, K.-S. Sze, C.-K. Chung, T. K.-M. Lee, K. Y. Zhang, W.-K. Hui, C.-K. Li, J. S.-Y. Lau, D. C.-M. Ng and N. Zhu, *Coord. Chem. Rev.*, 2007, **251**, 2292-2310.
14. M. J. Clarke, *Coord. Chem. Rev.*, 2002, **232**, 69-93.
15. F. P. Dwyer and E. C. Gyarfas, *J. Proc. R. Soc. N. S. W.*, 1949, **83**, 174-176.
16. X. Hua and A. von Zelewsky, *Inorg. Chem.*, 1995, **34**, 5791-5797.
17. C. Hiort, P. Lincoln and B. Norden, *J. Am. Chem. Soc.*, 1993, **115**, 3448-3454.
18. S. Bodige, A. S. Torres, D. J. Maloney, D. Tate, G. R. Kinsel, A. K. Walker and F. M. MacDonnell, *J. Am. Chem. Soc.*, 1997, **119**, 10364-10369.
19. W. R. Browne, D. Hesek, J. F. Gallagher, C. M. O'Connor, J. S. Killeen, F. Aoki, H. Ishida, Y. Inoue, C. Villani and J. G. Vos, *Dalton Trans.*, 2003, 2597-2602.
20. J. Lacour, S. Torche-Haldimann, J. J. Jodry, C. Ginglinger and F. Favarger, *Chem. Commun.*, 1998, 1733-1734.
21. N. C. Fletcher, P. C. Junk, D. A. Reitsma and F. Richard Keene, *J. Chem. Soc., Dalton Trans.*, 1998, 133-138.
22. J. G. Collins, J. R. Aldrich-Wright, I. D. Greguric and P. A. Pellegrini, *Inorg. Chem.*, 1999, **38**, 5502-5509.
23. N. C. Baker, N. McGaughey, N. C. Fletcher, A. V. Chernikov, P. N. Horton and M. B. Hursthouse, *Dalton Trans*, 2009, 965-972.
24. S. Torelli, S. Delahaye, A. Hauser, G. Bernardinelli and C. Piguet, *Chemistry (Easton)*, 2004, **10**, 3503-3516.
25. L. Gong, S. P. Mulcahy, K. Harms and E. Meggers, *J. Am. Chem. Soc.*, 2009, **131**, 9602-9603.
26. E. Meggers, *Chemistry (Easton)*, 2010, **16**, 752-758.
27. N. C. Fletcher, C. Martin and H. J. Abraham, *New J. Chem.*, 2007, **31**, 1407-1411.

28. N. C. Fletcher, M. Nieuwenhuyzen, R. Prabarahan and A. Wilson, *Chem. Commun.*, 2002, 1188-1189.
29. H. Weizman, J. Libman and A. Shanzer, *J. Am. Chem. Soc.*, 1998, **120**, 2188-2189.
30. P. Hayoz, A. Von Zelewsky and H. Stoeckli-Evans, *J. Am. Chem. Soc.*, 1993, **115**, 5111-5114.
31. A. von Zelewsky and O. Mamula, *J. Chem. Soc., Dalton Trans.*, 2000, 219-231.
32. S. E. Howson, L. E. N. Allan, N. P. Chmel, G. J. Clarkson, R. J. Deeth, A. D. Faulkner, D. H. Simpson and P. Scott, *Dalton Trans.*, 2011.
33. S. E. Howson, L. E. N. Allan, N. P. Chmel, G. J. Clarkson, R. van Gorkum and P. Scott, *Chem. Commun.*, 2009, 1727-1729.
34. S. E. Howson, L. E. N. Allan, N. P. Chmel, G. J. Clarkson, R. J. Deeth, A. D. Faulkner, D. H. Simpson and P. Scott, *Dalton Trans.*, 2011, **40**, 10416-10433.
35. S. E. Howson, G. J. Clarkson, A. D. Faulkner, R. A. Kaner, M. J. Whitmore and P. Scott, *Dalton Trans.*, 2013.
36. C. A. Hunter, J. Singh and J. M. Thornton, *J. Mol. Biol.*, 1991, **218**, 837-846.
37. C. A. Hunter and J. K. M. Sanders, *J. Am. Chem. Soc.*, 1990, **112**, 5525-5534.
38. S. E. Wheeler and K. N. Houk, *J. Am. Chem. Soc.*, 2008, **130**, 10854-10855.
39. M. O. Sinnokrot and C. D. Sherrill, *J. Phys. Chem. A*, 2004, **108**, 10200-10207.
40. M. O. Sinnokrot and C. D. Sherrill, *J. Phys. Chem. A*, 2006, **110**, 10656-10668.
41. E. C. Lee, D. Kim, P. Jurečka, P. Tarakeshwar, P. Hobza and K. S. Kim, *J. Phys. Chem. A*, 2007, **111**, 3446-3457.
42. S. Grimme, *Angew. Chem. Int. Ed. Engl.*, 2008, **47**, 3430-3434.
43. H. Adams, F. J. Carver, C. A. Hunter, J. C. Morales and E. M. Seward, *Angewe. Chem. Int. Ed. in English*, 1996, **35**, 1542-1544.
44. M. Seredyuk, A. B. Gaspar, V. Ksenofontov, Y. Galyametdinov, J. Kusz and P. Gutlich, *J. Am. Chem. Soc.*, 2008, **130**, 1431-1439.
45. P. Mobian, J.-P. Collin and J.-P. Sauvage, *Tetrahedron Lett.*, 2006, **47**, 4907-4909.
46. A. I. Prikhod'ko, F. Durola and J.-P. Sauvage, *J. Am. Chem. Soc.*, 2007, **130**, 448-449.
47. S. Durot, P. Mobian, J.-P. Collin and J.-P. Sauvage, *Tetrahedron*, 2008, **64**, 8496-8503.
48. J. D. Megiatto and D. I. Schuster, *J. Am. Chem. Soc.*, 2008, **130**, 12872-12873.
49. J.-P. Collin, J. Frey, V. r. Heitz, J.-P. Sauvage, C. Tock and L. Allouche, *J. Am. Chem. Soc.*, 2009, **131**, 5609-5620.
50. J.-P. Collin, J.-P. Sauvage, Y. Trolez and K. Rissanen, *New J. Chem.*, 2009, **33**, 2148-2154.
51. A. I. Prikhod′ko and J.-P. Sauvage, *J. Am. Chem. Soc.*, 2009, **131**, 6794-6807.
52. I. Aprahamian, O. Miljanic, Scaron, W. R. Dichtel, K. Isoda, T. Yasuda, T. Kato and J. F. Stoddart, *Bull. Chem. Soc. Jpn.*, 2007, **80**, 1856-1869.

53. J. D. Megiatto and D. I. Schuster, *Chem. Eur. J.*, 2009, **15**, 5444-5448.
54. J. P. Collman, N. K. Devaraj and C. E. D. Chidsey, *Langmuir*, 2004, **20**, 1051-1053.
55. S.-i. Fukuzawa, H. Oki, M. Hosaka, J. Sugasawa and S. Kikuchi, *Org. Lett.*, 2007, **9**, 5557-5560.
56. D. Gonzalez Cabrera, B. D. Koivisto and D. A. Leigh, *Chem. Commun.*, 2007, 4218-4220.
57. C. Haensch, M. Chiper, C. Ulbricht, A. Winter, S. Hoeppener and U. S. Schubert, *Langmuir*, 2008, **24**, 12981-12985.
58. M. Jauregui, W. S. Perry, C. Allain, L. R. Vidler, M. C. Willis, A. M. Kenwright, J. S. Snaith, G. J. Stasiuk, M. P. Lowe and S. Faulkner, *Dalton Transactions*, 2009, 6283-6285.
59. A. R. McDonald, H. P. Dijkstra, B. M. J. M. Suijkerbuijk, G. P. M. van Klink and G. van Koten, *Organometallics*, 2009, **28**, 4689-4699.
60. E. C. Constable, C. E. Housecroft, M. Neuburger and P. Rosel, *Chem. Commun.*, 2010, **46**, 1628-1630.
61. M. Whitmore, Warwick University, 2011.

Chapter 3

Design and synthesis of triplex metallohelices.

3.1 Introduction

As outlined in Chapter 1, ligands designed to form helicates are typically comprised of two pairs of bidentate coordinating groups A and B connected *via* some linker, i.e. **AB**–**BA**. Such ligands have C_2 or C_{2v} symmetry. As such, these ligands can result in the formation of three isomers, either of two homochiral helicates (*i.e.* Δ,Δ or Λ,Λ) or, should the ligand be suitably flexible, the mesocate (Δ,Λ). If however, lower symmetry *directional* ligands are employed in the formation of bimetallics $[M_2(\mathbf{AB}–\mathbf{CD})_3]$, a total of eight isomers may now be formed, because C_3 symmetric Head-to-Head-to-Head (HHH) and C_1 symmetric Head-to-Head-to-Tail (HHT) configurations are now possible (Figure 3.1). The expected statistical ratio HHT:HHH is 3:1; this is analogous to the *fac*:*mer* ratio in monometallic systems $[M(\mathbf{AB})_3]$.

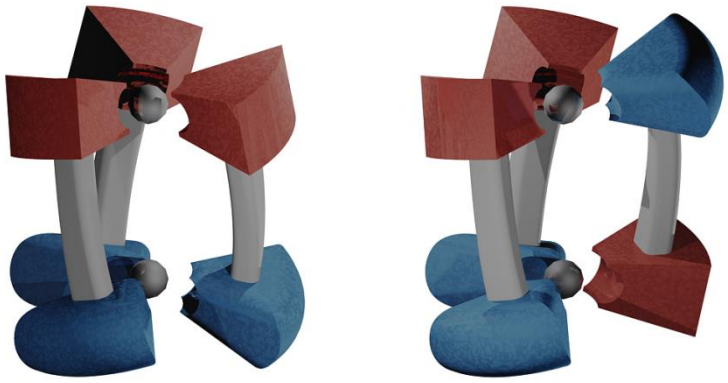

Figure 3.1 Schematic diagrams of the C_3 symmetric ΔΔ-Head-to-Head-to-Head (left), and C_1 symmetric ΔΔ-Head-to-Head-to-Tail (right) configurations.

As either a Δ or Λ configuration at each metal centre is possible, both the helicate (ΔΔ or ΛΛ), and mesocate structures (ΔΛ or ΛΔ), can be formed for each of the HHH and HHT geometries. Selective formation of C_3 symmetric hetrobimetallic systems has been achieved by employing either a multi-step synthesis in which an inert metal is coordinated, prior to a second binding site and metal being introduced into the complex,[1] or by incorporating two unique multidetate coordinating groups into the ligand design with each having a preference for a different metal.[2-4] In both cases, enantiomeric resolution of the products is often required. Recently, Scott and co-workers have shown that it is possible to selectively synthesise optically pure mixed iron(II) copper(I) systems using chiral (**AB–CD**) type ligands. In their system, the overall control arises from a combination of three concurrent π-stacking interactions around the iron(II) centre and the use of short rigid linkers both of which favour the formation of the C_3 helical isomers.[5] Unsurprisingly, the synthesis of C_1 symmetric HHT systems of triple stranded bimetallic helices is even more elusive.[2, 6] Although such systems have been observed in single crystals, they typically exist as mixture of regio- and optical isomers in solution that cannot be readily separated.[7-10]

In this chapter the possibility of diasteroselective synthesis of C_1 symmetric metallohelices is investigate, motivated principally by their potential applications as peptidometic therapeutic agents. The selectivity of these systems are investigated though both computational and synthetic studies. In addition the suitability of these systems to post complexation functionalisation through copper(I)-catalysed Huisgen 1,3-dipolar cycloaddation 'click' reactions is investigated.

3.2 **Results and Discussion**

3.2.1 A strategy for the selective synthesis of C_1 symmetric complexes.

Based on the previous work conducted by Scott and co-workers,[5, 11, 12] a new approach to the selective synthesis of C_1 symmetric HHT bimetallic systems is envisioned. Consider the replacement of one or two of the $\mathbf{L}^1$ ligands in the *tris* chelate $[Fe\mathbf{L}_3{}^1]^{2+}$ complex with for example either a bpy or phen ligand (Figure 3.2) If the diasteroselevtive preferences of the substituted complexes was sufficiently high and the absolute energies of the complexes sufficiently favourable the bis(bidentate) helicand of the type $\mathbf{H}^1$ or $\mathbf{H}^2$ (**a**, Figure 3.3) could lead to a diastereospecific synthesis of a C_1 symmetric HHT helix (**b**, Figure 3.3). To assess the validity of this approach the diasteroselective preferences of the substituted complexes were investigated by computational means.

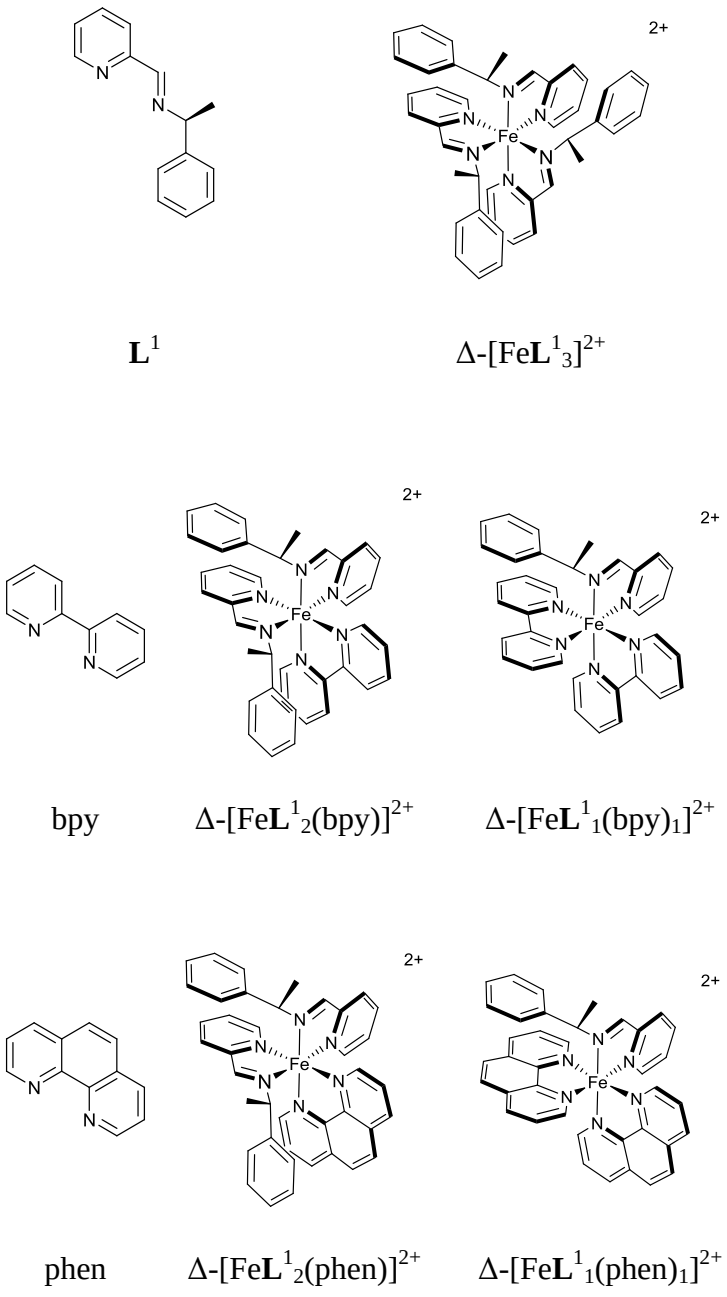

Figure 3.2 Top the tris chelate monometallic unit Δ-[Fe$\mathbf{L}^1_3$]$^{2+}$. The direct replacement of one or two $\mathbf{L}^1$ type ligands with bpy (middle) or phen (bottom) while maintain the overall stereochemistry.

(**a**) (**b**)

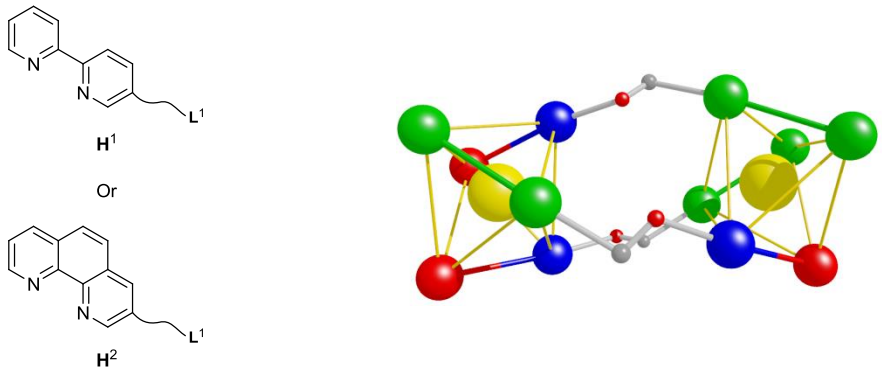

Figure 3.3 (**a**), proposed helicands of the type $\mathbf{H^1}$ and $\mathbf{H^2}$. (**b**) cartoon representation of the resulting C_1 symmetric HHT helix derived from the proposed helicands $\mathbf{H_1}$ and $\mathbf{H_2}$.

3.2.2 The selectivity of mixed ligand, monometallic complexes.

Each of the potential isomers that arise through the proposed substitution of an $\mathbf{L}^1$ type ligand, in the *tris* chelate $[Fe\mathbf{L}_3{}^1]^{2+}$ complex with either a 2,2'-bipyridine or 1,10-phenanthroline, was optimised using B3LYP-D3(BJ)[13] functional and the 6-31g* basis set as implemented in the Firefly quantum chemistry package,[14] with is partial based on the GAMESS(US) source code.[15] Single point energy calculations employing the B3LYP-D3(BJ)[13] functional were then performed on each of the optimised structures using the deff2-TZVP basis set. In the case where a single $\mathbf{L}^1$ ligand in $[Fe\mathbf{L}^1{}_3]^{2+}$ is replaced either 2,2'-bipyridine or 1,10-phenanthroline, six isomers for the resulting $[Fe\mathbf{L}^1{}_2(bpy)]^{2+}$ and $[Fe\mathbf{L}^1{}_2(phen)]^{2+}$ complexes are possible as shown in Table 3.1

The $\mathbf{a^3}$ isomers are characterised by the *trans* arrangement of the two pyridines of the $\mathbf{L}^1$ ligands which results in a C_2 symmetric system. Such symmetry would be undesirable as a monometallic unit in the target metallohelix as it cannot be combined with a second unit to create a C_1 symmetric assembly using a helicand of the type $\mathbf{H}^1$ or $\mathbf{H}^2$ (Figure 3.3). In any event the arrangement

of ligands in this case imposes significant steric clashes between the phenyl rings of the $\mathbf{L}^1$ ligands. As a result the $\mathbf{a}^3$ isomers of $[Fe\mathbf{L}^1{}_2(bpy)]^{2+}$ and $[Fe\mathbf{L}^1{}_2(phen)]^{2+}$ are found to be the *ca* 10 Kcal mol^{-1} higher in energy than both the $\mathbf{a}^1$ and $\mathbf{a}^2$ isomers.

$[FeL^1{}_2(bpy)]^{2+}$			$[FeL^1{}_2(phen)]^{2+}$		
Isomer $\Delta\mathbf{a}^1$	Isomer $\Delta\mathbf{a}^2$	Isomer $\Delta\mathbf{a}^3$	Isomer $\Delta\mathbf{a}^1$	Isomer $\Delta\mathbf{a}^2$	Isomer $\Delta\mathbf{a}^3$
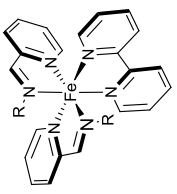	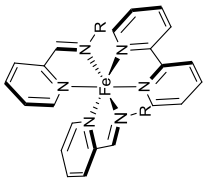	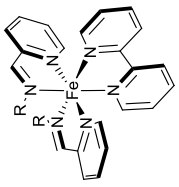	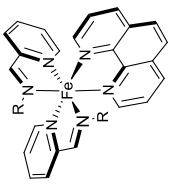	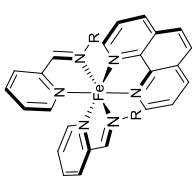	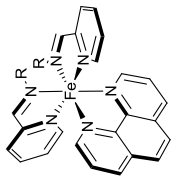
-1921767.45	-1921767.12	-1921777.55	-1969626.63	-1969626.45	-1969616.61
0.00	+0.34	+10.08	0.00	+0.18	+10.02
Isomer $\Lambda\mathbf{a}^1$	Isomer $\Lambda\mathbf{a}^2$	Isomer $\Lambda\mathbf{a}^3$	Isomer $\Lambda\mathbf{a}^1$	Isomer $\Lambda\mathbf{a}^2$	Isomer $\Lambda\mathbf{a}^3$
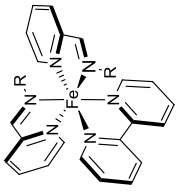	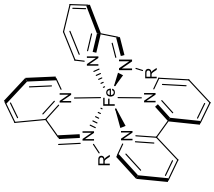	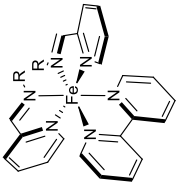	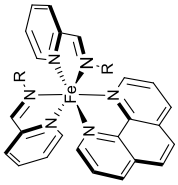	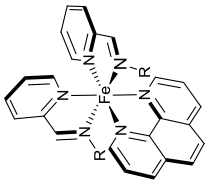	
-1921777.07	-1921774.12	-1921779.82	-1969617.06	-1969619.78	-1969614.27
+9.62	+6.67	+12.37	+9.56	+6.84	+12.36

Table 3.1 The six potential isomers of $[Fe\mathbf{L}^1{}_2(bpy)]^{2+}$ and $[Fe\mathbf{L}^1{}_2(phen)]^{2+}$. Where R = $CH(Ph)CH_3$. All energies (relative and absolute), are reported in kcal mol^{-1}. Energies are reported relative to isomer Δa^1 for the respectively substituted systems.

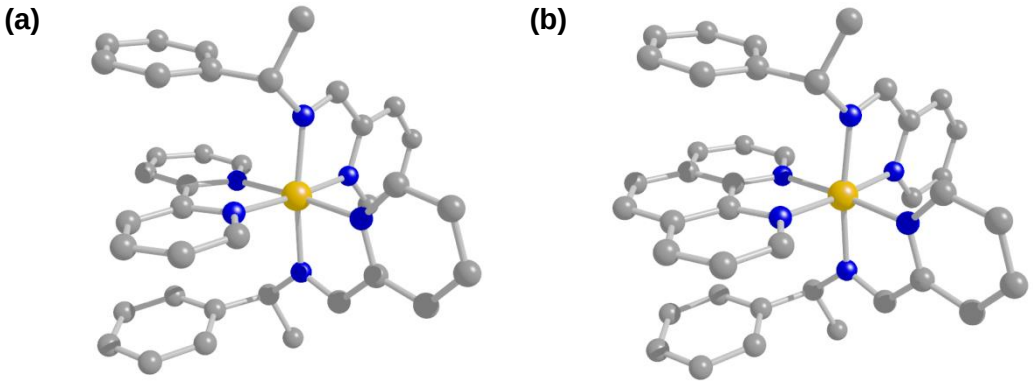

Figure 3.4 Calculated structure for the Δa^2 isomers showing the extended π-stacking arrangements between ligands of A) $[Fe\mathbf{L}^1{}_2(bpy)]^{2+}$ and B) $[Fe\mathbf{L}^1{}_2(Phen)]^{2+}$. Hydrogen atoms removed for clarity.

The $\mathbf{a}^2$ isomers also result in a C_2 symmetric system due to the *trans* placement of the two imine units of the $\mathbf{L}^1$ type ligands. In this configuration both the phenyl rings form extended face-to-face stacking interactions, with either the 2,2'-bipyridine or 1,10-phenanthroline (Figure 3.4). Although there are no known literature values for π-stacking arrangements of this type; the distance between ring planes (3.4 Å) and the horizontal displacement of the phenyl ring with respect to the closet pyridine ring (1.7 Å), are consistent with optimal values for an π-stacking interactions.[16]

There is a strong enantiomeric preference for the Δ enantiomer in the $\mathbf{a}^2$ isomers, 6.35 Kcal mol^{-1} in the case of $[Fe\mathbf{L}^1{}_2(bpy)]^{2+}$ and 6.84 Kcal mol^{-1} for $[Fe\mathbf{L}^1{}_2(phen)]^{2+}$. The $\mathbf{a}^1$ isomers are characterised by the *cis* arrangement of both the pyridine and imine components of the two $\mathbf{L}^1$ Ligands. This results in two unique π-stacking interactions. The first is observed between a pyridine ring of one $\mathbf{L}^1$ ligand and a phenyl ring of the adjacent $\mathbf{L}^1$ ligand. While the second is formed between the benzyl group of the $\mathbf{L}^1$ ligand and either the 2,2'-bipyridine or 1,10-phenanthroline ligand (Figure 3.5). As a direct consequence of this, the $\mathbf{a}^1$ isomers display C_1 symmetry. In both the $[Fe\mathbf{L}^1{}_2(bpy)]^{2+}$ and the

$[Fe\mathbf{L}^1{}_2(phen)]^{2+}$ series, the $\mathbf{a}^1$ isomer also found to be the lowest in energy by 0.34 and 0.18 kcal mol^{-1} respectively. Furthermore due to a steric clash arising between the two methyl groups in the Λ isomers, there is a significant preference for the Δ enantiomer in both cases. This makes them ideally suited as building blocks for C_1 symmetric bimetallic systems

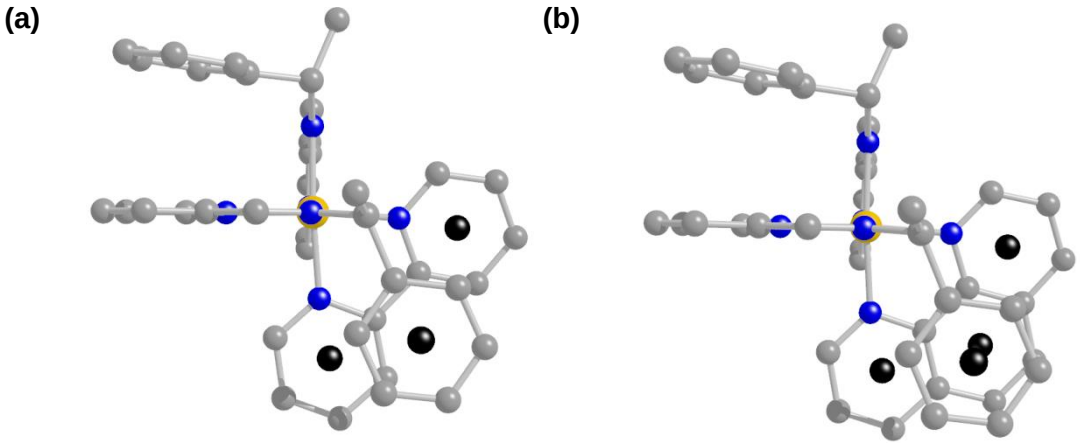

Figure 3.5 Calculated structures of isomer Δa^1 showing the offset π-stacking interactions between (**a**) The chiral phenyl and 2,2'-bipyridine and (**b**) The chiral phenyl and 1,10-phenanthroline. Ring centroids are shown as black spheres. Hydrogen atoms are removed for clarity.

For the doubly substituted complexes $[Fe\mathbf{L}^1(bpy)_2]^{2+}$ and $[Fe\mathbf{L}^1(phen)_2]^{2+}$ only two C_1 symmetric isomers are possible, both of which are shown in table 3.2. Although both isomers contain a single face-to-face π-stacking interaction between the phenyl ring and the adjacent ligand, there is a significant energy difference between them. In both cases the Δ enantiomer is found to be lower in energy, by 2.58 kcal mol^{-1} for the $[Fe\mathbf{L}^1(bpy)_2]^{2+}$ complex, and 2.51 kcal mol^{-1} for $[Fe\mathbf{L}^1(phen)_2]^{2+}$. The combination of low symmetry and the enantomeric selectivity of these disubstituted monometallic complexes makes them an ideal

partner to isomer Δ**a**[1] for the selective synthesis of C_1 symmetric bimetallic systems described above.

$[FeL^1(bpy)_2]^{2+}$		$[FeL^1(phen)_2]^{2+}$	
Isomer Δ**b**	Isomer Λ**b**	Isomer Δ**b**	Isomer Λ**b**
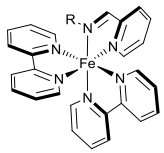	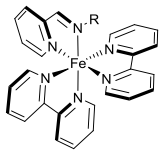	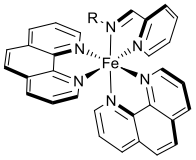	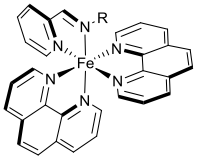
-1823806.51	-1823809.09	-1919524.38	-1919521.87
0.00	+2.58	0.00	+2.51

Table 3.2 The two potential isomers of $[Fe\mathbf{L}^1(bpy)_2]^{2+}$ and $[Fe\mathbf{L}^1(phen)_2]^{2+}$. Where R = $CH(Ph)CH_3$. All energies (relative and absolute), are reported in kcal mol^{-1}. Energies are reported relative to isomer Δb for the respectively substituted systems.

3.2.2 Formation of asymmetric monometallic complexes

As an experimental test of these computational predictions, the reaction between three equivalents of 2,2'-bipyridine and *fac*-Δ_{Fe},R_C-$[Fe\mathbf{L}^1{}_3][ClO_4]_2$ in dry d^3-acetonitrile was followed by ^{1}H NMR spectroscopy over a period of 73 h at 298 K. The initial spectrum shown in Figure 3.6 contains peaks which relate to only free 2,2'-bipyridine and *fac*-Δ_{Fe},R_C-$[Fe\mathbf{L}^1{}_3][ClO_4]_2$. The latter can easily be identified by the characteristic quartet at 5.3 ppm for the C*H* proton and by a singlet at 8.7 ppm associated with the imine proton for each of the three equivalent Schiff base ligands. As the reaction progresses these peaks decrease in intensity and peaks at 4.7 amd 8.44 ppm, corresponding to both the C*H* and imine protons in the unbound $\mathbf{L}^1$ ligand, begin to appear.

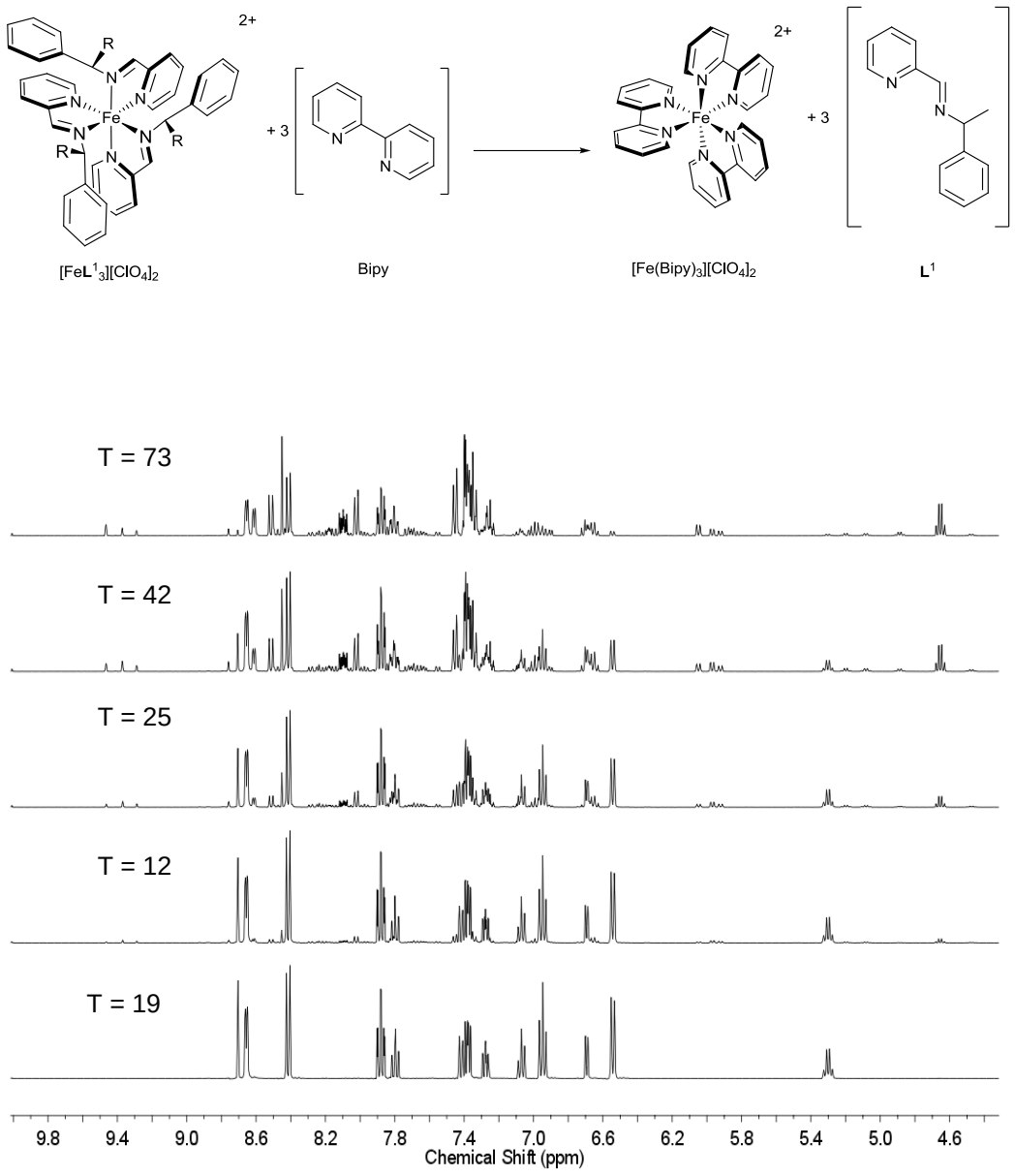

Figure 3.6 ^{1}H NMR spectra showing substitution of $\mathbf{L}^{1}$ with 2,2'-bipyridine in *fac*-Δ_{Fe},R_{C}-[Fe$\mathbf{L}^{1}_{3}$][ClO_4]$_2$ over a period of 73 h.

In addition, several new species can also be observed in the reaction mixture with new peaks appearing in the regions 9.5-8.7 ppm and 5.4 – 4.5 ppm. These can be identified as corresponding to the imine and C*H* protons of several 'mixed ligand' isomers *i.e.* compounds in which one or two of the initial $\mathbf{L}^{1}$ ligands have been substituted for 2,2'-bipyridine. Based on the computational results above, it is possible to assign these peaks to the mixed ligand isomers $\Delta\mathbf{a}^{1}$, $\Delta\mathbf{a}^{2}$ and $\Delta\mathbf{b}$.

Despite the large number of species, it is possible to assign the majority of the components in the reaction mixture at equilibrium as shown in Figure 3.7. Peaks for both *fac*-Δ_{Fe},R_C-[Fe$\mathbf{L}^1{}_3$][ClO_4]$_2$ (d), and free $\mathbf{L}^1$ (e) can easily be identified.

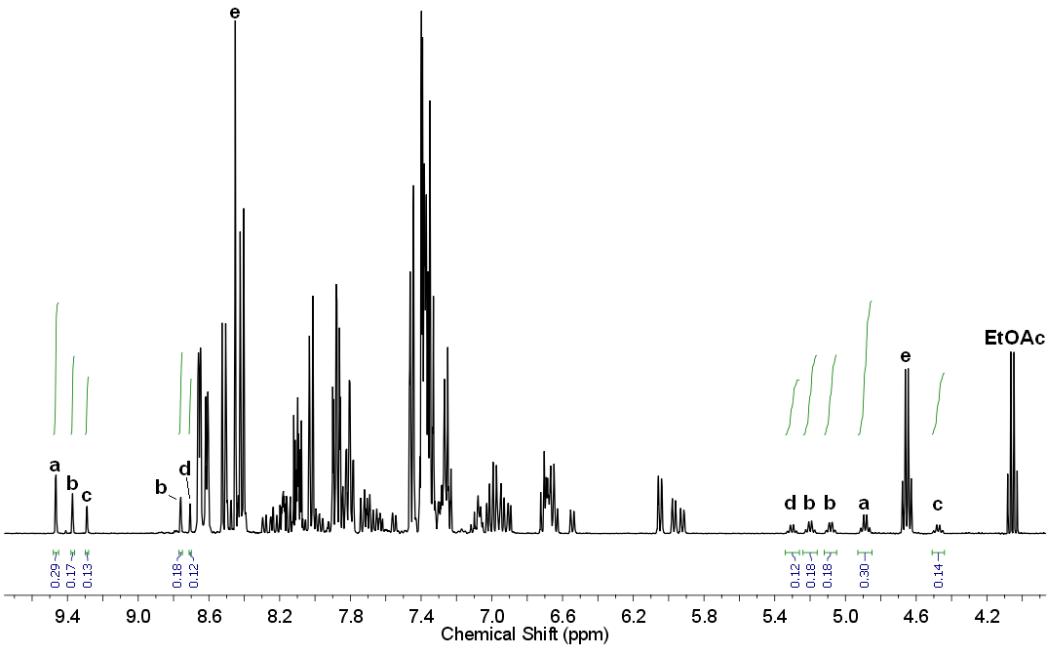

Figure 3.7 ^{1}H NMR spectra of reaction mix after 73 h showing the presence of multiple species with the chiral and imine protons assignments associated with each.

The two quartets associated with the inequivalent C*H* protons in C_1 symmetric compound $\mathbf{a}^1$ (b), are found at 5.1 and 5.2 ppm, along with the corresponding set of singlets for the inequivalent imine protons at 9.4 and 8.8 ppm. The quartet for the C*H* proton, and corresponding imine singlet for the C_2 symmetrically equivalent compound $\mathbf{a}^2$ (c), are identified at 4.2 and 9.3 ppm respectively. These two isomers are observed to be present in a ratio of approximately 2:1 $\Delta\mathbf{a}^1$:$\Delta\mathbf{a}^2$ ratio. The doubly substituted C_1 symmetric compound $\mathbf{b}^1$(a) can also be identified by its corresponding quartet at 4.9 ppm and its associated imine singlet at 9.5 ppm. While it is expected that the fully substituted [Fe(bpy)$_3$][ClO_4]$_2$ is

also present, the complex number of peaks in the region 7.2-8.6 ppm prevents its assignment.

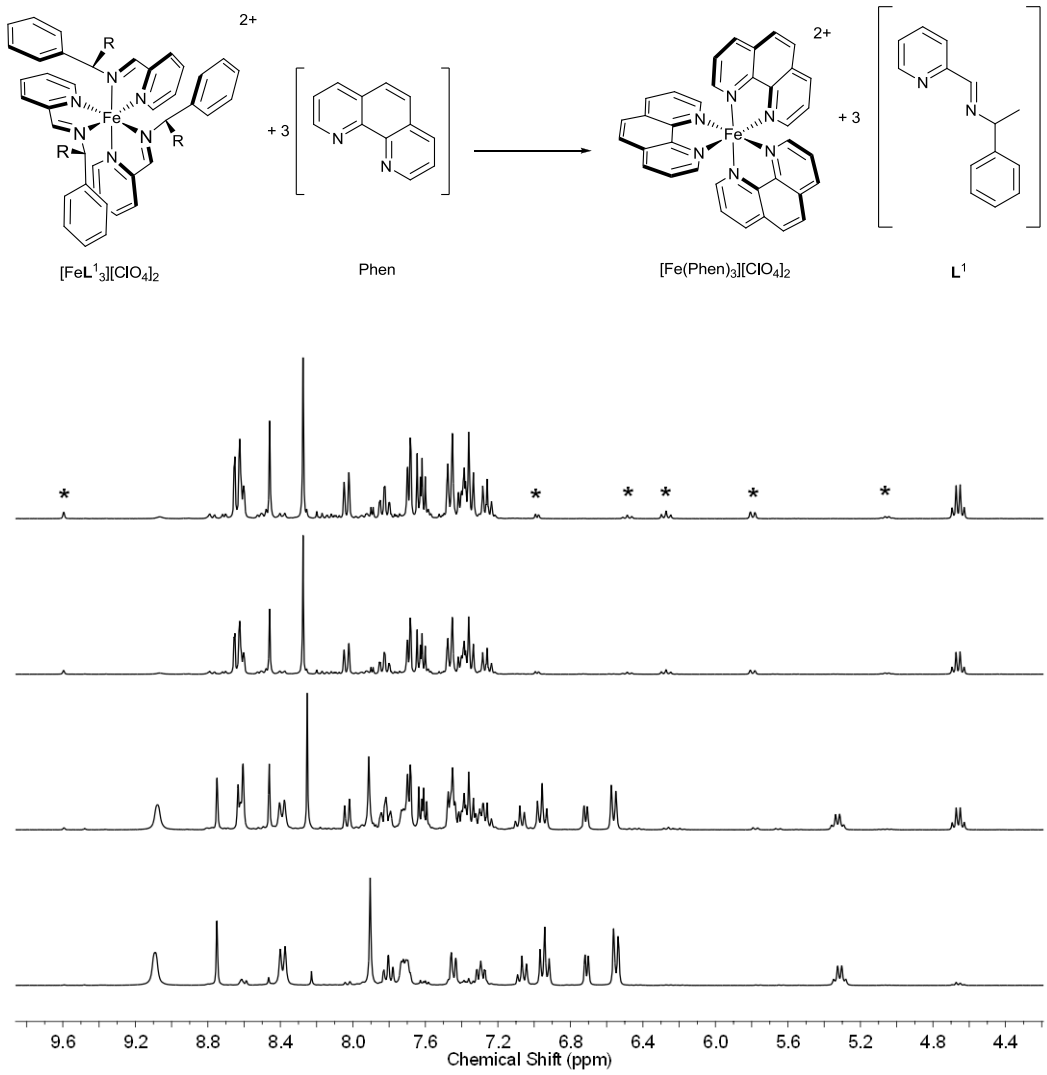

Figure 3.8 ^{1}H NMR spectra showing substitution of $\mathbf{L}^{1}$ with 1,10-phenanthroline in *fac*-Δ_{Fe},R_C-[Fe$\mathbf{L}^{1}_{3}$][ClO_4]$_2$ over a period of 24 hours.

The corresponding reaction between 1,10-phenanthroline and *fac*-Δ_{Fe},R_C-[Fe$\mathbf{L}^{1}_{3}$][ClO_4]$_2$ in dry d^3-acetonitrile was also followed by ^{1}H NMR spectroscopy. Characteristic peaks for the *fac*-Δ_{Fe},R_C-[Fe$\mathbf{L}^{1}_{3}$][ClO_4]$_2$ complex are again observed at 5.3 ppm (C*H)* and 8.7 ppm (imine), both of which decrease over the duration of the reaction. This decrease correlates directly with the

appearance of peaks at 4.65 and 8.45 ppm belonging to free ligand. Unlike the corresponding reaction with 2,2'-bipyridine, only a single mixed ligand species (* Figure 3.8) is observed in the ^{1}H NMR spectra at equilibrium. Due to the calculated energy difference between the $\Delta\mathbf{a}^1$ and $\Delta\mathbf{a}^2$ isomers, the presence of mono substituted $[Fe\mathbf{L}^1{}_2(phen)][ClO_4]_2$ complexes can be expected to result in three unique quartets in the region of 5.4 – 4.4 ppm, two for the C_1 symmetric $\Delta\mathbf{a}^1$ isomer and one for the C_2 symmetric $\Delta\mathbf{a}^2$ isomer. Conversely the doubly substituted C_1 symmetric $\Delta\mathbf{b}^1$ isomer is only expected to result in the single set of peaks in this region. Consequently, It is expected that the peaks observed belong to this isomer. This also suggests that the rate of a second addition of phen to $[Fe\mathbf{L}^1{}_3][ClO_4]_2$ is fast with respect to the first. Once again, the large number of peaks in the region 7.2-8.6 ppm prevents easy assignment of the $[Fe(phen)_3][ClO_4]_2$ complex.

3.2.4 Proposal for asymmetric ligands for the formation of bimetallic systems

Both of the previous studies highlight the synthetic viability of each of the computed mixed ligand monometallic systems. Although formation of the C_2 symmetric $\Delta\mathbf{a}^2$ isomer was observed, the *trans* placement of the imine groups would not be possible within a bimetallic system. As a consequence its presence when extending these systems to bimetallic complexes can be discounted. It is conceivable that if the two C_1 symmetric isomers were linked by a short bridge, the formation of the desired C_1 symmetric bimetallic systems would be possible. Therefore we proposed the following asymmetric ligands (Figure 3.9).

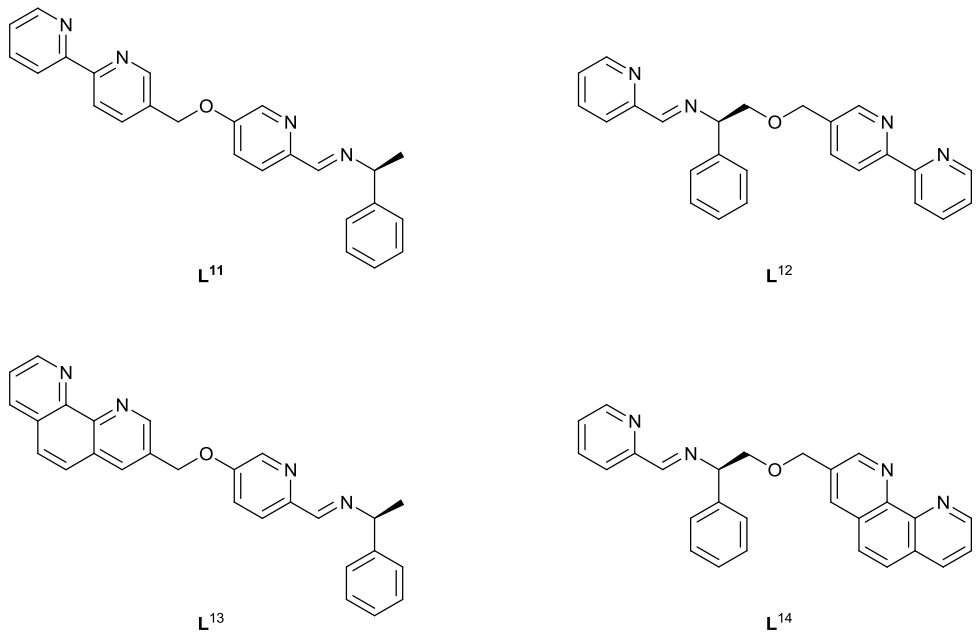

Figure 3.9 Proposed asymmetric ligands for the formation of asymmetrical bimetallic systems

Although the diasteroselction observed in each of the C_1 symmetric $\mathbf{a}^1$ and $\mathbf{b}^1$ isomers is expected to be preserved in the resulting bimetallic systems, the rigidity of the bridge may prove to be non-innocent in complex formations *i.e.* it may cause 'helication' or indeed 'mesocation'. As such, each of the possible isomers of $[Zn_2\mathbf{L}^n_3]^{+2}$ and $[Fe_2\mathbf{L}^n_3]^{+2}$ (where n = 11 or 12) were investigated by computational methods prior to synthesis. Each structure was first optimised using ligand field molecular mechanics (LFMM),[28] as implemented in the DommiMOE program,[29] before being simulated at 500 K for 1 ns to equilibrate, cooled to 0 K and re-optimised. Single point calculations were then performed at the B3LYP-D def2-TZVP level of theory on each of the resulting structures. The energies are shown in Table 3.3 and Table 3.4.

Isomer	Energy (Kcal mol^{-1})	$[Zn_2L^{11}{}_3]^{2+}$ Relative energy (Kcal mol^{-1})	Predicted isomer ratios at 298 K (%)
$\Delta_\alpha\Delta_\beta$**HHT**	-4606035.94	0.00	93.78
$\Delta_\alpha\Delta_\beta$**HHH**	-4606034.98	+0.95	6.18
$\Delta_\alpha\Lambda_\beta$**HHT**	-4606031.27	+4.66	0.04
$\Delta_\alpha\Lambda_\beta$**HHH**	-4606029.46	+6.48	0.00
$\Lambda_\alpha\Lambda_\beta$**HHT**	-4606027.87	+8.07	0.00
$\Lambda_\alpha\Lambda_\beta$**HHH**	-4606025.03	+10.91	0.00
$\Lambda_\alpha\Delta_\beta$**HHT**	-4606022.49	+13.44	0.00
$\Lambda_\alpha\Delta_\beta$**HHH**	-4606022.31	+13.63	0.00
Isomer	Energy (Kcal mol^{-1})	$[Fe_2L^{11}{}_3]^{2+}$ Relative energy (Kcal mol^{-1})	Predicted isomer ratios at 298 K (%)
$\Delta_\alpha\Delta_\beta$**HHT**	-3958862.28	0.00	97.42
$\Delta_\alpha\Delta_\beta$**HHH**	-3958860.78	+1.51	2.58
$\Delta_\alpha\Lambda_\beta$**HHH**	-3958854.67	+7.62	0.00
$\Delta_\alpha\Lambda_\beta$**HHT**	-3958853.46	+8.82	0.00
$\Lambda_\alpha\Lambda_\beta$**HHT**	-3958846.95	+15.33	0.00
$\Lambda_\alpha\Delta_\beta$**HHT**	-3958841.58	+20.70	0.00
$\Lambda_\alpha\Lambda_\beta$**HHH**	-3958841.32	+20.97	0.00
$\Lambda_\alpha\Delta_\beta$**HHH**	-3958836.19	+26.10	0.00

Table 3.3 Calculated energies for $[Zn_2\mathbf{L}^{11}{}_3]^{2+}$ and $[Fe_2\mathbf{L}^{11}{}_3]^{2+}$. An α subscript denotes a principally imine metal environment while β represents a principally bpy metal environment. Energies reported relative to isomer ΔαΔβ-HHT.

Isomer	Energy (Kcal mol^{-1})	$[Zn_2L^{12}{}_3]^{+2}$ Relative energy (Kcal mol^{-1})	Predicted isomer ratios at 298 K (%)
$\Delta_\alpha\Delta_\beta$**HHT**	-4606037.84	0.00	99.77
$\Delta_\alpha\Delta_\beta$**HHH**	-4606034.79	+3.05	0.19
$\Delta_\alpha\Lambda_\beta$**HHH**	-4606033.73	+4.11	0.03
$\Lambda_\alpha\Lambda_\beta$**HHT**	-4606027.46	+10.39	0.00
$\Delta_\alpha\Lambda_\beta$**HHT**	-4606023.91	+13.93	0.00
$\Lambda_\alpha\Lambda_\beta$**HHH**	-4606023.40	+14.45	0.00
$\Lambda_\alpha\Delta_\beta$**HHT**	-4606018.21	+19.64	0.00
$\Lambda_\alpha\Delta_\beta$**HHH**	-4606015.29	+22.55	0.00
Isomer	Energy (Kcal mol^{-1})	$[Fe_2L^{12}{}_3]^{+2}$ Relative energy (Kcal mol^{-1})	Predicted isomer ratios at 298 K (%)
$\Delta_\alpha\Delta_\beta$**HHT**	-3958865.98	0.00	99.05
$\Delta_\alpha\Delta_\beta$**HHH**	-3958863.49	+2.50	0.05
$\Delta_\alpha\Lambda_\beta$**HHH**	-3958853.44	+12.55	0.00
$\Delta_\alpha\Lambda_\beta$**HHT**	-3958848.35	+17.64	0.00
$\Lambda_\alpha\Lambda_\beta$**HHT**	-3958848.08	+17.90	0.00
$\Lambda_\alpha\Lambda_\beta$**HHH**	-3958842.43	+23.55	0.00
$\Lambda_\alpha\Delta_\beta$**HHT**	-3958839.54	+26.44	0.00
$\Lambda_\alpha\Delta_\beta$**HHH**	-3958834.33	+31.65	0.00

Table 3.4 Calculated energies for $[Zn_2\mathbf{L}^{12}{}_3]^{2+}$ and $[Fe_2\mathbf{L}^{12}{}_3]^{2+}$. An α subscript denotes a principally imine metal environment while β represents a principally bpy metal environment. Energies reported relative to isomer ΔαΔβ-HHT.

The diastereoselection observed for the C_1 symmetric monometallic $\mathbf{a}^{\mathbf{1}}$ and $\mathbf{b}^{\mathbf{1}}$ units above is retained in both the $\mathbf{L}^{11}$ and $\mathbf{L}^{12}$ systems leading to an overall thermodynamic preference for the Δ isomers. This energetic preference is likely to be have been further enhanced by the use of the short $–CH_2–O–$ bridge favouring the formation of helical systems. In all four systems the, $\Delta_\alpha\Delta_\beta$ isomers are found to be the most stable isomers. Of these, two isomers, the desired C_1 symmetric bimetallic $\Delta_\alpha\Delta_\beta$HHT isomer was found to be the lowest in energy, most notably for the $\mathbf{L}^{12}$ complexes where the $\Delta_\alpha\Delta_\beta$HHH is found to be 2.50 Kcal mol^{-1} and 3.05 Kcal mol^{-1} higher in energy for the respective $[Fe_2\mathbf{L}^{12}{}_3]^{+2}$ and $[Zn_2\mathbf{L}^{12}{}_3]^{+2}$ complexes. In comparison, the difference between the $\Delta_\alpha\Delta_\beta$HHT and $\Delta_\alpha\Delta_\beta$HHH was found to be only 0.95 Kcal mol^{-1} and 1.51 Kcal mol^{-1} for the $[Zn_2\mathbf{L}^{11}{}_3]^{+2}$ and $[Fe_2\mathbf{L}^{11}{}_3]$ systems respectively. Furthermore, by virtue of the number of possible combinations, the expected statistical ratio HHT:HHH of 3:1 also favours the asymmetric helicate. As such, if both thermodynamic and entropic considerations are accounted for, the predicted isomer ratios at 298K strongly favours the desired asymmetric $\Delta_\alpha\Delta_\beta$HHT isomer in all cases. Ultimately, these calculations appear to validate our proposed strategy to synthesise C_1 symmetric helices as outlined in Section 3.21.

We were interested to see if the thermodynamic preference for the HHT isomers arises from the differing π-stacking interactions in the two configurations, given that π-stacking interactions are at the heart of the mechanism of diasteroselectivity in $[Fe\mathbf{L}^{1}{}_3]^{2+}$ *tris* chelate systems.[11, 17, 18] While the HHH isomers contain exclusively pyridine/phenyl type π-stacking interactions, the HHT isomers contain a single pyridine/phenyl interaction and two bpy/phenyl interactions. In order to investigate this interaction in the absence

of any other competing factors, such as helication, model systems were studied by computational methods. In these systems a toluene molecule was used to represent the phenyl group, and either pyridin-2-ylmethanimine (Type 1) or 2,2'-bipyridine (Type 2) was chosen to represent the other component of the π-stacking interaction. Each of these components was optimised at the B3LYP-D def2-TZVP level of theory, prior to the model systems being constructed using the geometrical parameters shown in Figure 3.10.

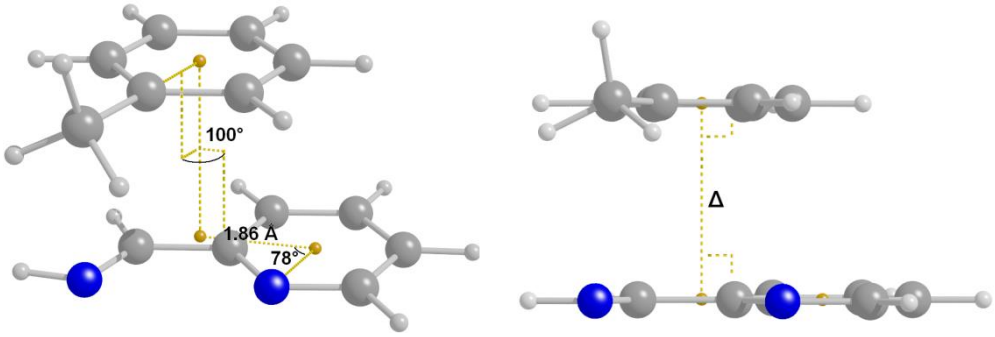

Figure 3.10 Geometrical parameters as used in toluene/pyridin-2-ylmethanimine and toluene/bpy dimers.

The toluene unit was then the displaced along the z-axis, from 3-7 Å in increments of 0.1 Å. Single point energy calculations were performed using the B3LYP-D def2-TZVP level of theory at each displacement. The resulting data (Figure 3.12), was then fitted using a Morse potential function shown in Equation 3.1.

$$V_{(r)} = D_e\left(1 - e^{-A(r-Re)}\right)^2 \qquad \textbf{Equation 3.1}$$

This allows both the effective binding energies of these systems (D_e) and the optimum separation of two components (R_e) to be calculated. In both systems the observed optimum separation for the aromatic groups was found to be

approximately 3.4 Å which is consistent with literate values for other π-stacking systems.[16] In contrast there is a considerable difference in the binding energy of the two systems, with the bpy/toluene system observed to be 1.2 kcal mol^{-1} more stable than the pyridine/toluene system. This is consistent with observations made by S. Grimme who has also noted that the magnitude of the π-stacking interaction in parallel-offset arrangement increases with the number of arenes involved.[19]

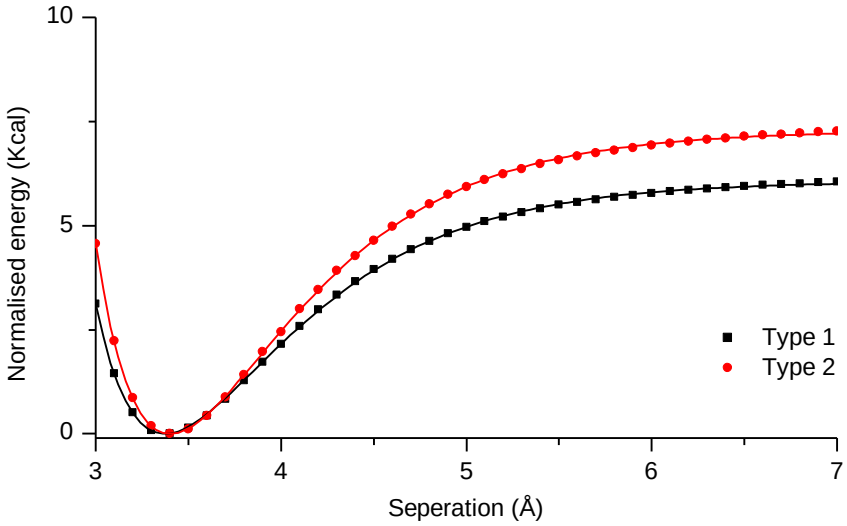

	Type 1	Type 2
A	1.44804	1.45549
D_e	6.06737	7.28608
R_e	3.37386	3.40109
χ^2	4.95485×10^{-4}	6.9444×10^{-4}
Adj. R-squared	0.99988	0.99989

Figure 3.11 Relative energy plots and fitting vales for each model π-stacking interaction.

In the C_3 symmetric HHH isomers three pyridine/toluene type interactions exist which, based on this study, are expected to stabilise these isomers by 18.2 kcal mol^{-1}. Conversely, by adopting the anti-parallel HHT arrangement of ligands, two bpy/toluene type π-staking interactions occur alongside a single

pyridine/toluene interaction contributing a total of 20.6 kcal mol^{-1} to the stability of the HHT isomers. As such, in the absence of other steric effects, this difference in π-stacking interactions results in the HHT isomers being *ca* 2.4 kcal mol^{-1} more stable than the equivalent HHH isomers. This value is in good agreement with that observed energy difference, of 2.5 kcal mol^{-1}, between the lowest two isomers, $\Delta_\alpha\Delta_\beta$HHT and $\Delta_\alpha\Delta_\beta$HHH, in the theoretical calculations for the $[Fe_2\mathbf{L}^3{}_3]$ series, although this close correspondence may arise from conflation of a number of factors.

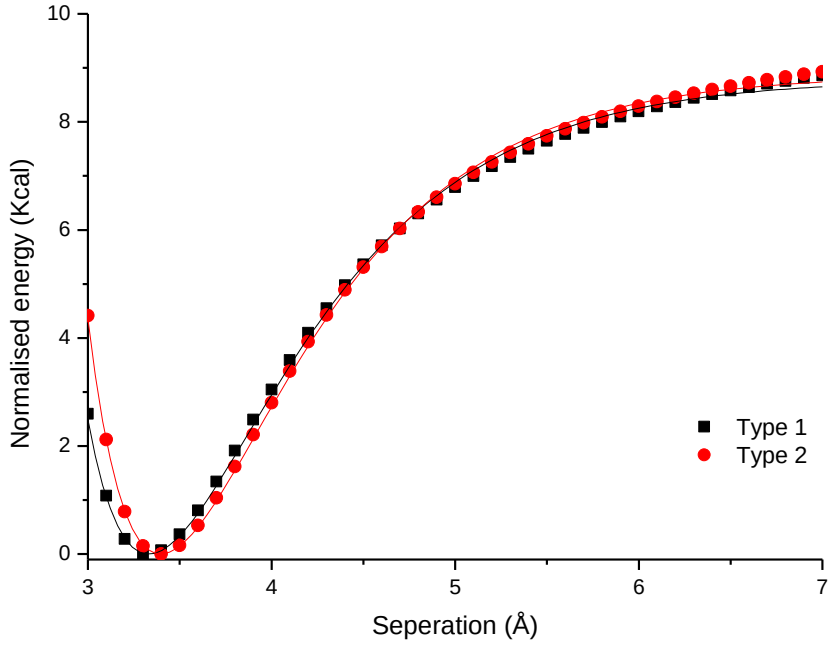

	Type 1	Type 2
A	1.29072	1.33771
$\boldsymbol{D_e}$	8.80524	8.88074
$\boldsymbol{R_e}$	3.33073	3.39680
χ^2	0.00888	0.0067
Adj. R-squared	0.99902	0.99926

Figure 3.12 Relative energy plots and fitting vales for each model lithium coordinated π-stacking interaction.

We were therefore interested in investigating how these π-stacking interactions changed on coordination of a metal. Consequently, both the pyridin-2-ylmethanimine and 2,2'-bipyridine components were coordinated to a lithium cation, optimised, and single point calculations were again conducted over a range of separations (3-7 Å) in 0.1 Å increments. The resulting data shown in Figure 3.12 was again fitted with a Morse potential function. Unlike the uncoordinated systems both of the model systems showed near identical binding energies (8.80 and 8.88 kcal mol^{-1}). These recorded binding energies are $\geq$ 1.6 kcal mol^{-1} greater than those observed for the un-coordinated model systems. This strongly suggests that metal coordination is likely to play a dominant role in the nature of these inter ligand π-stacking interactions.

Based on these calculations both the proposed $\mathbf{L}^2$ and $\mathbf{L}^3$ ligands appear suitable for the selective formation of C_1 symmetric bimetallic systems. However due to the marginal thermodynamic preference for the desired $\Delta_\alpha\Delta_\beta$HHT isomer shown for the $\mathbf{L}^3$ systems its synthesis was chosen over that of $\mathbf{L}^2$. The $\mathbf{L}^2$ systems have however been further investigated by a colleague and as such will not be further discussed here.

3.2.3 Synthesis of the asymmetrical ligand $\mathbf{L}^3$

2-Acetylpyridine was heated at 130˚C in the presence of iodine and pyridine to give the 1-(2-pyridylacetyl)pyridinium iodide salt. This was then treated with ammonium acetate and freshly distilled methacrolein in formamide, so as to afford 5-methyl-2,2'-bipyridine as a yellow oil in good yield after distillation under reduced pressure. Halogenation through radical bromination was initially

attempted using 1.1 eq. of *N*-bromosuccinimide and AIBN as a radical source in dry carbon tetrachloride under thermal conditions, but the resulting product was observed to contain up to 10% of the dibrominated species.[20-22] While a small amount of pure 5-bromomethyl-2,2'-bipridine could be obtained through repeated recrystallisation from hot hexane, this led to a dramatic reduction in yield.

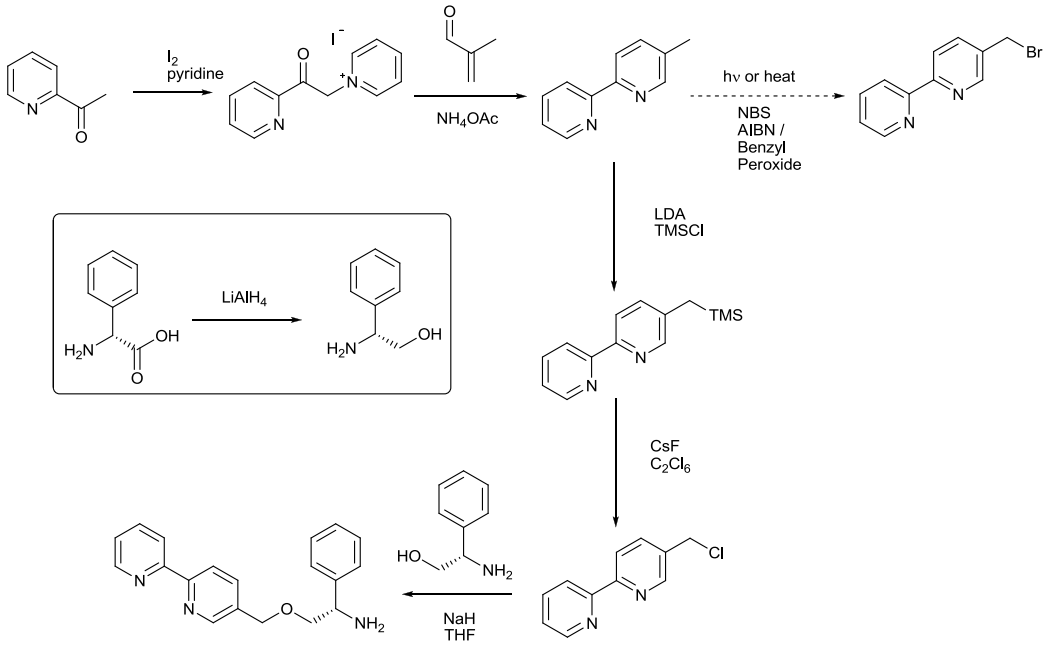

Scheme 3.1 The synthesis of (R)-2-(2,2'-bipyridine-5-ylmethoxy)-1-phenylethanamine.

Attempts to purify the product though silica gel chromatography were hampered by poor separation under a range of solvent conditions, while distillation of the crude product under reduced pressure resulted in decomposition. Consequently an alternative approach was investigated. A recent paper by Dallaire and co workers[22, 23] highlights an alternative method for the halogenation of biphenyl compounds; here, deprotonation of the 5-methyl-2,2'-bipyrdine with LDA at -78 ˚C, followed by the addition of 1.05 equivalents of trimethylsilyl chloride gave the product in good yield (>60%). This was converted to 5-chloromethyl-2,2'-bipyridene on reaction with caesium fluoride and hexachloroethane in dry

MeCN. The direct deprotonation of one equivalent of *R*-phenylglyciniol with NaH, followed by the addition of 0.9 equivalents of 5-chloromethyl-2,2'-bipyridene in THF resulted in the formation of the optically pure amine as a yellow solid in good yield (Scheme 3.1).

3.2.4 Self-assembly and analysis

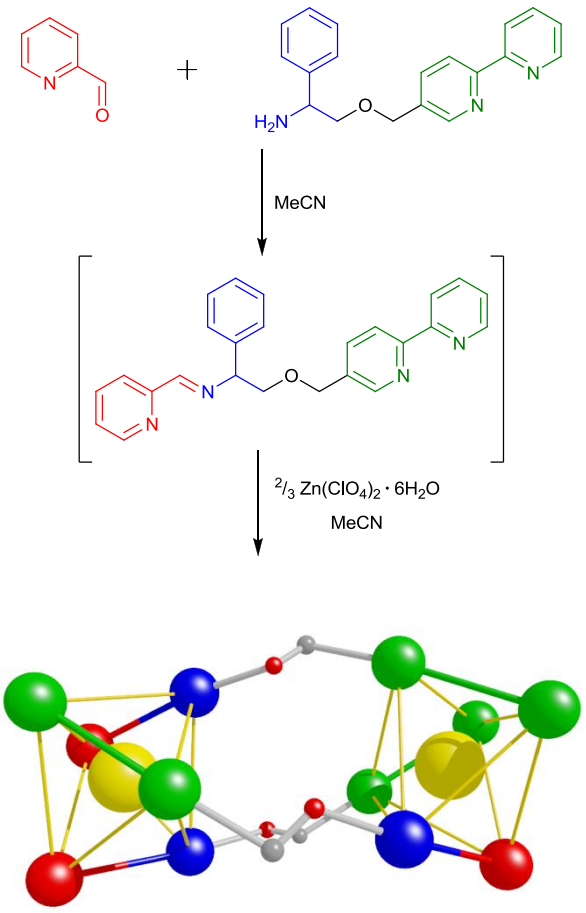

Scheme 3.2 Synthesis of R_c,Δ_{Zn},HHT-$[Zn_2\mathbf{L}^{12}{}_3][ClO_4]_4$.

The use of three equivalents of (*R*)-2-(2,2'-bipyridin-5-ylmethoxy)-1-phenylethanamine in a one-pot synthesis with three equivalents of 2-pyridinecarboxaldehyde and two equivalents of $Zn(ClO_4)_2{\cdot}6H_2O$ led to the

formation of the asymmetric complex R_c,Δ_{Zn},HHT-[$Zn_2\mathbf{L}^{12}{}_3$][ClO_4]$_4$ (Scheme 3.2). ^{1}H NMR spectra of this complex (Figure 3.13), indicate the presence of three unique ligand environments. Despite the relative complexity of the spectra it is possible to easily identify the three separate imine signals (a) in the region 9.31-8.91 ppm. The benzylic CH protons (f) for each ligand are found at 5.52, 5.01 and 4.89 ppm along with the corresponding adjacent diasterotopic CH_2 groups (h) at 4.37-4.12 ppm and 3.66-3.48 ppm. While the inequivalent OCH_2 groups (g) are also seen in the region 5.24-5.17 ppm and 4.58-4.50 ppm as a series of overlapping doublets. Finally, peaks in the region of 6.65-5.85 ppm can be identified as aromatic protons belonging to the phenyl groups that are experiencing a strong through-space shielding from the 2,2'-bypyridine of an adjacent ligand.

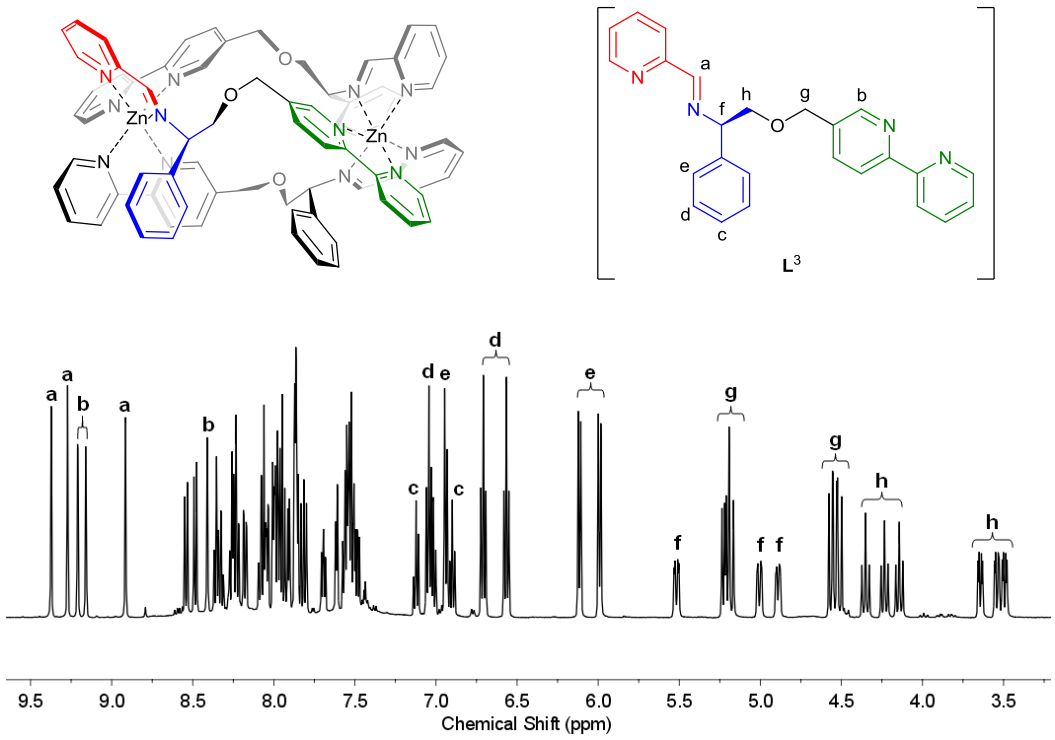

Figure 3.13 ^{1}H NMR spectrum and assignment of ligand peaks for $\Delta_\alpha\Delta_\beta$HHT-[$Zn_2\mathbf{L}_3{}^3$][$ClO_4$]$_4$

The complex R_c,Δ_{Zn},HHT-$[Zn_2\mathbf{L}^{12}{}_3][ClO_4]_4$ gave excellent electrospray mass spectrometry data, with a strong peak at m/z 328.6 Da for the $[Zn_2\mathbf{L}^{12}{}_3]^{4+}$ species (Figure 3.14). The isotope peaks observed for this molecular ion are separated by 0.25 Da, confirming the tetracationic charge. It is therefore possible to rule out the presence of larger (8+) structures comprising four zinc(II) centres arranged in a tetrahedral fashion linked by six ligands. Such supramolecular tetrahedral (*T*) structures have been observed previously in related systems by Raymond [24] and Nitschke,[25-28] the latter using our own method for steroselection.

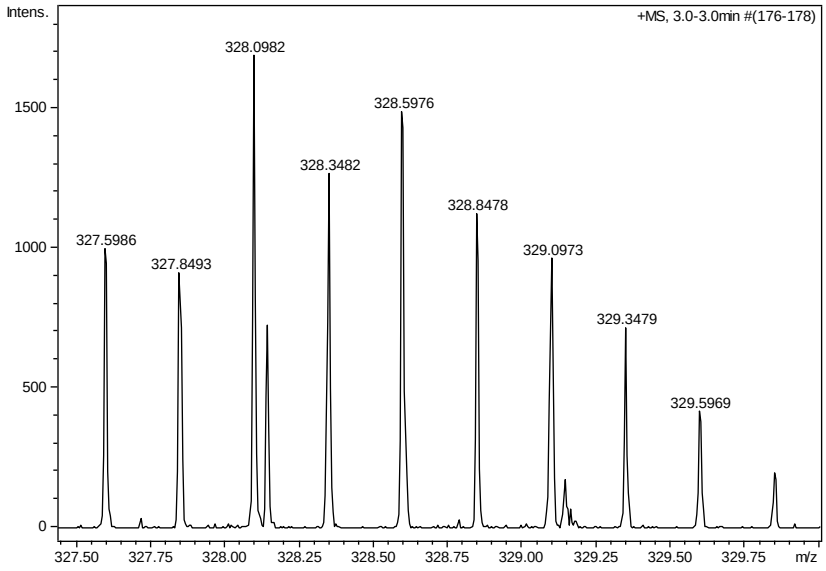

Figure 3.14 Esi mass spectra of R_c,Δ_{Zn},HHT-$[Zn_2\mathbf{L}^{12}{}_3][ClO_4]_4$.

3.2.5 Single Crystal XRD studies of $\Delta_\alpha\Delta_\beta$HHT-$[Zn_2L^3{}_3][ClO_4]_4$

Single needle like crystals of R_c,Δ_{Zn},HHT-$[Zn_2\mathbf{L}^{12}{}_3][ClO_4]_4$ were obtained *via* slow vapour diffusion of ethyl acetate into acetonitrile solutions, and proved to be suitable for X-ray diffraction studies. The complex crystallises in the monoclinic space group C_2 with the asymmetric unit containing the complex, ethyl acetate, two fully occupied and one half occupied acetonitrile, and three

fully occupied and two half occupied perchlorate counter ions. Some additional electron density was modelled as a water molecule disordered over three very closely related positions (too close to be bonded), and each position was refined isotropically at $^1/_3$ occupancy, although no hydrogen atoms were located for the disordered water.

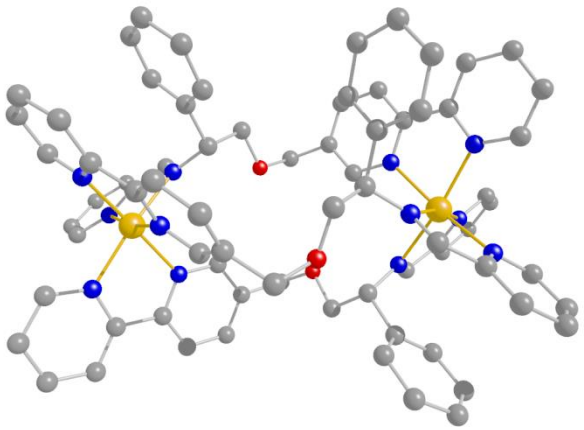

Figure 3.15 Structure of the cationic unit in R_c,Δ_{Zn},HHT-$[Zn_2\mathbf{L}^{12}{}_3][ClO_4]_4$. H atoms and solvent molecules have been removed for clarity.

Both of the zinc(II) metal centres are found in the Δ configuration and each metal centre is approximately octahedral with a mean Zn–N bond length of 2.16 Å, which is comparable to the observed average in the structurally similar complex $[Zn(bpy)_3][ClO_4]_2$ (2.16 Å).[29] As indicated by the solution state data, the configuration of the ligands around the metals is asymmetric as two ligands are orientated in one direction while the third ligand is observed to be in an anti-parallel orientation. This asymmetric configuration of ligands leads to differential ligation of the metal centres, with one end containing two face-to-face π-stacking interactions, one between the a benzyl groups and the pyridine of the adjacent ligand, and the second similar interaction between the remaining benzyl group and the 2,2'-bipyridine component of the reversed ligand. The other end of the

complex by comparison, contains only a single face-to-face π-stacking interaction between the benzlic group and one of the two 2,2'-bipyridine. This is configuration of ligands about the two metals is consistent with that predicted by the computational studies above, with each end of the molecule being composed of either the Δ**a**^{1} and Δ**b**^{1} mixed ligand monometallic isomer, while the overall structure is indistinguishable from that of the predicted $\Delta_\alpha\Delta_\beta$-HHT isomer. We have previously considered that the centroid–centroid distance between rings gives the readiest assessment of π-stacking interactions since all the other distances and angles have an impact on it.[30] For R_c,Δ_{Fe},HHT-[Fe_2**L**$^{12}{}_3$][ClO_4]$_4$ it was observed that the single centroid–centroid distance between the benzyl group and the pyridine ring was 3.63 Å, which is consistent with the calculated structure (3.48 Å) and falls within the region reported previously for an identical type interaction found within the *tris*-chelate [Zn**L**$^1{}_3$]$^{2+}$ complexes[30] described in Chapter 2. The remaining two interactions between benzylic group and the 2,2'-bipyridine are however not as easy to quantify as two centroid–centroid distance are between the benzylic group and either of the two constituent pyridine rings are possible. The shorter of the two distances is in the region of 3.62-3.67 Å and is found between the benzylic ring and the terminal pyridine with the second interaction between the benzylic ring and the remaining pyridine unit was observed to be between 4.64-4.36 Å. Once again these values agree strongly with the calculated structures, where they were observed to be in the regions of 3.60-3.72 Å and 4.09-4.19 Å respectively. The average distance between the planes of the two rings was observed to be 3.41 Å and correlates well with the predicted structure (3.24 Å) and previously computed values for π-stacking arenes of 3.5

Å.[19] In addition the mean angle between planes is observed to be 6.7˚ which again agrees with the computationally predicted mean of 4.8˚.

3.2.6 Incorporation of functionality into asymmetric complexes.

For most conceivable applications of *triplexes*, such as their use as biological agents, the ability to precisely incorporate functional groups into the systems is highly desirable. This can be readily achieved through the substitution of the pyridine carboxaldehyde component of the ligand with either pyrazine-2-carbaldehyde or 5-hydroxypyridine. Pyrazine-2-carbaldehyde (Scheme 3.3) was readily synthesised from of 2-pyrazinecarboxylic acid in a two-step process in good yields (>70%).[31]

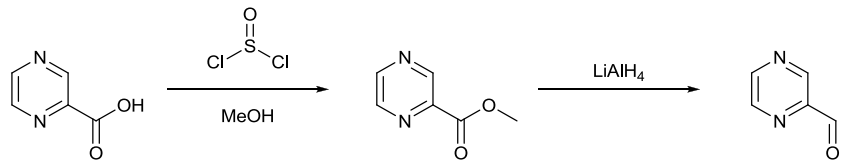

Scheme 3.3 synthesis of pyrazine-2-carbaldehyde**.**

The reaction between three equivalents of (S)-2-(2,2'-bipyridin-5-ylmethoxy)-1-phenylethanamine with three equivalents of pyrazine-2-carbaldehyde and two equivalents of $Zn(ClO_4)_2 \cdot 6H_2O$ in the standard one pot synthesis again results in the formation of R_c,Δ_{Zn},HHT-$[Zn_2\mathbf{L}^{15}{}_3][ClO_4]_4$ as an off white solid after precipitation with ethyl acetate.

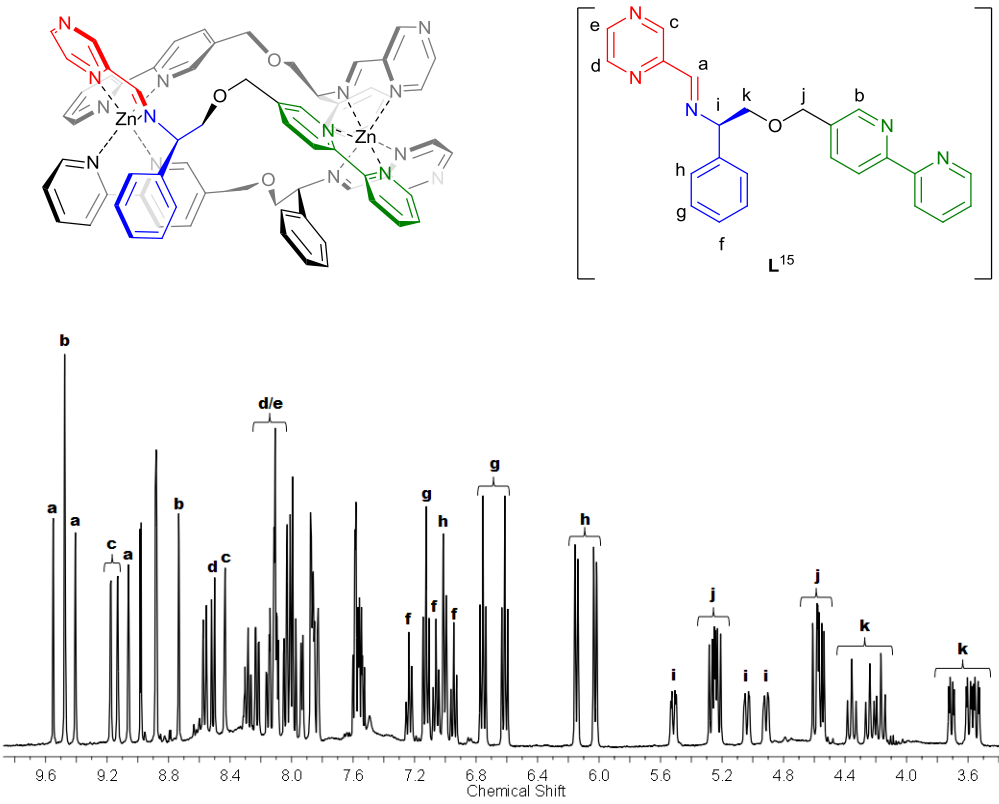

Figure 3.16 ^{1}H NMR spectra and assignment of ligand peaks for R_c,Δ_{Zn},HHT-[Zn_2**L**$^{15}_3$][ClO_4]$_4$.

Once again ^{1}H NMR spectroscopy indicates that each of the three ligands are inequivalent with three set of peaks being observed for both the benzylic C*H* (f) and the diasterotopic CH_2 (h) (Figure 3.16). There is also a noticeable up field shift of the benzylic protons (d and e) due to an increased shielding effect resulting from the π-stacking interaction between the benzyl groups and the 2,2'-bipyridine components for the adjacent ligands. Mass spectroscopy and micro analysis are also consistent with the formation of the desired *triplex* structure. Alternatively pyridine carboxaldehyde can be substituted for 5-hydroxypyridine aldehyde which can be further functionalised through a Williamson ether synthesis with a range of halides and thus provides easy access to ligand **L**^{16} – **L**^{18} (Figure 3.17). Complexation with a zinc perchlorate afforded the desired

functionalised *triplex* structures after precipitation with ethyl acetate as white solids.

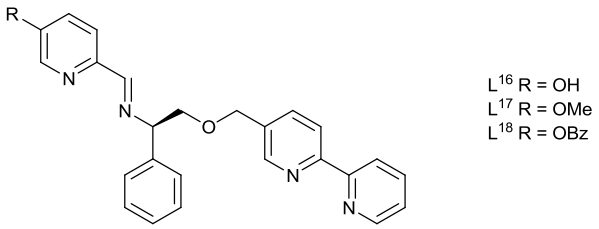

Figure 3.17 Ligands $\mathbf{L}^{16}$– $\mathbf{L}^{18}$ formed in situ via condensation with the appropriate chiral amine.

In all cases, each of the functionalised complexes was characterised by NMR spectroscopy, mass spectrometry, and micro analysis. In the case of R_c,Δ_{Zn},HHT-$[Zn_2L^{16}{}_3][ClO_4]_4$ Single needle like crystals were obtained via slow vapour diffusion of ethyl acetate into a solution of acetonitrile and menthol that were suitable for X-ray diffraction studies.

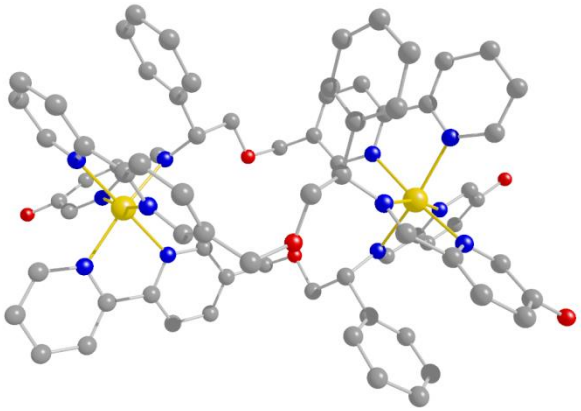

Figure 3.18 Structure of the cationic unit in R_c,Δ_{Zn},HHT-$[Zn_2\mathbf{L}^{16}{}_3][ClO_4]_4$. All solvents, hydrogen atoms and counter ions are removed for clarity.

The complex was found to crystallise in the C_2 space group with the asymmetric unit containing the triplex structure, four perchlorate counter ions one of which modelled at half occupancy. A molecule of ethyl acetate, a half occupied

acetonitrile and two half occupied methanol molecules were also present although no hydrogen atoms could be located for the methanol molecules. The structure can be considered analogous to the one found for the asymmetric parent compound R_c,Δ_{Zn},HHT-$[Zn_2L^{16}_3][ClO_4]_4$.

3.2.7 Functionalisation post complexation though 'Click' chemistry

As outlined previously in Chapter 2, the inclusion of 5-(propargyl)picolinaldehyde in the ligand structure provides an interesting route to further functionalistion post complexation through the means of copper(I)-catalysed Huisgen 1,3-dipolar cycloaddition (CuAAC) 'click' chemistry. We were interested to see if *triplex* systems were suitably stable to undergo such reactions as, in particular the asymmetrical HHT arrangement, precludes formation of three concurrent triazole rings preventing the coordinating copper during the reaction. Using 5-(propargyl)picolinaldehyde in the standard one-pot synthesis method already described afforded the desired alkynyl functionalised *Triplex* structure after precipitation with ethyl acetate as a white solid. ^{1}H NMR spectroscopy (Figure 3.19) shows three sets of ligand peaks consistent with triplex formation, with three singlets (**j**) observed in the region 2.5-3.0 ppm being reliably assignable to the three inequivalent alkynes.

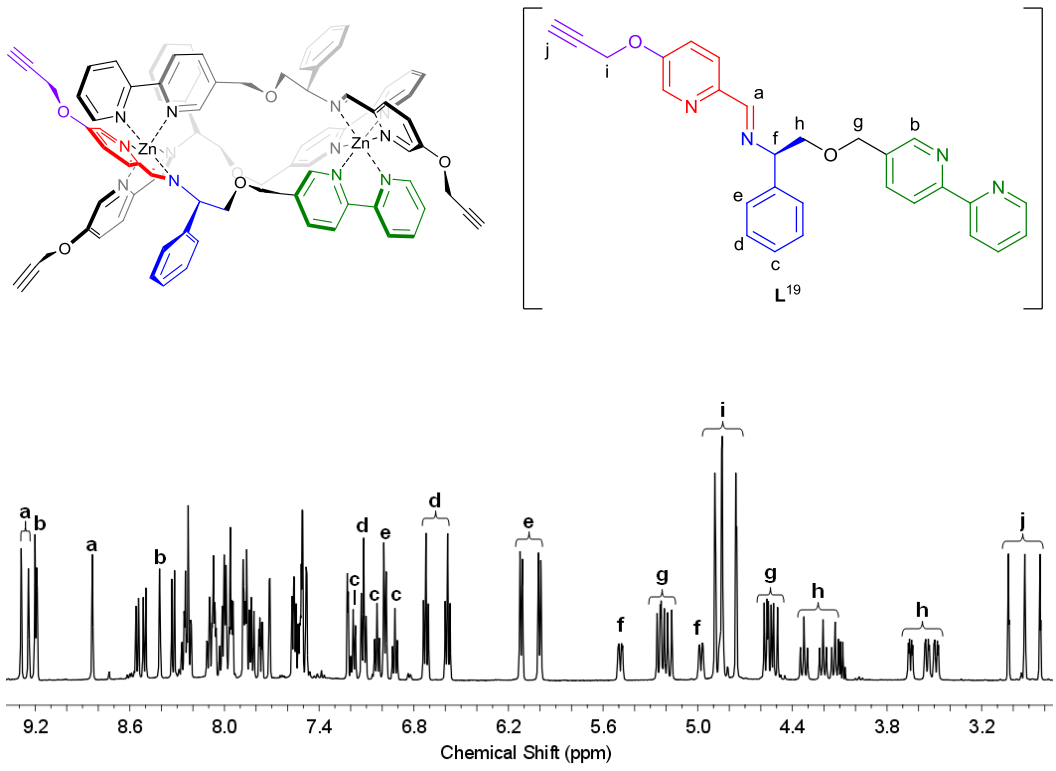

Figure 3.19 ^{1}H NMR spectrum of R_c,Δ_{Zn},HHT-[Zn_2**L**$^{19}_3$][ClO_4]$_4$.

The synthesis of a suitable azide, 4-fluorobenzylazide was achieved through the reaction of sodium azide and 4-fluorobenzyl bromide in DMSO in good yields (>70%)(Scheme 3.4)

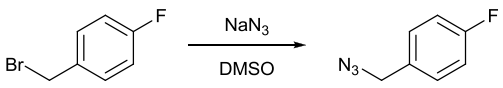

Scheme 3.4 Synthesis of 4-fluorobenzylazide.

The reaction between three equivalents of this azide and R_c,Δ_{Zn},HHT-[Zn_2**L**$^{19}_3$][ClO_4]$_4$ was conducted in the presence of three equivalents of copper(I) and triethylamine in dry acetonitrile. The resulting suspension was filtered through celite and desired product could be isolated as a pale yellow solid on precipitation with ethyl acetate.

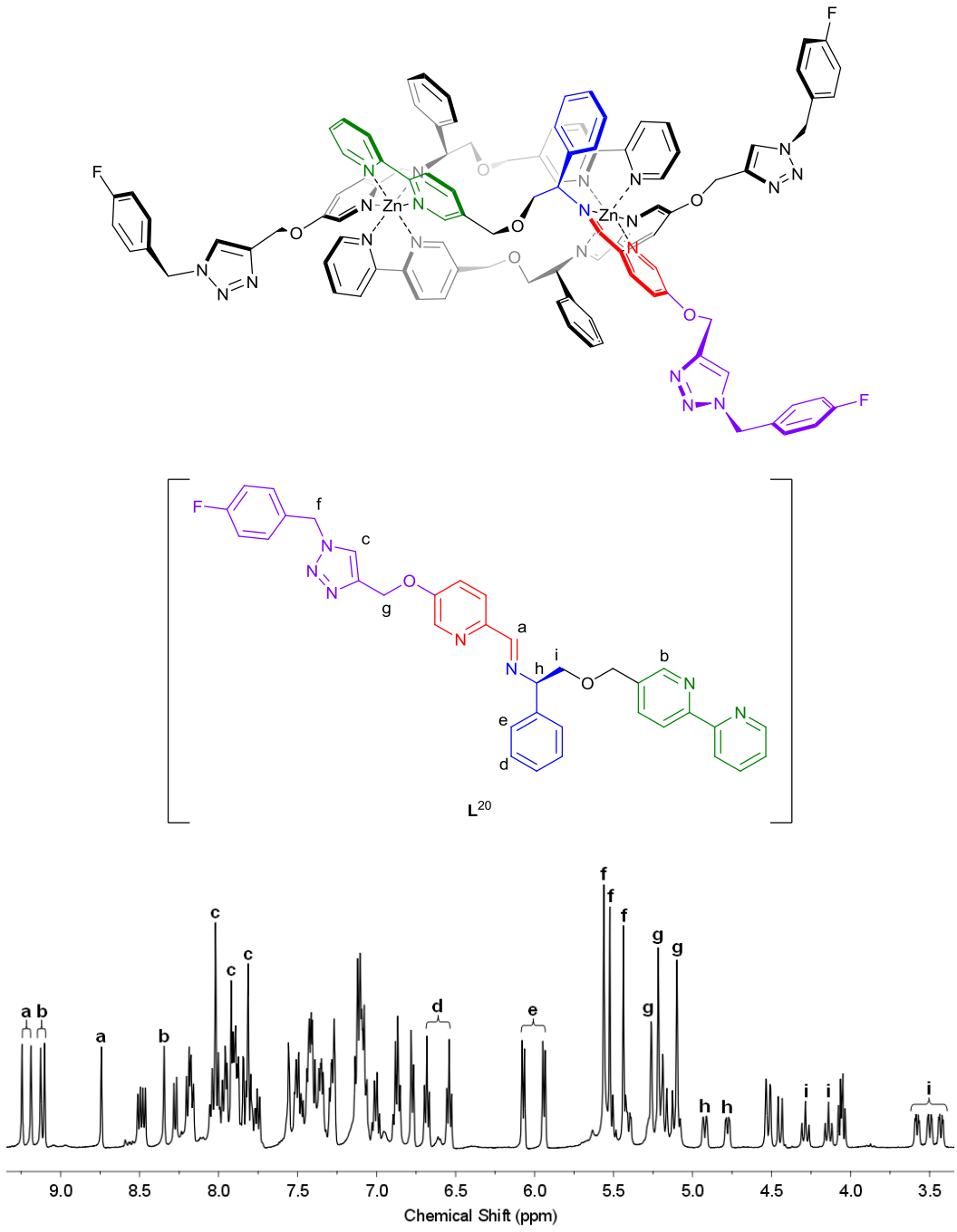

Figure 3.20 ^{1}H NMR spectrum of R_c,Δ_{Zn},HHT-[Zn_2**L**$^{20}{}_3$][ClO_4]$_4$.

The resulting ^{1}H NMR R_c,Δ_{Zn},HHT-[Zn_2**L**$^{20}{}_3$][ClO_4]$_4$ (Figure 3.20), also shows three sets of peaks corresponding to each of the in equivalent ligands making up the core triplex structure. The three characteristic singlets between 2.5-3.0 ppm belonging to the alkyne group (**j**, Figure 3.19) are no longer observable, however three singlets are now observable at 8.02, 7.92 and 7.81 ppm (**c,** Figure 3.20)

These can be assigned to triazole protons in three separate ligand environments. This suggests that complete conversion of R_c,Δ_{Zn},HHT-[$Zn_2\mathbf{L}^{\mathbf{19}}{}_3$][$ClO_4$]$_4$ to the desired R_c,Δ_{Zn},HHT-[$Zn_2\mathbf{L}^{\mathbf{20}}{}_3$][$ClO_4$]$_4$ species has occurred. Due to the incorporation of fluorine from 4-fluorobenzyl azide, it becomes possible to investigate the complex through ^{19}F NMR spectroscopy. The ^{19}F{H} NMR spectra (**a**, Figure 3.21) shows two signals with a ratio of 1:2 which is consistent with the asymmetric incorporation of the azide at the ends of the *Triplex* structure. Furthermore the complex R_c,Δ_{Zn},HHT-[$Zn_2\mathbf{L}^{\mathbf{20}}{}_3$][$ClO_4$]$_4$ also gave electrospray mass spectrometry data consistent with [$Zn_2\mathbf{L}^{20}{}_3$]$^+$ species (**b**, Figure 3.23). Microanalytical data however indicates the presence of Cu(I) iodide in a 1:1 ratio with the complex. Similar observations have been made previously following CuAAC 'click' reactions on preformed complexes as outlined in Chapter 2.

(**a**) (**b**)

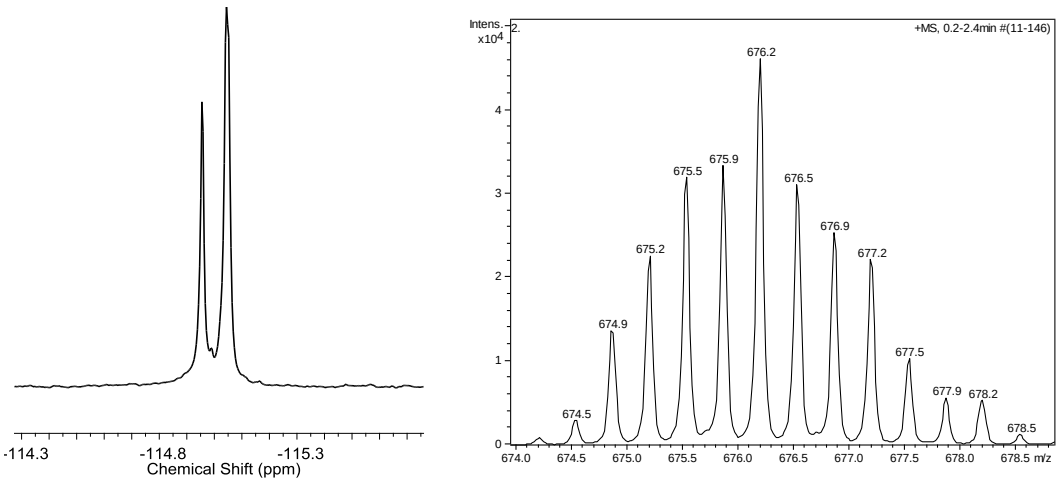

Figure 3.21 (**a**) ^{19}F{H} NMR spectrum of R_c,Δ_{Zn},HHT-[$Zn_2\mathbf{L}^{\mathbf{20}}{}_3$][$ClO_4$]$_4$ showing two separate fluorine environments. (**b**) ESI mass spectra of R_c,Δ_{Zn},HHT-[$Zn_2\mathbf{L}^{\mathbf{16}}{}_3$][$ClO_4$]$_4$.

3.3 Conclusion

A strategy for the selective formation of asymmetric HHT triple stranded helices has been successfully established though molecular modelling and experimental studies. Ultimately the maximisation of secondary π-stacking interactions between ligands while reducing unfavourable steric clashes is crucial to the selectivity of these compounds, however the role played by ligand helication in these complexes cannot be ruled out as a further factor in their formation.

Ligands comprising both a pyridyl imine and 2,2'-bipyridine components were synthesised and their resulting self-assembly on coordination with Zn(II) was investigated. This resulted in the highly selective asymmetric formation of triple stranded bimetallic complexes in the solution state. Single crystal XRD shows that one of the ligands orientates itself to lie anti-parallel to the other two, consistent with the computed asymmetric structure.

These asymmetric triplex systems can be functionalised readily by substituting the pyridine carboxaldehyde component of the ligand with either pyrazine-2-carbaldehyde, or 5-hydroxypyridine in a one-pot synthesis. The latter also provides access to a range of functionalised species via Williamson ether syntheses, in this case OMe and OBn. Through the inclusion of an alkyne group it becomes possible to carry out further copper(I)-catalysed Huisgen 1,3-dipolar cycloaddition (CuAAC) ‘click’ reactions to further functionalise these systems.

3.3 **References**

1. N. C. Fletcher, R. T. Brown and A. P. Doherty, *Inorg. Chem.*, 2006, **45**, 6132-6134.
2. M. Albrecht and R. Fröhlich, *J. Am. Chem. Soc.*, 1997, **119**, 1656-1661.
3. S. Torelli, S. Delahaye, A. Hauser, G. Bernardinelli and C. Piguet, *Chemistry*, 2004, **10**, 3503-3516.
4. F. E. Hahn, C. Schulze Isfort and T. Pape, *Angew. Chem. Int. Ed. Engl.*, 2004, **43**, 4807-4810.
5. S. E. Howson, G. J. Clarkson, A. D. Faulkner, R. A. Kaner, M. J. Whitmore and P. Scott, *Dalton Trans.*, 2013.
6. C. R. Rice, C. J. Baylies, J. C. Jeffery, R. L. Paul and M. D. Ward, *Inorg. Chim. Acta*, 2001, **324**, 331-335.
7. M. J. Hannon, S. Bunce, A. J. Clarke and N. W. Alcock, *Angew. Chem. Int. Ed.*, 1999, **38**, 1277-1278.
8. E. C. Constable, F. R. Heirtzler, M. Neuburger and M. Zehnder, *Supramol. Chem.*, 1995, **5**, 197-200.
9. M. Albrecht, M. Napp, M. Schneider, P. Weis and R. Frohlich, *Chem. Commun.*, 2001, 409-410.
10. C. Schulze Isfort, T. Kreickmann, T. Pape, R. Frohlich and F. E. Hahn, *Chemistry*, 2007, **13**, 2344-2357.
11. S. E. Howson, L. E. N. Allan, N. P. Chmel, G. J. Clarkson, R. J. Deeth, A. D. Faulkner, D. H. Simpson and P. Scott, *Dalton Trans.*, 2011, **40**, 10416-10433.
12. S. E. Howson, A. Bolhuis, V. Brabec, G. J. Clarkson, J. Malina, A. Rodger and P. Scott, *Nat Chem*, 2012, **4**, 31-36.
13. S. Grimme, S. Ehrlich and L. Goerigk, *J. Comput. Chem.*, 2011, **32**, 1456-1465.
14. A. A. Granovsky, *Firefly version 8.0*, http://classic.chem.msu.su/gran/firefly/index.html.
15. M. W. Schmidt, K. K. Baldridge, J. A. Boatz, S. T. Elbert, M. S. Gordon, J. H. Jensen, S. Koseki, N. Matsunaga, K. A. Nguyen, S. Su, T. L. Windus, M. Dupuis and J. A. Montgomery, *J. Comput. Chem.*, 1993, **14**, 1347-1363.
16. C. A. Hunter and J. K. M. Sanders, *J. Am. Chem. Soc.*, 1990, **112**, 5525-5534.
17. V. Brabec, S. E. Howson, R. A. Kaner, R. M. Lord, J. Malina, R. M. Phillips, Q. M. A. Abdallah, P. C. McGowan, A. Rodger and P. Scott, *Chemical Science*, 2013.
18. S. E. Howson, L. E. Allan, N. P. Chmel, G. J. Clarkson, R. van Gorkum and P. Scott, *Chemical communications*, 2009, 1727-1729.
19. S. Grimme, *Angew. Chem. Int. Ed. Engl.*, 2008, **47**, 3430-3434.
20. L. Della Ciana, I. Hamachi and T. J. Meyer, *J. Org. Chem.*, 1989, **54**, 1731-1735.
21. J. Uenishi, T. Tanaka, K. Nishiwaki, S. Wakabayashi, S. Oae and H. Tsukube, *J. Org. Chem.*, 1993, **58**, 4382-4388.
22. S. A. Savage, A. P. Smith and C. L. Fraser, *J. Org. Chem.*, 1998, **63**, 10048-10051.
23. C. Dallaire, I. Kolber and M. Gingras, *Org. Synth.*, 2002, **78**, 82.

24. A. V. Davis, D. Fiedler, M. Ziegler, A. Terpin and K. N. Raymond, *J. Am. Chem. Soc.*, 2007, **129**, 15354-15363.
25. P. Mal, B. Breiner, K. Rissanen and J. R. Nitschke, *Science*, 2009, **324**, 1697-1699.
26. P. Mal, D. Schultz, K. Beyeh, K. Rissanen and J. R. Nitschke, *Angew. Chem. Int. Ed. Engl.*, 2008, **47**, 8297-8301.
27. N. Ousaka, J. K. Clegg and J. R. Nitschke, *Angew. Chem. Int. Ed. Engl.*, 2012, **51**, 1464-1468.
28. N. Ousaka, S. Grunder, A. M. Castilla, A. C. Whalley, J. F. Stoddart and J. R. Nitschke, *J. Am. Chem. Soc.*, 2012, **134**, 15528-15537.
29. X. M. Chen, R. Q. Wang and X. L. Yu, *Acta Crystallographica Section C Crystal Structure Communications*, 1995, **51**, 1545-1547.
30. S. E. Howson, L. E. N. Allan, N. P. Chmel, G. J. Clarkson, R. J. Deeth, A. D. Faulkner, D. H. Simpson and P. Scott, *Dalton Trans.*, 2011, **40**, 10416-10433.
31. O. Branytska, L. J. W. Shimon and R. Neumann, *Chem. Commun.*, 2007, 3957-3959.

Chapter 4

Biological applications of triplex metallohelices.

4.1 Introduction

The nature of the triplex metallohelices outlined in chapter three is such that a thermodynamic preference for the formation of only single enantiomer exists, circumnavigating both the need to conduct post complexation resolution and avoiding racemisation, making them well suited for biological study.

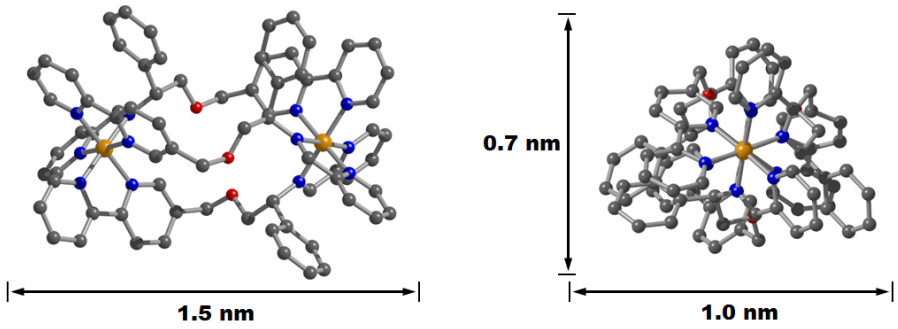

Figure 4.1 The parent triplex system, Rc,ΔFe,HHT-[$Fe_2\mathbf{L}^{12}{}_3$]Cl_4. Hydrogen atoms have been removed for clarity

While triplex metallohelices are slightly smaller than either LL-37 or the α-helix component of p53 which are discussed in Chapter 1, this allows scope for

introduction of functional groups within the target size envelope. Furthermore unlike either Hannon's D_{3h} cylinders[1] or Scott's D_3 flexicate systems,[2] triplex metallohelices display the same C_1 symmetry as natural peptide α-helix structures. This combined with the ability to incorporate different functionalities into the asymmetric ligand design, provides easy access to a range of potential synthetic drug candidates that approach the level of complexity typically associated protein systems. This chapter looks to addresses the biological applications of triplex metallohelices.

4.2 **Synthesis of water soluble triplex metallohelices**

4.2.1 Synthesis of water-soluble triplexes.

For triplex systems to be of practical use in biological applications the complexes are required to be soluble in water, however the zinc perchlorate species outlined in Chapter 3 however exhibits little to no solubility in aqueous media. In order to improve the solubility of these systems, chloride salts of ten iron(II) triplex complexes Δ_{Fe}/Λ_{Fe}-$[Fe_2\mathbf{L}^n{}_3]Cl_4$ (where n = 12, 15-18)(Figure 4.2), were prepared by heating appropriate proportions of the amine and various aldehydes with $FeCl_2$ in methanol. The resulting dark purple chloride salts were found to be highly soluble in aqueous media.

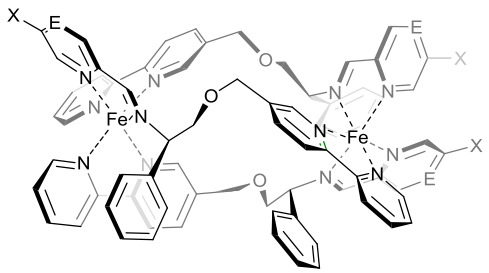

R_C,Δ_{Fe},HHT-[Fe_2**L**$^{12}{}_3$] (X = H, E = CH)
R_C,Δ_{Fe},HHT-[Fe_2**L**$^{15}{}_3$] (X = H, E = N)
R_C,Δ_{Fe},HHT-[Fe_2**L**$^{16}{}_3$] (X = OH, E = CH)
R_C,Δ_{Fe},HHT-[Fe_2**L**$^{17}{}_3$] (X = OMe, E = CH)
R_C,Δ_{Fe},HHT-[Fe_2**L**$^{18}{}_3$] (X = OBn, E = CH)

S_C,Λ_{Fe},HHT-[Fe_2**L**$^{12}{}_3$] (X = H, E = CH)
S_C,Λ_{Fe},HHT-[Fe_2**L**$^{15}{}_3$] (X = H, E = N)
S_C,Λ_{Fe},HHT-[Fe_2**L**$^{16}{}_3$] (X = OH, E = CH)
S_C,Λ_{Fe},HHT-[Fe_2**L**$^{17}{}_3$] (X = OMe, E = CH)
S_C,Λ_{Fe},HHT-[Fe_2**L**$^{18}{}_3$] (X = OBn, E = CH)

Figure 4.2 Substituted triplex metallohelices.

Unlike their zinc(II) perchlorate counterparts, ^{1}H NMR spectra for all iron(II) triplex metallohelices were found to be too broad to assign however, well resolved ^{13}C NMR spectra and mass spectra were both consistent with the predicted structures. IR spectra of complexes Δ_{Fe}/Λ_{Fe}-[Fe_2**L**$^n{}_3$]Cl_4 (where n = 12, 15-18) showed a broad peak in the region of 3600-3100 cm^{-1} indicating the presence of water. This was later confirmed by both thermal gravimetric analysis (see Appendix 1) and microanalysis to correspond to between eight and ten water molecules per complex. CD spectra of each of the triplex compounds, Δ_{Fe}/Λ_{Fe}-[Fe_2**L**$^n{}_3$]Cl_4 (where n = 12, 15-18) recorded in water contain bands spanning the whole UV-Visible region and were observed to be equal and opposite for the two enantiomers of the same complex (Figure 4.3 and Appendix 2).

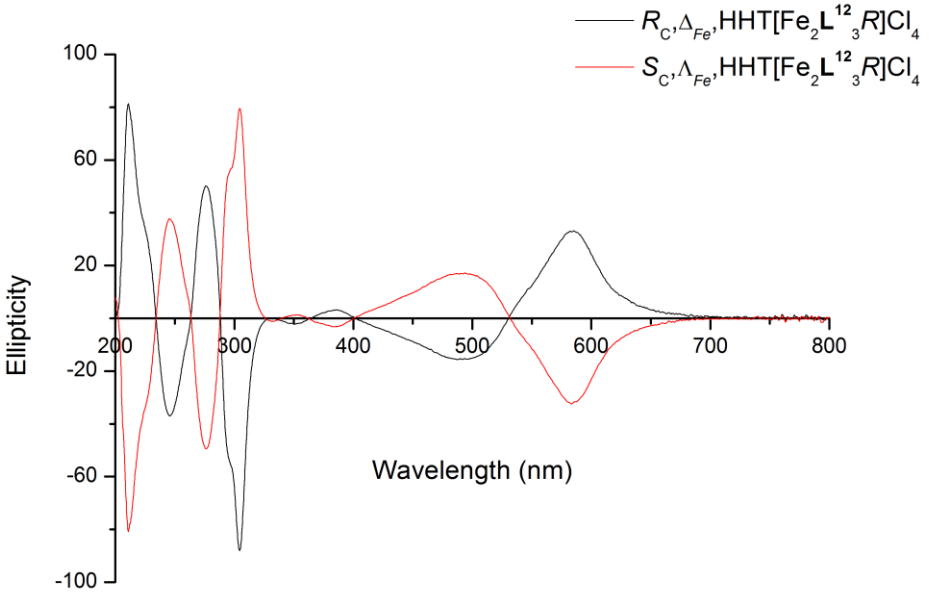

Figure 4.3 CD spectra of HHT-[Fe_2**L**$^{12}_3$]Cl_4.

4.2.2 UV-Vis stability studies.

In addition to good water solubility the chloride variants of triplex metallohelices they need to be sufficiently stable in aqueous media, e.g. with respect to hydrolysis, for most biological applications. Solutions of triplexes R_C,Δ_{Fe},HHT-[Fe_2**L**$^{n}_3$]Cl_4 (n = 12, 15-18) were prepared and their stabilities in various media have been followed by UV-visible spectroscopy, by observing the decrease in the metal-to-ligand charge transfer band (in the region of 500 - 550 nm) over an extended periods of time. The intensity of the UV peaks for all complexes in aqueous solutions were observed to decrease by *ca* 8 % over a period of 10 days at 22 °C. While identical stability studies were also carried out in 0.2 M HCl in which the UV intensities of all complexes were observed to decrease by *ca* 12 % at 22 °C over a period of five days. In both cases the resulting decrease in the intensity of the UV bands does not follow simple first order kinetics. It is likely that the stability of these complexes to decomposition in both aqueous and acidic

media is a result of the unique π-stacking interactions between ligands, and as such makes triplex metallohelices ideally suited for biological studies.

4.3 **Biological activity of triplex metallohelices**

4.3.1 Cytotoxicity of triplex metallohelices.

Triplex metallohelices are approximately the same size as Hannon's cylinders, Scott's flexicates and several naturally occurring α-helices, all of which have been shown to display cylotoxicity towards cancer cells. We were therefore interested in ascertaining weather these systems were suitability as potential anticancer drug candidates. As such, MTT assays were conducted by Rebecca Kaner at Bradford Institute of Cancer Therapeutics. Both enantiomers of HHT-$[Fe_2\mathbf{L}^{n}_3]Cl_4$ (Where n = 12, 15-18) were screened alongside a cisplatin control against MDA-MB-468 (human breast adenocarcinoma) and HCT116 $p53^{++}$ (human colon carcinoma) cell lines.[†]

[†] While all the tested compounds were found to be sufficiently soluble under assay conditions, the component ligands were found to be insoluble in aqueous media making them unsuitable for testing.

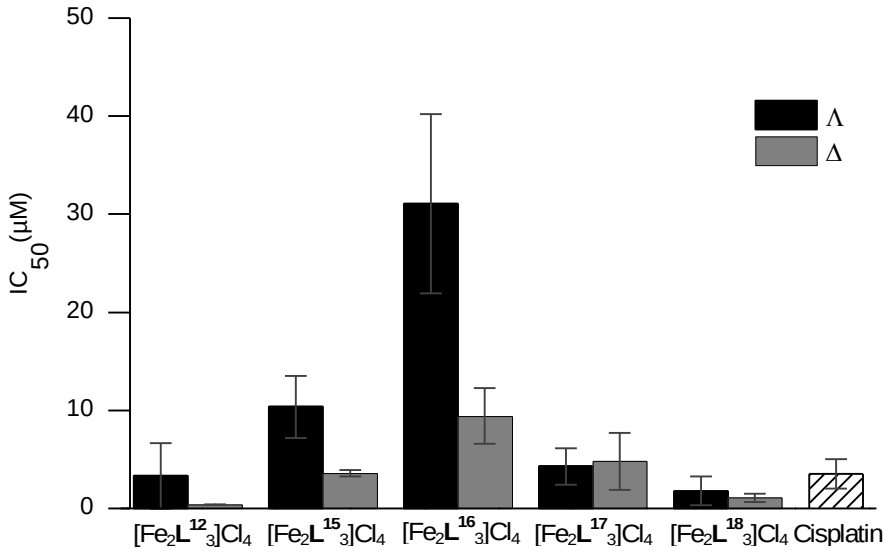

Figure 4.4 IC_{50} values for triplex metallohelices and a cisplatin control calculated after a 96 h incubation period in RPMI media with HCT116 $p53^{++}$ (human colon carcinoma) cells.

It was observed that all of the tested triplex metallohelices were active against HCT116 $p53^{++}$ cell with IC_{50} values being recorded in the range of 0.4-31.0 nm (Figure 4.4). Compound R_c,Δ_{Fe},HHT-$[Fe_2\mathbf{L}^{\mathbf{12}}{}_3]Cl_4$ showed IC_{50} values in the nanomolar range, actives which are up to ten times greater than those observed for the cisplatin control. Interestingly it was observed that the hydroxyl substituted complex, HHT-$[Fe_2\mathbf{L}^{\mathbf{16}}{}_3]Cl_4$ exhibited significantly lower activities than the other triplex metallohelices with IC_{50} values >10 higher than the most active compound R_c,Δ_{Fe},HHT-$[Fe_2\mathbf{L}^{\mathbf{12}}{}_3]Cl_4$. A less marked reduction in activity against HCT116 $p53^{++}$ cells was also recorded for the pyrazine compounds HHT-$[Fe_2\mathbf{L}^{\mathbf{15}}{}_3]Cl_4$.

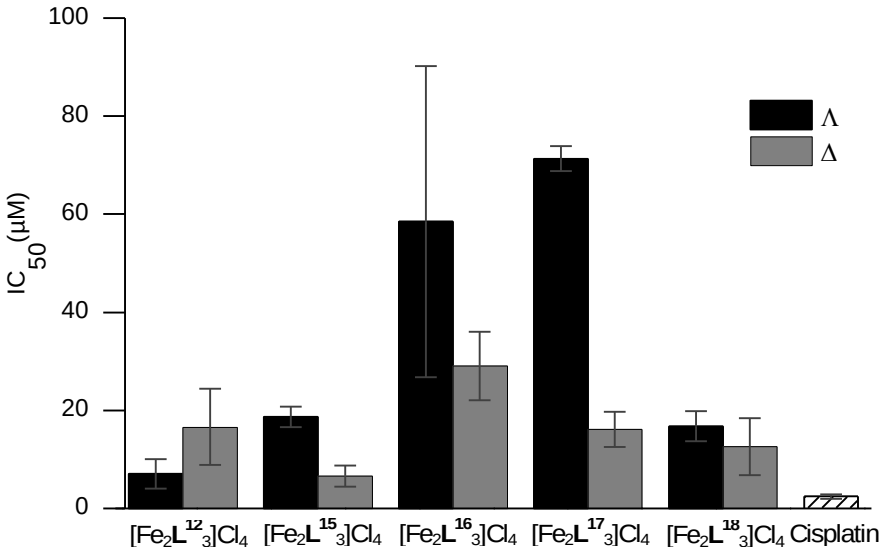

Figure 4.5 IC_{50} values for triplex metallohelices and a cisplatin control calculated after a 96 h incubation period in RPMI media with MDA-MB-468 (human breast adenocarcinoma) cells.

In general all triplex metallohelices were found to be less active against the MDA-MB-468 (Figure 4.5) than HCT116 $p53^{++}$ with IC_{50} values for all complexes found to be greater than the cisplatin control. Incorporation of either hydroxyl or methoxy groups in to the ligand structure (compounds HHT-$[Fe_2\mathbf{L}^{\mathbf{16}}{}_3]Cl_4$ and HHT-$[Fe_2\mathbf{L}^{\mathbf{17}}{}_3]Cl_4$), was observed to result in a reduction in the overall potency of these complexes when compared to the parent HHT-$[Fe_2\mathbf{L}^{\mathbf{12}}{}_3]Cl_4$ complexes. By contrast the inclusions of either a benzyl or pryazine group into the ligand structure appears to have little effect on the activity of these systems with IC_{50} values being comparable to those observed for the unsubstituted parent HHT-$[Fe_2\mathbf{L}^{\mathbf{12}}{}_3]Cl_4$ complexes.

4.3.2 Assessment of DNA damage caused by triplex metallohelicates.

In an effort to elucidate a possible mode of action for these compounds, the effects of R_c,Δ_{Fe},HHT-[$Fe_2\mathbf{L}^{\mathbf{12}}{}_3$]$Cl_4$ and S_c,Λ_{Fe},HHT-[$Fe_2\mathbf{L}^{\mathbf{12}}{}_3$]$Cl_4$ on HCT116 $p53^{++}$ colon carcinoma cells was further investigated. Single cell gel electrophoresis (SCGE) assays referred to as 'comet' assays, due to the comet like appearance of the results obtained from this technique,[3] were conducted by Rebecca Kaner at the Bradford Institute of Cancer Therapeutics, to establish weather these complexes induced single-strand breaks (SSBs) in cellular DNA. HCT116 $p53^{++}$ cells were treated with 20 μM solutions of either R_c,Δ_{Fe},HHT-[$Fe_2\mathbf{L}^{\mathbf{12}}{}_3$]$Cl_4$ or S_c,Λ_{Fe},HHT-[$Fe_2\mathbf{L}^{\mathbf{12}}{}_3$]$Cl_4$ (which is substantially higher than the recorded IC_{50} values) for 24 h. Control samples of untreated cells was also prepared along with a further positive control in which HCT116 $p53^{++}$ cells were treated with H_2O_2, which has been shown to induce random single stand breaks in DNA[4, 5] were also prepared. Each of these samples was then deposited onto an agar matrix before undergoing cell membrane lysis and further incubation in alkaline media. The resulting samples were subjected to gel electrophoresis and staining with a DNA-specific stain allowing the cells to be visualised by florescence spectroscopy. Undamaged DNA is observed to move relatively slowly forming the 'head' of the comet while the single strand fragments move more quickly giving the impression of a tail. As such calculation of the tail moment (Percentage of DNA in tail times tail length; where tail length is measured form the centre of the head)[3] gives an indication of the degree of SSBs that occur within the HTC116 $p53^{++}$ cells from treatment with either R_c,Δ_{Fe},HHT-[$Fe_2\mathbf{L}^{\mathbf{12}}{}_3$]$Cl_4$ or S_c,Λ_{Fe},HHT-[$Fe_2\mathbf{L}^{\mathbf{12}}{}_3$]$Cl_4$. The untreated cells gave no tail moment, while cells that were treated with H_2O_2 can be considered to

have undergone 100% induced SSBs. As shown in Table 4.1, both enantiomers of $[Fe_2\mathbf{L}^{\mathbf{12}}{}_3]Cl_4$ resulted tail moments that were comparable to those of the untreated HCT116 $p53^{++}$ cells strongly suggesting that these complexes do not induce SSBs.

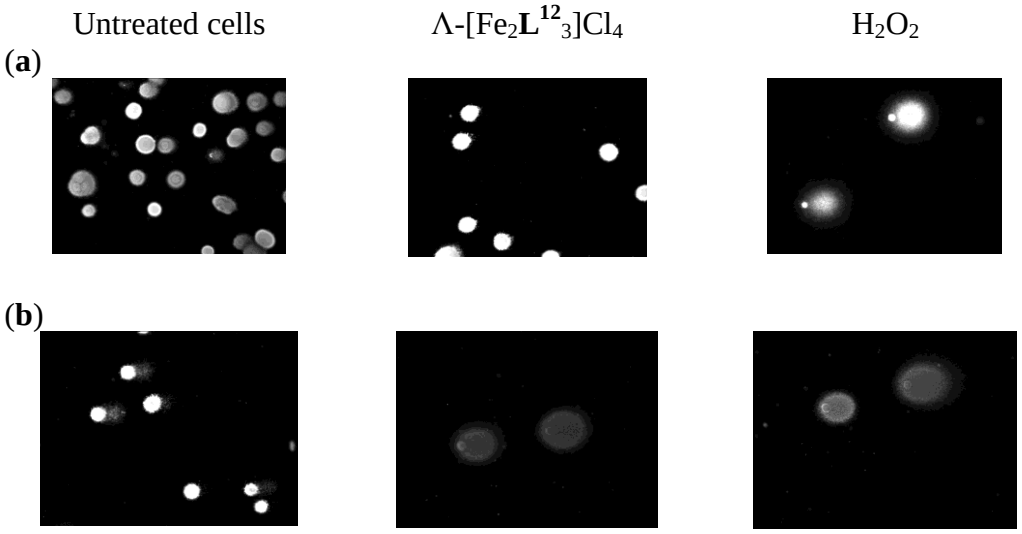

Figure 4.6 Microscope images of (**a**) SSB comet assasy and (**b**) ICLs comet assays showing the comparsion between cells treated with Λ-$[Fe_2L^{12}{}_3]Cl_4$ and those either incubated with H_2O_2 or left untreated.

	SSB tail moment (esd)	ICLs tail moment (esd)
Untreated Cells	3.51 (1.30)	1.87 (0.39)
H_2O_2	36.04 (6.77)	36.44 (4.02)
Λ-$[Fe_2L^{12}{}_3]Cl_4$	4.35 (1.11)	41.90 (12.13)
Δ-$[Fe_2L^{12}{}_3]Cl_4$	3.77 (1.45)	38.53 (1.68)

Table 4.1 SSB and ICL tail moments of HTC11 $p53^{++}$ cells after treatment with $[Fe_2\mathbf{L}^{\mathbf{12}}{}_3]Cl_4$.

Although neither of the parent triplex metalloheciates induces SSBs in HCT116 $p53^{++}$ cells they can potentially cause inter-strand crosslinking (ICL) which prevents both DNA replication and transcription; in the absence of cellular repair mechanisms this can lead to cell death.[6] Consequently, both R_c,Δ_{Fe},HHT-

$[Fe_2\mathbf{L}^{\mathbf{12}}{}_3]Cl_4$ and S_c,Λ_{Fe},HHT-$[Fe_2\mathbf{L}^{\mathbf{12}}{}_3]Cl_4$ were subjected to further ICL comet assays. Once again HCT116 $p53^{++}$ cells were treated with 20 μM solutions of both triplex metallohelices and incubated for 24 h, deposited on an agar matrix prior to cell membrane lyses. The liberated DNA from the treated cells was exposed to H_2O_2 to induce random SSBs prior to undergoing gel electrophoresis and staining with an appropriate fluorescent DNA stain. Should ICLs occur, migration of the DNA in the comet assay is similar to that of untreated cells if not reduced,[5] as the presence of ICLs prevents the complete denaturation of DNA strands resulting in a decreases of DNA fragmentation.[6] Comparing the tail moments of cells treated with either R_c,Δ_{Fe},HHT-$[Fe_2\mathbf{L}^{\mathbf{12}}{}_3]Cl_4$ or S_c,Λ_{Fe},HHT-$[Fe_2\mathbf{L}^{\mathbf{12}}{}_3]Cl_4$ to a control sample, in which HCT116 $p53^{++}$ cells have been treated with only H_2O_2 and as such are considered to have undergone no ICL, strongly suggests that neither of these complexes cause any crosslinking of DNA strands (Table 4.1).

To confirm that triplex metallohelices do not cause DNA damage, H2AX expression studies have also conducted by Qasem Abdullah at Bradford Institute of Cancer Therapeutics. H2AX is a histone that becomes rapidly phosphorylated to γ-H2AX at sites of double-strand breaks (DSBs) where it initiates DNA repair.[7-10] DSBs can occur either directly or as a result of SSBs, ICL, intercalation or inhibition of other DNA repair enzymes.[7] As such H2AX expression is considered as a powerful tool to assess DNA damage.[7, 11] Following incubation of HCT116 $p53^{++}$ cells with R_c,Δ_{Fe},HHT-$[Fe_2\mathbf{L}^{\mathbf{12}}{}_3]Cl_4$ (10 μM) for 24 h the cells were treated with γ-H2AX and fluorescent antibodies. The resulting cells, along with a control of untreated HCT116 $p53^{++}$ cells were analysed using fluorescent-activated cell sorting (FACS).

Drug (10 μM)	γ-H2AX foci/cell (esi)
Control	30.07 (7.30)
Δ_{Fe}-[Fe_2**L**$^{1a}{}_3$]Cl_4	40.46 (8.90)

Table 4.2 γ-H2AX expression FACS assay of HCT116 p53++ cells treated with 10 μM triplex metallohelices for 24 h.

As shown in Table 4.2, both of the triplex metallohelices tested did not significantly alter the production of γ-H2AX, suggesting that neither DNA damage or interruption of the γ-H2AX pathway occurs. The data from this study combined with the results from both the SSBs and ICLs comet assays consistently indicated that the cyclotoxicity of *R*$_c$,Δ_{Fe},HHT-[Fe_2**L**$^{12}{}_3$]Cl_4 and *S*$_c$,Λ_{Fe},HHT-[Fe_2**L**$^{12}{}_3$]Cl_4 does not result from DNA damage.

4.3.3 Cell cycle analysis

During replication each cell undergoes a series of distinct phases. In the G_1 phases the cell increases in size, synthesising both mRNA and proteins in preparation for DNA replication. The cell then proceeds to the S phase, in which new DNA is synthesised prior to the cell preparing for mitosis (G_2 Phase). Finally the cell undergoes mitosis (M phase).[41] If the cell is determined to be unsuitable for replication during any part of this cycle its further development is arrested and it enters into a state of apoptosis (sub G_1 phase),[12, 13] thus removing it from the cell cycle. As such, abnormalities in this cycle, which occur on treatment of the cells with a potential drug molecule, can help in elucidation of its mode of action.

Metallohelices have previously been shown to interact with the cell cycle. Hannon *et al.*[14] have reported that their iron(II) cylinders cause arrestment in the cell cycle of HL60 promyelocytic leukemia cells during the sub G_1/G_1 phases. Hannon postulates that this results from the complex binding to the DNA, preventing its replication and as such leading to a reduction in the proportion of cells in the S phase from 39 % to 21 % over a 48 h period. Scott *et al.* have also previously identified that their flexicate systems affect the cell cycle of HCT116 $p53^{++}$ cells. They observed an increase in the proportion of cells in the G_2/M phase by between 20-40% of that observed for untreated cells.[15] Furthermore these complexes were also noted to cause an increase in the number of cells present in the sub G_1 phase by 13-30%. Scott therefore speculates that this increase is the result of flexicate systems inducing programmed cell death.[15] As such we were interested in ascertaining weather triplex metallohelicates also disrupted the cell cycle of HCT116 $p53^{++}$ cells.

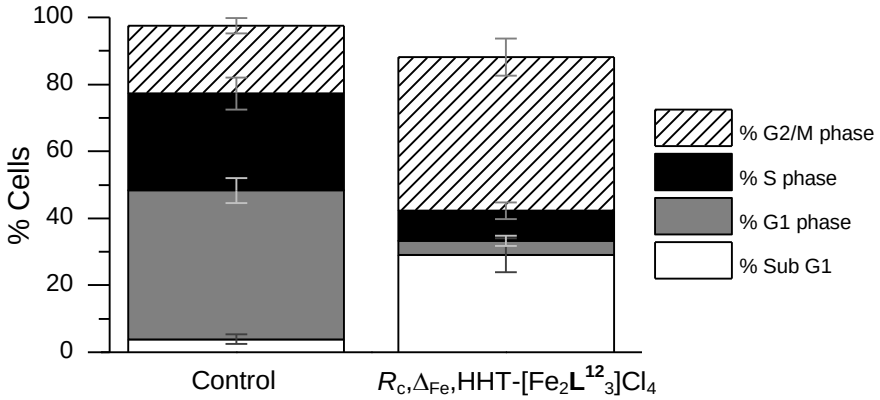

Figure 4.7 Cell Cycle FACS assay showing the % population of HCT116 p53++ cells when treated with Rc,ΔFe,HHT-[$Fe_2\mathbf{L}^{12}{}_3]Cl_4$ (10 μM) for 24 h compared to a control of untreated cells.

Cell cycle studies were conducted by Qasem Abdullah at Bradford Institute of Cancer Therapeutics in which HCT116 $p53^{++}$ cells were incubated with

R_c,Δ_{Fe},HHT-[Fe_2**L**$^{12}{}_3$]Cl_4 (10 μM) for 24 h prior to staining and analysis by FACS.[44] Compared to the control, cells treated with R_c,ΔFe-HHT-[Fe_2**L**$^{12}{}_3$]Cl_4 show a significant increase in the population of cells in the G_2/M phase (*ca.* 26 % increase) and the sub G_1 phase (ca. 4 to 30 %, Figure 4.7) compared with the untreated control. The proportion of cells in the G_1 and S phases are reduced from 44 % to 4 % and 29 % to 9 % respectively. These observations suggest that the compound R_c,Δ_{Fe},HHT-[Fe_2**L**$^{12}{}_3$]Cl_4 may be inhibiting mitosis in the HCT116 $p53^{++}$ cells, ultimately leading to programed cell death (apoptosis). Further research is ongoing to ascertain the validity of this hypothesis.

4.3.4 Antimicrobial studies

As a result of the widespread emergence of acquired resistance in bacterial pathogens to many antibiotic agents, the need for novel antibacterial compounds is paramount.[16] Despite this the use of coordination complexes as antimicrobial agents has received relatively little attention in the literature. Pioneering work by Dwyer *et al.* in 1952 highlighted the bacteriostatic/bacteriocidal activity of several metal coordination complexes against both *Escherichia coli* and *Staphylococcus hameolyticus.*[17] More recently Aldrich-Wright and co-workers have investigated ruthenium(II) complexes as potential antimicrobial agents, observing minimum inhibitory concentrations (MICs) as low as ≥ 2 mg/L against Gram-positive bacteria. Interestingly the same systems were found to be inactive against the Gram-negative bacterium *E. coli*.[18] While Hannon and co-workers have shown that their iron(II) helicates display limited antimicrobial activity (MIC ≥ 32 mg/L) against both Gram-positive and Gram-negative bacteria.[19] Scott and co-workers have also looked at the antimicrobial activity of their

flexicate systems; reporting antimicrobial activity against both the Gram-negative bacterium *E.coli* (MC4100) and the Gram-positive bacterium methicillin-resistant *S. aureus* (MRSA252) with MICs as low as 4 μg ml^{-1} (~2 μM) against *E. coli*.[2]

In order to ascertain weather triplex metallohelices also displayed bactericidal properties, antimicrobial experiments were conducted by Daniel Simpson at the University of Warwick. *Staphylococcus aureus* (USA300) bacteria cells were incubated with both enantiomers of each triplex matallohelces HHT-$[Fe_3\mathbf{L^n}_3]Cl_4$ (Where n = 12, 15-18) at a range of dilution factors (2 - 128 μg/ml) in Müeller-Hinton broth over a 20 h period at 37 °C, prior to the determination of MIC values from the optical density at 600 nm. After MIC testing, any concentrations which exhibited no growth other the 20 h period were diluted with phosphate buffered saline (PBS, 1:20) and spread on two separate sterile LB-agar plates. The lowest concentrations showing no bacterial colonies on either plate after a further 20 h incubation period at 37 °C was quoted as the minimum bactericidal concentrations (MBC). In general triplex metallohelices failed to show any inhibition of bacterial growth, even the most active pryazine compounds, R_c,Δ_{Fe},HHT-$[Fe_2\mathbf{L^{18}}_3]Cl_4$ and S_c,Λ_{Fe},HHT-$[Fe_2\mathbf{L^{18}}_3]Cl_4$ display MIC and MBC values ten times lower than the ampicillin control (**Table 4.3**).

	MIC	MBC
Ampicillin (Control)	<2	
R_c,Δ_{Fe},HHT-[$Fe_2\mathbf{L}^{\mathbf{12}}{}_3$]$Cl_4$	≥ 128	≥ 128
S_c,Λ_{Fe},HHT-[$Fe_2\mathbf{L}^{\mathbf{12}}{}_3$]$Cl_4$	≥ 128	≥ 128
R_c,Δ_{Fe},HHT-[$Fe_2\mathbf{L}^{\mathbf{15}}{}_3$]$Cl_4$	≥ 128	≥ 128
S_c,Λ_{Fe},HHT-[$Fe_2\mathbf{L}^{\mathbf{15}}{}_3$]$Cl_4$	≥ 43	≥ 128
R_c,Δ_{Fe},HHT-[$Fe_2\mathbf{L}^{\mathbf{16}}{}_3$]$Cl_4$	≥ 128	≥ 128
S_c,Λ_{Fe},HHT-[$Fe_2\mathbf{L}^{\mathbf{16}}{}_3$]$Cl_4$	≥ 128	≥ 128
R_c,Δ_{Fe},HHT-[$Fe_2\mathbf{L}^{\mathbf{17}}{}_3$]$Cl_4$	≥ 128	≥ 128
S_c,Λ_{Fe},HHT-[$Fe_2\mathbf{L}^{\mathbf{17}}{}_3$]$Cl_4$	≥ 128	≥ 128
R_c,Δ_{Fe},HHT-[$Fe_2\mathbf{L}^{\mathbf{18}}{}_3$]$Cl_4$	≥ 32	≥ 64
S_c,Λ_{Fe},HHT-[$Fe_2\mathbf{L}^{\mathbf{18}}{}_3$]$Cl_4$	≥ 32	≥ 64

Table 4.3 MIC and MBC values determined for triplex metallohelics in Müeller-Hinton broth over a 20 h period at 37 °C against Staphylococcus aureus (USA300).

4.4 **Conclusion**

Due to its low symmetry (C_1), comparable size to α-helix peptides and the ease with through which substituents can be incorporated into overall ligand design, triplex metallohelices are the first example of a coordination complex that approaches the level of complexity typically associated with α-helixes. In this chapter water soluble, iron(II) chloride, variants of triplex metallohelices described in Chapter 3 have been synthesised. Remarkably, the thermodynamic stability of these systems, arising from novel π-stacking interactions between ligands, results in these complexes being stable for extended periods of time in both aqueous and acidic media. This stability combined with the inherent enationselectivity of these complexes makes them ideally suited for biological studies. MTT assays have shown that these complexes are active against two separate cancer cell lines. With the most promising actives being observed between the parent complex HHT-[$Fe_2\mathbf{L}^{\mathbf{12}}{}_3$]$Cl_4$ and the HTC116 $p53^{++}$ cell line, with IC_{50} values reported in the nanomolar range. Primary investigations of the

mode of action for these complexes indicate that they do not cause direct damage to cellular DNA. Cell cycle analysis indicates that the complex, R_c-Δ_{Fe},HHT-[Fe_2**L**$^{12}_3$]Cl_4 causes a significant increase in the population of cells in the G2/M phase and sub G1 phase. This suggests that these compounds may be inducing apoptosis, although further work is needed in this area. Interestingly, unlike previously reported compounds, triplex metallohelices appear only to be active against the tested mammalian cancer cells, displaying no inhibition or bactericidal activity towards either of the tested Gram-positive or Gram-negative bacteria. As such, triplex metallohelices provide a novel approach to optically pure, metallo-peptidomimetic systems, which selectively display anticancer activities in the nanomolar range.

4.5 **References**

1. M. J. Hannon, V. Moreno, M. J. Prieto, E. Moldrheim, E. Sletten, I. Meistermann, C. J. Isaac, K. J. Sanders and A. Rodger, *Angew. Chem. Int. Ed.*, 2001, **40**, 879-884.
2. S. E. Howson, A. Bolhuis, V. Brabec, G. J. Clarkson, J. Malina, A. Rodger and P. Scott, *Nat Chem*, 2012, **4**, 31-36.
3. W. Liao, M. A. McNutt and W.-G. Zhu, *Methods*, 2009, **48**, 46-53.
4. L. Szmigiero and K. Studzian, *Anal. Biochem.*, 1988, **168**, 88-93.
5. S. Pfuhler and H. Uwe Wolf, *Environ. Mol. Mutagen.*, 1996, **27**, 196-201.
6. J. Wu and N. Jones, in *Genetic Toxicology*, eds. J. M. Parry and E. M. Parry, Springer New York, Editon edn., 2012, vol. 817, pp. 165-181.
7. L. J. KUO and L.-X. YANG, *In Vivo*, 2008, **22**, 305-309.
8. C. Redon, J. Dickey, A. Nakamura, O. Martin and W. Bonner, in *Molecular Determinants of Radiation Response*, eds. T. L. DeWeese and M. Laiho, Springer New York, Editon edn., 2011, pp. 3-33.
9. W. M. Bonner, C. E. Redon, J. S. Dickey, A. J. Nakamura, O. A. Sedelnikova, S. Solier and Y. Pommier, *Nat. Rev. Cancer*, 2008, **8**, 957-967.
10. J. Kobayashi, *Journal of Radiation Research*, 2004, **45**, 473-478.
11. A. Ivashkevich, C. E. Redon, A. J. Nakamura, R. F. Martin and O. A. Martin, *Cancer Lett.*, 2012, **327**, 123-133.
12. I. Nicoletti, G. Migliorati, M. C. Pagliacci, F. Grignani and C. Riccardi, *Journal of Immunological Methods*, 1991, **139**, 271-279.
13. M. Kajstura, H. D. Halicka, J. Pryjma and Z. Darzynkiewicz, *Cytometry Part A*, 2007, **71A**, 125-131.
14. A. C. G. Hotze, N. J. Hodges, R. E. Hayden, C. Sanchez-Cano, C. Paines, N. Male, M.-K. Tse, C. M. Bunce, J. K. Chipman and M. J. Hannon, *Chem. Biol.*, 2008, **15**, 1258-1267.
15. V. Brabec, S. E. Howson, R. A. Kaner, R. M. Lord, J. Malina, R. M. Phillips, Q. M. A. Abdallah, P. C. McGowan, A. Rodger and P. Scott, *Chemical Science*, 2013.
16. A. J. Neill and I. Chopra, *Expert Opin. Invest. Drugs*, 2004, **13**, 1045-1063.
17. F. P. Dwyer, E. C. Gyarfas, W. P. Rogers and J. H. Koch, *Nature*, 1952, **170**, 190-191.
18. A. Bolhuis, L. Hand, J. E. Marshall, A. D. Richards, A. Rodger and J. Aldrich-Wright, *Eur. J. Pharm. Sci.*, 2011, **42**, 313-317.
19. A. D. Richards, A. Rodger, M. J. Hannon and A. Bolhuis, *International Journal of Antimicrobial Agents*, 2009, **33**, 469-472.

Chapter 5

Experimental section.

5.1 General Considerations

All solvents and chemicals purchased from commercial sources (Sigma-Aldrich, Acros, Fisher Scientific or Alfa Aesar) were used without further purification. Sodium hydride dispersions in mineral oil were placed in a Schlenk vessel under an inert atmosphere and washed three times with diethyl ether to remove the oil. The sodium hydride powder was then dried and stored in an MBraun dry box.

Where appropriate, reactions were carried out under argon using a dual manifold argon/vacuum line and standard Schlenk techniques or MBraun dry box. Necessary solvents were dried by heating to reflux for 3 d under dinitrogen over the appropriate drying agents (potassium for THF, and calcium hydride for acetonitrile, pyridine, diisopropyl amine and triethylamine) and degassed before use. THF was additionally pre-dried over sodium wire. Dried solvents were stored in glass ampoules under argon. All glassware and cannulae were stored in an oven at > 375 K. Deuterated solvents were purchased from Sigma-Aldrich and Cambridge Isotope laboratories.

NMR spectra were recorded on Bruker Spectrospin 300/400/500 spectrometers. Routine NMR assignments were confirmed by ^{1}H-^{1}H (COSY) and ^{13}C-^{1}H (HMQC) correlation experiments where necessary. The spectra were internally referenced using the residual protio solvent ($CDCl_3$, CD_3CN *etc.*) resonance relative to tetramethylsilane (δ = 0 ppm). ESI mass spectra were recorded on Bruker Esquire 2000 and Bruker MicroTOF spectrometers. Infra-Red spectra were measured using a Perkin-Elmer FTIR spectrometer. Elemental analyses were performed by Warwick Analytical Services, Coventry, UK and MEDAC Ltd, Surrey, UK.

UV-Visible absorbance spectra were recorded using a Jasco V-660 spectrometer. Measurements were collected in a 1 cm path-length quartz cuvette using the following standard parameters: bandwidth 1 nm, response time 1 sec, wavelength scan range 200 – 800 nm, data pitch 0.2 nm, scanning speed 100 nm/min and accumulation 2. CD spectra were measured on a Jasco J-815 spectrometer, which was calibrated conventionally using 0.060% ACS for intensity and a holmium filter for wavelength and against the more recently introduced Na[Co(EDDS)] system.[1] Measurements were collected in a 1 cm path-length quartz cuvette using the following standard parameters: bandwidth 1 nm, response time 1 sec, wavelength scan range 200 – 800 nm, data pitch 0.2 nm, scanning speed 100 nm/min and accumulation 4.

Optical rotation measurements were performed on a Perkin Elmer Polarimeter 341 by Warwick Analytical Services, Coventry, UK. In all cases, the following parameters were used: solvent methanol, temperature 20°C, pathlength 100 mm, wavelength 589 nm.

We are grateful to the National Crystallographic Service[2] for recording the data for compounds R_c,Δ_{Fe},HHT-$[Zn_2\mathbf{L^{12}}_3][ClO_4]_4$ and R_c,Δ_{Fe},HHT-$[Zn_2\mathbf{L^{16}}_3][ClO_4]_4$. Structural data for all other compounds was recorded in house using a Siemens SMART CCD single crystal diffractometer, using a MoKα (λ = 0.71073 Å) or a CuKα (λ = 1.54184 Å) radiation source. All structures were solved by direct methods using SHELX (TREF),[3, 4] with additional light atoms found by Fourier methods. Crystal refinement was performed using SHELX97.[4]

Starting points for geometry optimisations were taken from crystallographic data where available, where this was unavailable, starting structures were created from existing crystallographic fragments. Monometallic structures were first optimised using B3LYP-D3(BJ)[5] functional and the 6-31g* basis set, with a convergence criteria of 0.0001 a.u. as implemented in the Firefly quantum chemistry package,[6] which is partially based on the GAMESS(US) source code.[7] Bimetallic systems were optimised using ligand field molecular mechanics (LFMM)[8] as implemented in the DommiMOE program,[9] before being annealed at 500 K for 1 ns prior to re-optimisation. Single point energies of all structures were performed using the B3LYP-D3(BJ)[5] functional and the deff2-TZVP basis set with energy convergence criteria of 0.0001 a.u. as implemented in the Firefly quantum chemistry package.[6]

5.2 **Experimental for chapter 2**

5.2.1 Ligand components

5.2.1.1 5-hydroxy-2-methylpyridine-1-oxide.[10]

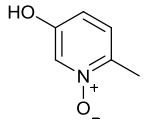

5-hydroxy-2-mehylpyridine (25.1 g, 0.23 mol) was suspended in a solution of *m*-chlorperbenzoic acid (44.1 g, 0.26 mol) in 500 ml of chloroform and heated to reflux for 2 h. After which time the solution was cooled to ambient temperature and stirred for a further 2 h before solvents were removed under reduced pressure. The resulting yellow solid was extracted into hot ethyl acetate and the insoluble product was isolated by filtration, washed with further portions of hot ethyl acetate (2 x 100ml), and dried to give the desired product as a pale yellow solid. Yield 23.4 g, 81%

^{1}H NMR (300 MHz, DMSO) δ_H ppm 10.22 (1H, s, OH), 7.81 (1H, d, $^{4}J_{HH}$ = 2.3, Py), 7.24 (1H, d, $^{3}J_{HH}$ = 8.5, Py), 6.76 (1H, dd, $^{3}J_{HH}$ = 8.5, $^{4}J_{HH}$ = 2.3, Py), 2.22 (3H, s, Me).

^{13}C {^{1}H} NMR (75 MHz, DMSO) δ_C ppm 154.0, 139.0, 127.4, 126.1, 113.7 (Py), 16.30 (Me).

ESI ms 126.2 $[M+H]^+$ 148.1 $[M+Na]^+$.

IR cm^{-1} 2288 (bm), 1624 (w), 1571 (m), 1528 (m), 1458 (m), 1421 (m), 1386 (m), 1308 (m), 1275 (w), 1226 (m), 1161 (m), 1116 (s), 1034 (w), 1001 (m), 965 (w), 888 (w), 858 (s), 825 (s), 776 (m), 740 (w), 691 (w).

5.2.1.2 6-(acetoxymethyl)pyridin-3-yl acetate.[10]

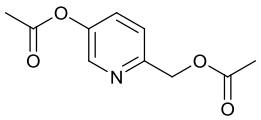

5-hydroxy-2-methylpyridine-1-oxide (23.0 g, 0.13 mol) was suspended in acetic anhydride (400 ml) and heated to reflux for 4 h. After cooling to ambient temperature solvents were removed under reduced pressure to give the titular product as a black oil which was suitable for use without further purification. Yield 34.2g, 96.6%

^{1}H NMR (300 MHz, 298 K, DMSO) δ_H ppm 8.40 (1H, d, $^{4}J_{HH}$ = 2.5, Py), 7.66 (1H, dd, $^{3}J_{HH}$ = 8.5, $^{4}J_{HH}$ = 2.5, Py), 7.50 (1H, d, $^{3}J_{HH}$ = 8.5, Py), 5.15 (2H, s, CH_2), 2.31 (3H, s, CH_3) 2.11 (3H, s, CH_3).

^{13}C NMR (75 MHz, 298 K, DMSO) δ_C ppm 170.1 (C=O), 169.1 (C=O) 153.0, 146.5, 142.9, 130.4, 122.5 (Py), 65.7 (CH_2), 20.7 (Me), 20.6 (Me).

ESi m/s 232.1 $[M+Na]^+$.

5.2.1.3 6-(hydroxymethyl)pyridin-3-ol.[10]

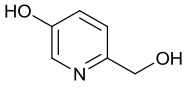

Crude 6-[(acetyloxy)methyl]pyridin-3-yl acetate (34.0 g, 0.16 mol) was dissolved in conc. HCl (200 ml) and boiled over a period of 24h. After cooling the solution was evaporated and dissolved in water, then it was neutralized with sufficient amount of sodium hydroxide. The precipitated sodium chloride was

filtered off, and the filtrate was evaporated to give a dark residue which was taken up with boiling acetonitrile (3 × 100 ml). Fractions were combined and evaporated to dryness to give the desired product as a yellow solid. Yield 12.8g, 63.9%

^{1}H NMR (300 MHz, 298 K, DMSO) δ_H ppm 8.04 (1H, d, $^{4}J_{HH}$ = 2.7 Hz, Py), 7.28 (1H, d, $^{3}J_{HH}$ = 8.6 Hz, Py), 7.16 (1H, dd, $^{3}J_{HH}$ = 8.6, $^{4}J_{HH}$ = 2.8 Hz), 4.46 (2H, s CH_2).

^{13}C NMR (100 MHz, 298 K, DMSO) δ_C ppm 152.4, 152.1, 136.5, 122.6, 121.1 (Py), 64.0 (CH_2).

ESI MS 126.2 $[M+H]^+$

IR cm^{-1} 2882 (w), 2840 (w), 2360 (br), 1751 (br), 1570 (m), 1496 (m), 1445 (m), 1375 (w), 1334 (w), 1293 (w), 1271 (m), 1209 (s), 1127 (w), 1117 (w), 1072 (s), 1028 (m), 893 (w), 867 (w), 858 (w), 831 (s), 760 (w), 714 (w), 657 (s).

5.2.1.4 5-(hydroxy)picolinaldehyde.[10]

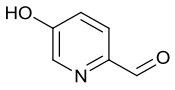

Activated MnO_2 (16.0 g, 192 mmol 2.5 eq.) was added to a solution of 6-(hydroxymethyl)pyridin-3-ol (12.0g, 96 mmol) in isopropanol (250 ml) and the resulting suspension was refluxed for 4 h, cooled to ambient temperature and stirred overnight. The suspension was filtered through celite and the residue was washed with isopropanol (2x 100 ml). Solvents were removed under reduced pressure to give the crude produce as a yellow brown solid, which was

recrystallized from hot water to give the desired product as a brown solid. Yield 6.7g, 56%.

^{1}H NMR (400 MHz, 298 K, DMSO) δ_H ppm 8.82 (1H, s, CO*H*), 8.31 (1H, d, $^{4}J_{HH}$ = 2.5, Py), 7.83 (1H, d, $^{3}J_{HH}$ = 8.4, Py), 7.32 (1H, dd, $^{3}J_{HH}$ = 8.6, $^{4}J_{HH}$ = 2.5, Py), 3.42 (1H, bs, OH).

^{13}C {^{1}H} NMR (100 MHz, 298 K, DMSO) δ_C ppm 191.9 (C=O), 158.0, 144.8, 138.8, 123.8, 122.4 (Py).

ESi m/s 124.2 $[M+H]^{+}$.

IR cm^{-1} 2883 (w), 2839 (w), 2399 (b), 1707 (b), 1570 (m), 1492 (m), 1460 (w), 1444 (w), 1374 (w), 1333 (w), 1270 (s), 1208 (s), 1127 (m), 1117 (m), 1071 (s), 1027 (m), 892 (w), 858 (w), 829 (s), 760 (w), 713 (w).

5.2.1.5 5-methoxypicolinaldehyde.

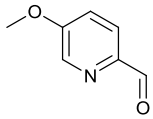

5-(hydroxy)picolinaldehyde (2.0g, 16.2 mmol), methyl iodide (2.3g, 1ml, 16.2mmol), and potassium carbonate (2.69g 19.4 mmol) were dissolved in acetonitrile (50 ml) and refluxed for 18 h, after which the dark brown solution was cooled to ambient temperature and filtered through silica. Solvents were removed under reduced pressure to give the desired compound as a white solid. Yield = 1.2 g, 72%.

^{1}H NMR: (300 MHz, 298 K, $CDCl_3$) δ_H ppm 9.92 (1H, s, CO*H*), 8.36 (1H, d, $^{4}J_{HH}$ = 2.8, Py), 7.90 (1H, d, $^{3}J_{HH}$ = 8.7, Py), 7.24 (1H, dd, $^{3}J_{HH}$ = 8.6, $^{4}J_{HH}$ = 2.7, Py), 3.89 (3H, s, OMe).

^{13}C NMR {^{1}H} (75 MHz, 298 K $CDCl_3$) δ_C ppm 192.1 (C=O), 159.1, 146.4, 138.7, 123.5, 120.0 (Py), 56.0 (OMe).

ESi m/s 138.1 $[M+H]^+$, 160.0 $[M+Na]^+$.

IR cm^{-1} 3099 (w), 3052 (w) 3033 (w), 2984 (w), 2947 (w), 2831 (w), 1692 (s), 1572 (s), 1489 (m), 1452 (m), 1380 (w), 1308 (m), 1261 (m), 1222 (m), 1117 (m), 1007 (s), 898 (m), 852 (s), 750 (m), 734 (m).

Melting point 38-40˚C.

Elemental Analysis found (Calculated for $C_7H_7NO_2$) % C 61.00 (61.31), H 4.98 (5.14), N 10.00 (10.21).

5.2.1 5-(Propargyloxy)picolinaldehyde**.**

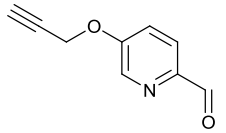

Potassium carbonate (0.59 g, 4.26 mmol) was added to a solution of 5-(hydroxy)picolinaldehyde (0.50 g, 4.06 mmol) in acetonitrile (40 ml). Propargyl bromide (80 wt% in toluene, 0.475 ml) was added. The solution was stirred at reflux temperature (ca. 85 °C) overnight, cooled to ambient temperature and passing a short column of silica. The solvent was evaporated and the crude

product was dissolved in dichloromethane, filtered and evaporated under reduced pressure to leave a dark orange oil. Yield = 0.45 g, 2.79 mmol, 69%.

^{1}H NMR (400 MHz, 298 K, DMSO) δ_H 9.90 (1H, s, HC=O), 8.53 (1H, d, $^{4}J_{HH}$ = 3.0 Hz), 7.97 (1H, d, $^{3}J_{HH}$ = 8.5 Hz), 7.64 (1H, dd, $^{3}J_{HH}$ = 8.5 Hz, $^{4}J_{HH}$ = 3.0 Hz, Py), 5.05 (2H, d, $^{4}J_{HH}$ = 2.5 Hz, CH_2–C≡C), 3.71 (1H, t, $^{4}J_{HH}$ = 2.5 Hz, C≡CH).

$^{13}C^{1}$ NMR (100 MHz, 298 K, DMSO) δ_C 191.9 (CO), 156.7, 146.1, 138.8, 123.3, 121.7 (Py), 79.4 (C≡CH), 78.9 (C≡CH), 56.3 (CH_2).

MS (ESI) m/z 162.2 $[M + H]^+$, 184.1 $[M + Na]^+$.

IR v cm^{-1} 3213 w, 2127 w, 1692 s, 1569 s, 1490 w, 1474 w, 1379 w, 1308 m, 1282 w, 1259 s, 1203 s, 1132 m, 1006 s, 975 m, 916 w, 835 s, 800 s, 762 m, 732 m, 694 s, 659 s.

Elemental Analysis found (Calculated for $C_9H_7NO_2$) % C 66.85 (67.07), H 4.02 (4.38), N 8.52 (8.69).

5.2.1.1 Benzyl azide[11]

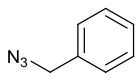

Benzyl bromide (2.0 ml, 16.84 mmol) was dissolved in DMSO (40 ml). Sodium azide (1.64 g, 25.26 mmol) was added as a solid and the reaction was stirred overnight at ambient temperature. Water (75 ml) was added slowly (exothermic)

before extracting the product into diethyl ether (3 × 150 ml). The combined diethyl ether layers were washed with brine (2 × 150 ml), dried over sodium sulfate and the solvent removed under reduced pressure to leave a clear colourless oil. Yield = 1.63 g, 12.24 mmol, 73%.

^{1}H NMR (400 MHz, 298 K, $CDCl_3$) δ_H 7.42–7.32 (5H, m, Ph), 4.35 (2H, s, CH_2).

^{13}C {^{1}H} NMR (100 MHz, 298 K, $CDCl_3$) δ_C 135.4, 128.9, 128.3, 128.2 (Py), 54.8 (CH_2).

MS (EI/CI) m/z 105.1 $[M - 2N]^+$.

IR v cm^{-1} 2090 s, 1497 w, 1455 m, 1253 m, 876 w, 735 m, 696 s.

Elemental Analysis found (Calculated for $C_7H_7N_3$) % C 63.53 (63.14), H 5.72 (5.30), N 31.34 (31.56).

5.2.2 Complexes

5.2.2.1 General procedure for $[Zn\mathbf{L}^{n}_{3}][ClO_4]_2$ complexes (*n* = 1-5).

2-Pyridinecarboxaldehyde (0.50 g, 3.1 mmol) and the desired substituted α-methylbenzylamine (3.1 mmol) were dissolved in acetonitrile (15 ml) to form a yellow solution. Zinc(II) perchlorate hexahydrate (1.0 eq.) in acetonitrile (5 ml) was added to give a yellow solution. This was stirred for 4 h at ambient temperature before the solvent was removed under reduced pressure. The product

was recrystallised from acetonitrile and ethyl acetate and the resulting purple crystals were filtered and dried *in vacuo*.

5.2.2.1.1 $[Zn\mathbf{L}^{\mathbf{1}}{}_3][ClO_4]_2$

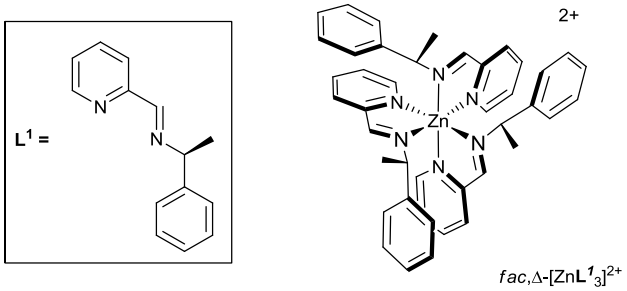

Yield = 0.28 g, 78 %.

^{1}H NMR**:** (300 MHz, 298 K, CD_3CN) δ_H ppm 8.21 (3H, s, HC=N), 8.07 (3H, t, $^{3}J_{HH}$ = 7.3 Hz, Py), 7.54 (6H, m, Ph), 7.44 (3H, m, Py), 7.41 (6H, m, Py), 7.08 (3H, t, $^{3}J_{HH}$ = 6.9, Ph) 6.91 (6H, d, $^{3}J_{HH}$ = 7.2 Hz, Ph), 6.65 (6H, d, $^{3}J_{HH}$ = 7.4 Hz, Ph), 5.47 (3H, m, CH), 1.63 (9H, d, $^{3}J_{HH}$ = 6.2 Hz, Me).

^{13}C {^{1}H} NMR (100 MHz, 298 K, CD_3CN) δ_C ppm 162.7 (N=CH), 148.7, 147.2, 142.4, 141.6, 131.0, 130.3, 129.7, 128.6, 126.1, 118.4 (Ar), 65.2 (CH), 23.8 (Me).

IR ν cm^{-1}: 1646 (m), 1597 (m), 1493 (m), 1444 (m), 1321 (m), 1231 (w), 1070 (s), 1016 (s), 923 (m).

Elemental Analysis found (calculated for $C_{42}H_{42}Cl_2ZnN_6O_8$) % C 55.56 (56.36), H 4.53 (4.73), N 9.16 (9.38)

5.2.2.1.2 $[Zn\mathbf{L}^{\mathbf{2}}_3][ClO_4]_2$

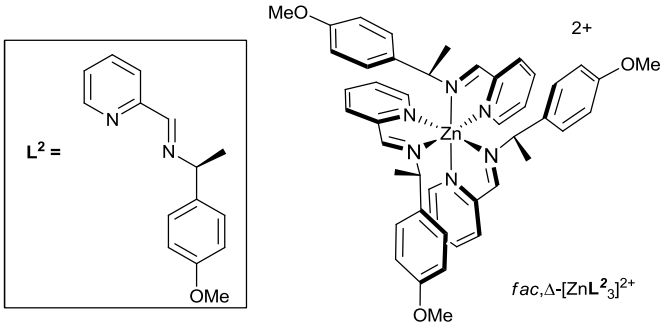

Yield = 0.36 g, 92 %.

^{1}H NMR: (400 MHz, 298 K, CD_3CN) δ_H ppm 8.27 (3H, s, HC=N), 8.08 (3H, td, $^3J_{HH}$ = 7.7 Hz, $^4J_{HH}$ = 1.5 Hz, Py), 7.55-7.48 (6H, m, Py), 7.38 (3H, d, $^3J_{HH}$ = 4.7 Hz, Py), 6.56 (6H, d, $^3J_{HH}$ = 8.6 Hz, Ph), 6.44 (6H, d, $^3J_{HH}$ = 8.6 Hz, Ph), 5.41 (3H, q, $^3J_{HH}$ = 6.5, CH), 3.73 (9H, s, OMe), 1.63 (9H, d, $^3J_{HH}$ = 6.5 Hz, Me).

^{13}C {^{1}H} NMR (100 MHz, 298 K, CD_3CN) δ_C ppm 160.9, 158.5, 147.4, 146.1, 140.9, 131.9, 129.3, 129.0, 126.6, 113.6 (Ar), 63.4 (CH), 54.7 (OMe), 22.3 (Me).

IRν cm^{-1}: 1728 (m), 1612 (sh), 1597 (m), 1571 (m), 1514 (s), 1485 (w), 1444 (m), 1390 (m),1321 (w), 1307 (m), 1277 (m), 1247 (s), 1178 (m), 1076 (s), 1035 (s), 1015 (sh), 982 (w), 921 (m), 832 (s), 811 (m).

MS (ESI) m/z 392.8 $[Zn\mathbf{L}^{\mathbf{2}}_3]^{2+}$.

Elemental Analysis found (calculated for $C_{45}H_{48}Cl_2ZnN_6O_{11}$) % C 53.64 (54.86), H 5.24 (4.91), N 8.31 (8.53)

Crystallography:

fac,Δ_{Zn},*R*$_C$-$[Zn\mathbf{L}^{\mathbf{2}}_3][ClO_4]_2$, *M* = 1108.33, Orthorhombic, *P*213, colourless block 0.50 × 0.50 × 0.50 mm, *a* = 17.41117(9), *b* = 17.41117(9), *c* = 17.41117(9) Å, α

= 90°, β = 90°, γ = 90°, U = 5278.17(5) Å^3, Z = 4, T = 100(2) K, radiation Mo-Kα (λ = 0.71073), 30966 total reflections, 4718 unique (R_{int} = 0.0211), R_1 = 0.0336 (obs. data), wR_2 = 0.0866 (all data), GooF 1.043, Flack 0.017(10).

5.2.2.1.3 [Zn$\mathbf{L}^{\mathbf{3}}_3$][$ClO_4$]$_2$

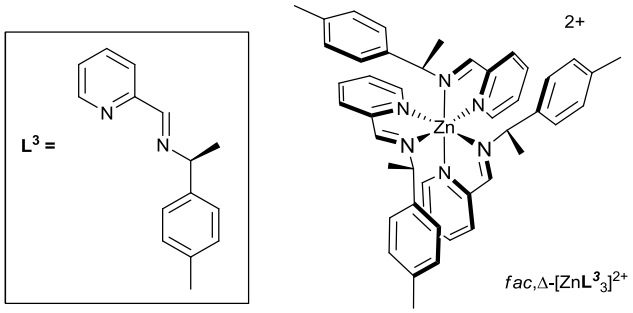

Yeild = 0.26 g, 70%.

^{1}H NMR: (400 MHz, 298 K, CD_3CN) δ_H ppm 8.20 (3H, s, HC=N), 8.08 (3H, td, $^3J_{HH}$ = 7.8 Hz, $^4J_{HH}$ = 1.4 Hz, Py), 7.53-7.49 (3H, m, Py), 7.45 (3H, d, $^3J_{HH}$ = 7.8 Hz, Py), 7.38 (3H, d, $^3J_{HH}$ = 4.81 Hz, Py), 6.69 (6H, d, $^3J_{HH}$ = 7.8 Hz, Ph), 6.51 (6H, d, $^3J_{HH}$ = 7.8 Hz, Ph), 5.41 (3H, q, $^3J_{HH}$ = 5.8, CH), 2.23 (9H, s, Me), 1.63 (9H, d, $^3J_{HH}$ = 6.8 Hz, Me).

^{13}C {^{1}H} NMR (100 MHz, 298 K, CD_3CN) δ_C ppm 161.0, 147.4, 146.0 140.7, 137.1, 137.0, 134.8, 129.2, 128.9, 125.3 (Ar), 63.6 (CH), 22.2, 19.6 (Me).

IRν cm^{-1}: 2985 (w), 2324 (w), 1730 (m), 1644 (m), 1597 (m), 1571 (w), 1515 (m), 1484 (m), 1444 (m), 1390 (m), 1320 (m), 1235 (m), 1074 (s), 1014 (m), 982 (m), 920 (m), 845 (w), 820 (m).

MS (ESI) m/z 368.2 [Zn$\mathbf{L}^{\mathbf{3}}_3$]$^{2+}$.

Elemental Analysis found (calculated for $C_{45}H_{48}Cl_2ZnN_6O_8$) % C 56.51 (57.67), H 5.55 (5.16), N 8.66 (8.96)

Crystallography:

fac,Δ_{Zn},R_C-[Zn$\mathbf{L}^3_3$][ClO_4]$_2$, M = 978.22, Orthorhombic, P213, colourless block 0.40 × 0.30 × 0.30 mm, a = 16.77238(9), b = 16.77238(9), c = 16.77238(9) Å, α = 90°, β = 90°, γ = 90°, U = 4718.29(4) Å^3, Z = 4, T = 100(2) K, radiation Mo-Kα (λ = 0.71073), 24927 total reflections, 4857 unique (R_{int} = 0.0250), R_1 = 0.0355 (obs. data), wR_2 = 0.0808 (all data), GooF 1.044, Flack 0.010(9).

5.2.2.1.4 [Zn$\mathbf{L}^4_3$][ClO_4]$_2$

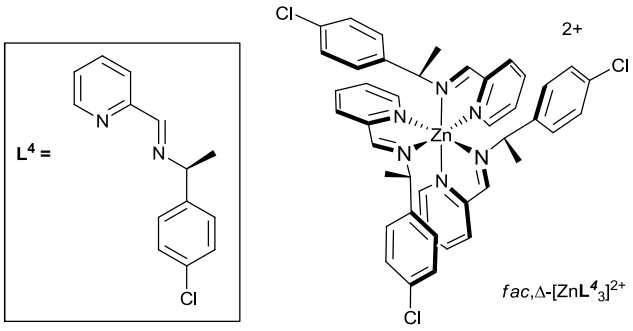

Yield = 0.30 g, 74 %.

^{1}H NMR: (400 MHz, 298 K, CD_3CN) δ_H ppm 8.32 (3H, s, HC=N), 8.14 (3H, td, $^3J_{HH}$ = 7.6 Hz, $^4J_{HH}$ = 1.3 Hz, Py), 7.59-7.52 (6H, m, Ph), 7.4 (3H, d, $^3J_{HH}$ = 5.1 Hz, Py), 6.90 (6H, d, $^3J_{HH}$ = 8.7 Hz, Ph), 6.65 (6H, d $^3J_{HH}$ = 8.8 Hz, Ph), 5.46 (3H, q, $^3J_{HH}$ = 6.3 Hz, CH), 1.63 (9H, d, $^3J_{HH}$ = 6.6 Hz, Me).

^{13}C {^{1}H} NMR (100 MHz, 298 K, CD_3CN) δ_C ppm 163.3, 149.1, 147.1, 142.4, 140.1, 134.0, 130.9, 130.7, 129.7, 128.3 (Ar), 64.6 (CH), 23.6 (Me).

IRν cm^{-1}: 3568 (w), 2984 (w), 1644 (m), 1597 (m), 1572 (w), 1484 (m), 1444 (m), 1409 (w), 1388 (w), 1319 (m), 1231 (m), 1068 (s), 1009 (s), 919 (m), 828 (m).

MS (ESI) m/z 398.1 $[Zn\mathbf{L^4}_3]^{2+}$.

Elemental Analysis found (calculated for $C_{42}H_{39}Cl_5ZnN_6O_8$) % C 49.23 (50.52), H 3.85 (3.94), N 8.12 (8.41).

5.2.2.1.5 $[Zn\mathbf{L^5}_3][ClO_4]_2$

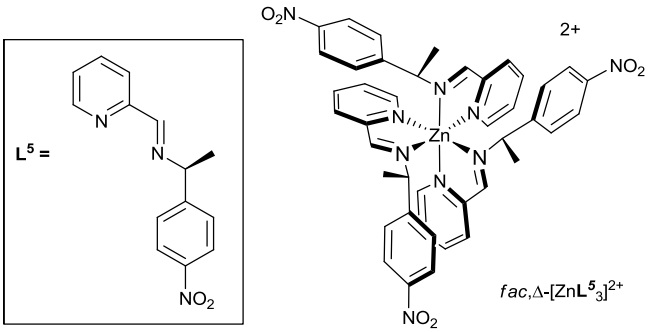

Yeild = 0.35 g, 84%.

^{1}H NMR: (300 MHz, 298 K, CD_3CN) δ_H ppm 8.30 (3H, s, HC=N), 8.11 (3H, td, $^{3}J_{HH}$ = 7.9 Hz, $^{4}J_{HH}$ = 1.6 Hz, Py), 7.73 (6H, d $^{3}J_{HH}$ = 8.8 Hz, Ph), 7.62 (3H, m, Py), 7.48 (6H, m, Py), 6.90 (6H, d, $^{3}J_{HH}$ = 8.8 Hz, Ph), 5.66 (3H, m, CH), 1.64 (9H, d, $^{3}J_{HH}$ = 6.7 Hz, Me).

^{13}C {^{1}H} NMR (75 MHz, 298 K, CD_3CN) δ_C ppm 164.29 (C=N), 159.9, 150.1, 149.29, 148.53, 144.8, 142.79, 131.18, 127.73, 124.79 (Ar), 64.70 (CH), 25.58 (Me).

IRν cm^{-1}: 1645 (m), 1598 (m), 1523 (s), 1484 (m), 1443 (m), 1389 (m), 1350 (s), 1312 (m), 1236 (m), 1073 (s), 1011 (m), 989 (w), 975 (w), 923 (m), 880 (w), 875 (s).

MS (ESI) m/z 414.7 $[Zn\mathbf{L}^{5}_{3}]^{2+}$.

Elemental Analysis found (calculated for $C_{42}H_{39}Cl_2ZnN_9O_{14}$) % C 48.26 (48.97), H 3.61 (3.82), N 11.66 (12.23)

Crystallography:

fac,Δ_{Zn},R_C-$[Zn\mathbf{L}^{5}_{3}][ClO_4]_2$, M = 1030.09, Orthorhombic, $P2_13$, colourless block 0.30 × 0.30 × 0.20 mm, a = 16.53113(5), b = 16.53113(5), c = 16.53113(5) Å, α = 90°, β = 90°, γ = 90°, U = 4571.60(2) $Å^3$, Z = 4, T = 100(2) K, radiation Mo-Kα (λ = 1.54184 Å), 30381 total reflections, 2903 unique (R_{int} = 0.0279), R_1 = 0.0345 (obs. data), wR_2 = 0.0919 (all data), GooF 1.050, Flack 0.001(19).

5.2.2.2 General procedure for $[Zn\mathbf{L}^{n}_{3}][ClO_4]_2$ complexes (n = 6,7).

The desired substituted aldehyde (3.1 mmol) and (*S*)-α-methylbenzylamine (0.38 g, 3.1 mmol) were dissolved in acetonitrile (15 ml) to form a yellow solution. Zinc(II) perchlorate hexahydrate (1.0 eq.) in acetonitrile (5 ml) was added to give

a yellow solution. This was stirred for 4 h at ambient temperature, before the solvent was removed under reduced pressure. The product was recrystallised from acetonitrile and ethyl acetate and the resulting purple crystals were filtered and dried *in vacuo*.

5.2.2.2.1 $[Zn\mathbf{L^6}_3][ClO_4]_2$

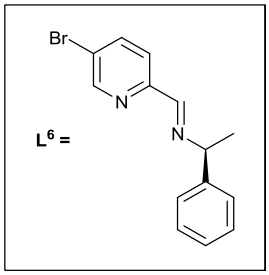

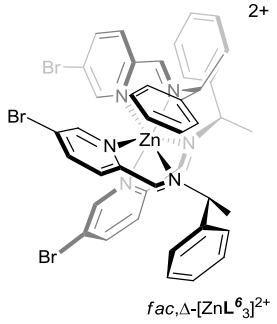

fac,Δ-$[Zn\mathbf{L^6}_3]^{2+}$

Yield = 0.38 g, 83%.

^{1}H NMR (400 MHz, 298 K, CD_3CN) δ_H ppm 8.25 (3H, s, HC=N), 8.24 (3H, dd, $^3J_{HH}$ = 8.4 Hz, $^4J_{HH}$ = 2,3 Hz, Py), 7.58 (3H, d, $^4J_{HH}$ = 2.03 Hz, Py), 7.33 (3H, d, $^3J_{HH}$ = 8.4 Hz, Py), 7.12 (3H, t, $^3J_{HH}$ = 7.4 Hz, Ph), 6.44 (6H, t, $^3J_{HH}$ = 7.9 Hz, Ph), 6.69 (6H, d, $^3J_{HH}$ = 7.9 Hz, Ph), 5.42 (3H, q, $^3J_{HH}$ = 6.5, CH), 1.65 (9H, d, $^3J_{HH}$ = 6.7 Hz, Me).

^{13}C {^{1}H} NMR (100 MHz, 298 K, CD_3CN) δ_C ppm 162.8 (C=N), 150.5, 145.9, 145.3, 141.4, 131.85, 129.9, 128.9, 126.7, 126.6 (Ar), 65.4 (CH), 23.9 (Me).

IRν cm^{-1}: 2978 (w), 1726 (m), 1642 (m), 1583 (m), 1554 (m), 1494 (w), 1476 (w), 1454 (m) 1374 (m) 1325 (w), 1246 (m), 1081 (s), 1030 (s), 1010 (m), 991 (sh), 925 (m), 872 (w), 849 (m).

MS (ESI) m/z 310.2 $[Zn\mathbf{L^6}_3]^{2+}$.

Elemental Analysis found (calculated for $C_{42}H_{39}Br_3Cl_2ZnN_6O_8$) % C 44.43 (44.57), H 3.94 (3.47), N 6.7 (7.42)

Crystallography:

fac,Δ_{Zn},R_C-[Zn$\mathbf{L}^{\mathbf{6}}_3$][$ClO_4$]$_2$, M = 1162.58, Orthorhombic, $P2_13$, colourless block 0.50 × 0.50 × 0.50 mm, a = 18.02363(12), b = 18.2363(12), c = 18.2363(12) Å, α = 90°, β = 90°, γ = 90°, U = 5585.00(7) Å^3, Z = 4, T = 100(2) K, radiation Mo-Kα (λ = 1.54184), 34442 total reflections, 3748 unique (R_{int} = 0.0452), R_1 = 0.0698 (obs. data), wR_2 = 0.1918 (all data), GooF 1.078, Flack 0.03(4).

5.2.2.2.2 [Zn$\mathbf{L}^{\mathbf{7}}_3$][$ClO_4$]$_2$

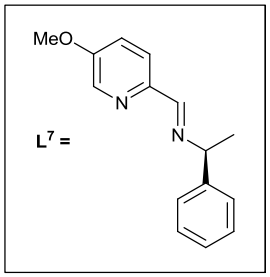

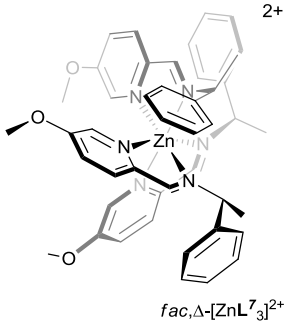

fac,Δ-[Zn$\mathbf{L}^{\mathbf{7}}_3$]$^{2+}$

Yield = 0.36 g, 91%.

^{1}H NMR (400 MHz, 298 K, CD_3CN) δ_H ppm 8.08 (3H, s, HC=N), 7.55 (3H, dd, $^3J_{HH}$ = 8.7 Hz, $^4J_{HH}$ = 2.7 Hz, Py), 7.43 (3H, d, $^3J_{HH}$ = 8.72 Hz, Py), 7.09 (3H, t, $^3J_{HH}$ = 7.6 Hz, Ph), 6.98-6.91 (9H, m, Ph/Py), 6.70 (6H, d, $^3J_{HH}$ = 7.8 Hz, Ph), 5.42 (3H, q, $^3J_{HH}$ = 6.6, CH), 3.38 (9H, s, OMe), 1.59 (9H, d, $^3J_{HH}$ = 6.7 Hz, Me).

^{13}C {^{1}H} NMR (100 MHz, 298 K, CD_3CN) δ_C ppm 160.3, 159.5, 140.6, 138.8, 137.1, 130.8, 128.3, 127.2, 125.3, 122.5 (Ar), 63.5 (CH), 56.1 (OMe), 22.4 (Me).

IRν cm^{-1}: 3057 (w), 1707 (w), 1640 (w), 1592 (w), 1570 (s), 1492 (m), 1452 (m), 1411 (m), 1411 (w), 1389 (m), 1312 (m), 1262 (m), 1227 (m), 1184 (w), 1143 (w), 1078 (s), 1010 (m), 924 (m).

MS (ESI) m/z 368.1 $[Zn\mathbf{L}^{7}_{3}]^{2+}$.

Elemental Analysis found (calculated for $C_{45}H_{48}Cl_2ZnN_6O_{11}$) % C 54.24 (54.86), H 4.58 (4.91), N 8.50 (8.53)

Crystallography:

fac,Δ_{Zn},R_C-$[Zn\mathbf{L}^{7}_{3}][ClO_4]_2$, M = 1067.27, Orthorhombic, $P2_12_12_1$, colourless block 0.38 × 0.38 × 0.16 mm, a = 17.3753(3), b = 17.80903(18), c = 19.6784(2) Å, α = 90°, β = 90°, γ = 90°, U = 6089.24(14) $Å^3$, Z = 4, T = 100(2) K, radiation Mo-Kα (λ = 1.54184), 40252 total reflections, 11624 unique (R_{int} = 0.0517), R_1 = 0.0720 (obs. data), wR_2 = 0.1994 (all data), GooF 1.071, Flack 0.01(2).

5.2.2.3 $[Fe\mathbf{L}^{9}_{3}][ClO_4]_2$.

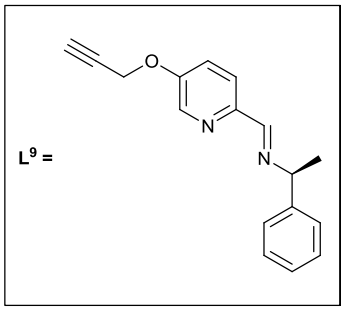

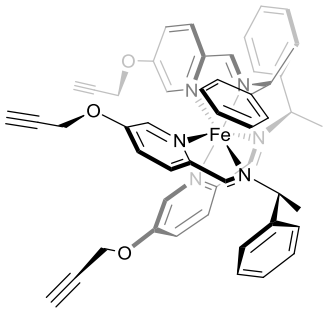

fac,Δ_{Fe},S_c-$[Fe\mathbf{L}^{9}_{3}][ClO_4]_2$

5-(Propargyloxy)picolinaldehyde (0.50 g, 3.1 mmol) and (S)-α-methylbenzylamine (0.38 g, 3.1 mmol) were dissolved in acetonitrile (15 ml) to form a yellow solution. Iron(II) perchlorate hexahydrate (0.38 g, 1.0 mmol, 1.0 eq.) in acetonitrile (5 ml) was added to give a purple solution. This was stirred overnight at ambient temperature before the solvent was removed under reduced pressure. The product, was recrystallised from acetonitrile and ethyl acetate and the resulting purple crystals were filtered and dried in vacuo. Yield = 0.65 g, 0.59 mmol, 59%.

^{1}H NMR (400 MHz, 298 K, CD_3CN) δ_H 8.62 (3H, s, HC=N), 7.42–7.35 (6H, m, Py), 7.09 (3H, t, $^{3}J_{HH}$ = 7.5 Hz, Ph para), 7.00 (6H, t, $^{3}J_{HH}$ = 7.5 Hz, Ph meta), 6.62 (6H, d, $^{3}J_{HH}$ = 7.5 Hz, Ph ortho), 6.35 (3H, d, $^{4}J_{HH}$ = 2.5 Hz, Py), 5.22 (3H, q, $^{3}J_{HH}$ = 6.5 Hz, CH), 4.72 (3H, dd, $^{2}J_{HH}$ = 16.5 Hz, $^{4}J_{HH}$ = 2.5 Hz, CH_2–C≡C), 4.64 (3H, dd, $^{2}J_{HH}$ = 16.5 Hz, $^{4}J_{HH}$ = 2.5 Hz, CH_2–C≡C), 2.94 (3H, t, $^{4}J_{HH}$ = 2.5 Hz, C≡CH), 1.92 (9H, d, $^{3}J_{HH}$ = 6.5 Hz, CH_3).

^{13}C{^{1}H} NMR (100 MHz, 298 K, CD_3CN) δ_C 170.5 (C=N), 156.7, 152.9, 142.9, 140.9, 130.9, 130.0, 128.4, 125.5, 124.5 (Ar), 79.0 (C≡CH), 77.7 (C≡CH), 69.4 (CH), 57.3 (CH_2), 26.3 (CH_3).

MS (ESI) m/z 424.2 $[Fe\mathbf{L}^{\mathbf{9}}_3]^{2+}$.

IR v cm^{-1} 3256 w, 1592 w, 1560 m, 1496 m, 1452 w, 1383 w, 1297 w, 1278 m, 1229 m, 1070 s, 1007 s, 928 m, 838 m, 760 m, 740 w, 700 s.

Elemental Analysis found (calculated for $C_{51}H_{48}Cl_2FeN_6O_{11}$) % C 58.61 (58.47), H 4.52 (4.62), N 7.94 (8.02).

5.3 **Experimental for Chapter 3**

5.3.1 Ligand Components

5.3.1.1 1-(2-Pyridylacetyl)pyridinium iodide.[12]

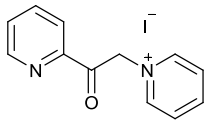

2-Acetylpyridine (6.05 g, 5.6 ml, 50 mmol) was added via syringe to a solution of iodine (12.69 g, 50 mmol) in dry pyridine (50 ml) in a 250 ml round bottomed Schlenk vessel. The round bottomed Schlenk was fitted with a condenser and a N_2 bubbler, and the reaction was stirred and heated at reflux (130^{o}C) for 2 h. The solution was then cooled to ambient temperature. A 9:1 mixture of diethyl ether/ethanol (20 ml) was added and the solution was cooled to 0^{o}C using an ice/water bath. The resulting black precipitate was filtered off, washed with a 9:1 mixture of diethyl ether/ethanol (20 ml), and dried in air. The solid was then dissolved in boiling methanol (200 ml) with activated charcoal (20 g) and stirred at reflux for 10 min. The solution was filtered through celite in a fritted funnel and the solvent was removed under reduced pressure to leave the crude product. Recrystallisation from hot methanol (100 ml) resulted in light brown crystals which were filtered, washed with cold methanol (25 ml), and dried *in vacuo*. Yield = 6.07 g, 18.61 mmol, 37%.

^{1}H NMR (400 MHz, 298 K, DMSO) δ_H ppm 9.02 (2H, dd, $^3J_{HH}$ = 6.5 Hz, $^4J_{HH}$ = 1.0 Hz, Py), 8.87 (1H, dt, $^3J_{HH}$ = 4.5 Hz, $^4J_{HH}$ = 1.0 Hz, Py), 8.73 (1H, tt, $^3J_{HH}$ = 8.0 Hz, $^4J_{HH}$ = 1.5 Hz, Py), 8.28 (2H, m, Py), 8.14 (1H, td, $^3J_{HH}$ = 7.5 Hz, $^4J_{HH}$ =

1.5 Hz, Py), 8.07 (1H, dt, $^{3}J_{HH}$ = 8.0 Hz, $^{4}J_{HH}$ = 1.0 Hz, Py), 7.84 (1H, m, Py), 6.51 (2H, s, CH_2).

$^{13}C\{^{1}H\}$ NMR (100 MHz, 298 K, DMSO) δ_C ppm 191.49 (C=O), 150.46, 149.58, 146.36, 146.31, 138.17, 129.16, 127.73, 122.06 (Py), 66.66 (CH_2).

MS (ESI) m/z 199.1 [M+].

5.3.1.2 5-methyl-2,2'-bipyridine.[13]

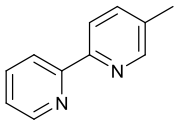

1-(2-Pyridylacetyl)pyridinium iodide (43.58 g, 134 mmol) and ammonium acetate (23.69 g, 307 mmol) were dissolved in formamide (250 ml). Freshly distilled methacrolein (10.3 g, 12.1 ml, 145 mmol) was then added *via* syringe and the reaction was stirred at 80°C for 6 h. The solution was then cooled to ambient temperature and water (150 ml) was added and the reaction mixture was extracted into DCM (3 × 250 ml). The DCM extracts were combined, dried over sodium sulphate and the solvent was removed under reduced pressure to leave the crude product as a yellow liquid. Distillation under vacuum at 110˚C gave the desired product as a pale yellow oil. Yield = 20.12 g, 89%.

^{1}H NMR (400 MHz, 298 K, $CDCl_3$) δ_H ppm 8.65 (1H, d, $^{3}J_{HH}$ = 5.0 Hz, Py), 8.50 (1H, d, $^{4}J_{HH}$ = 2.0 Hz, Py), 8.34 (1H, d, $^{3}J_{HH}$ = 8.0 Hz, Py), 8.27 (1H, d, $^{3}J_{HH}$ = 8.0 Hz, Py), 7.78 (1H, td, $^{3}J_{HH}$ = 7.5 Hz, $^{4}J_{HH}$ = 2.0 Hz, Py), 7.61 (1H, dd, $^{3}J_{HH}$ = 8.0 Hz, $^{4}J_{HH}$ = 2.0 Hz, Py), 7.28-7.24 (1H, m, Py), 2.38 (3H, s, CH_3).

$^{13}C\{^{1}H\}$ NMR (100 MHz, 298K, $CDCl_3$) δC ppm 156.41, 153.75, 149.75, 149.23, 137.58, 136.98, 133.53 , 123.49, 120.91, 120.72 (Py), 18.46 (CH_3).

MS (ESI) m/z 171.1 $[M+H]^+$, 193.1 $[M+Na]^+$.

5.3.1.3 5-((trimethylsilyl)methyl)-2,2'-bipyridine.[14]

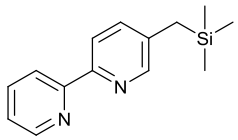

A Schelnk vessel was charged with dry THF (30 ml), diisopropylamine (1.18 ml, 8.4 mmol) and the solution was cooled to -78˚C, at which point n-butyllithium (2.8ml, 2.5 M, 7.0 mmol) was added and the resulting solution was stirred for 10 min before being warmed to 0˚C for a further 10 min. The reaction mixture was then cooled again to -78˚C and a solution of 5-methyl-2,2'-bipyridine (1.0 g, 5.9 mmol) in dry THF was added dropwise. The resulting maroon solution was stirred for a 1 h at -78˚C. Chlorotrimethylsilane (0.9 ml, 7.1 mmol) was then added rapidly to the solution and after 1 min the reaction was quenched by the rapid addition of absolute ethanol. The resulting pale yellow/green solution was allowed to warm up to room temperature before a saturated solution of $NaHCO_3$ (150 ml), was added and the reaction mixture was extracted into DCM (3 x 75 ml). The organic fractions were combined, washed with brine, dried over sodium sulphate, filtered and solvents removed under reduced pressure to yield the titular product as a white solid that was used without purification. Yeild = 1.89 g 84%

^{1}H NMR (400 MHz, 298 K, $CDCl_3$) δ_H ppm 8.69 (1H, dq, $^{3}J_{HH}$ = 4.7 Hz, $^{4}J_{HH}$ = 0.9 Py), 8.41 (2H, m, Py), 8.33 (1H, d, $^{3}J_{HH}$ = 8.3 Hz, Py), 7.78 (1H, td, $^{3}J_{HH}$ =

7.8 Hz, $^{4}J_{HH}$ = 2.0 Hz, Py), 7.46 (1H, dd, $^{3}J_{HH}$ = 8.0 Hz $^{4}J_{HH}$= 2.5, Hz Py), 7.25 (1H, ddd, $^{3}J_{HH}$ = 7.5 Hz $^{3}J_{HH}$ = 4.7 Hz $^{4}J_{HH}$ = 1.2, Py), 2.14 (2H, s, CH_2), 0.05 (9H, s, $SiMe_3$).

$^{13}C\{^{1}H\}$ NMR (100 MHz, 298K, $CDCl_3$) δ_C ppm 156.2, 152.1, 148.9, 148.3, 136.6, 136.2, 135.8, 122.9, 120.4, 120.3 (py), 23.8 (*C*H_2), 2.2 (Si*C*H_3).

MS (ESI) m/z 243.0 $[M+H]^+$,

IR cm^{-1}: 3050.3 (w), 3002.1 (w), 2921.0 (w), 1588.8 (m), 1575.0 (m), 1557.1 (w), 1491.0 (w), 1458.2 (s), 1431.7 (s), 1378.8 (m), 1269.2 (w), 1244.1 (w), 1218.0 (w), 1145.2 (w), 1127.57 (m), 1040.32 (m), 1027.3 (m), 991.3 (m), 922.1 (w), 898.9 (w) 874.0 (m).

5.3.1.4 5-(chloromethyl)-2,2'-bipyridine.[14]

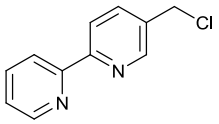

5-((trimethylsilyl)methyl)-2,2'-bipyridine (1.16 g, 4.5 mmol), hexachloroethane (4.06 g, 9.0 mmol) and caesium fluoride (1.46 g, 9.0 mmol) were suspended in dry acetonitrile (75 ml) and heated to 60˚C for 4 H. The reaction mixture was cooled to 25˚C, water (100 ml) was added and the product was extracted in to ethyl acetate (3 x 150 ml). The organic fractions were combined, washed with brine, dried over sodium sulphate, filtered and solvents were removed under reduced pressure. The product was purified by sublimation of any residual hexachloroethane at 60˚C under vacuum to leave the desired product as a beige solid. Yield = 0.84 g, 84 %.

^{1}H NMR (300 MHz, 298 K, $CDCl_3$) δ_H ppm 8.71-8.66 (2H, m, Py), 8.45-8.38 (2H, m, Py), 7.89-7.79 (2H, m, Py), 7.32 (1H, ddd, $^{3}J_{HH}$ = 7.4 Hz $^{3}J_{HH}$ = 4.9 Hz $^{4}J_{HH}$ = 1.1, Py), 4.65 (2H, s, C*H*$_2$).

^{13}C{^{1}H} NMR (75 MHz, 298K, $CDCl_3$) δ_C ppm 156.2 (py), 155.6 (py), 149.3 (py), 149.0 (py), 137.3 (py), 137.0 (py), 133.2 (py), 124.0 (py), 121.3 (py), 121.0 (py), 43.2 (*C*H$_2$).

MS (ESI) m/z 205.0 $[M+H]^+$.

IR cm^{-1}: 3053 (w), 3008 (w), 2969 (w), 1598 (m), 1587 (m), 1573 (m), 1557 (m), 1493 (w), 1458 (m), 1436 (m), 1392 (m), 1263 (m), 1219 (w), 1196 (w), 1149 (w), 1128 (w), 1090 (w), 1062 (w), 1041 (w), 1028 (m), 993 (w), 935 (w), 904 (s), 857 (w), 834 (m).

Elemental Analysis found (Calculated for $C_{11}H_9N_2Cl$) % C 64.56 (64.56), H 4.32 (4.43), N 13.58 (13.68).

5.3.1.5 *R*-phenylglycinol.[15]

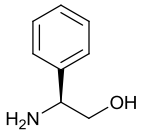

A solution of (*R*)-phenylglycine (15.0 g, 99.2 mmol) in THF (100 ml) was added dropwise to a stirred suspension to lithium aluminium hydride (7.5 g, 19.8 mmol) in THF (100 ml) over 30 min at 0 °C. The resulting solution was heated to refluxed overnight at 70 °C under an atmosphere of dinitrogen. On cooling to room temperature the reaction was quenched by the careful addition of saturated

potassium carbonate solution. The crude product was obtained as a yellow solid after filtration of solids and removal of solvents under reduced pressure. Recrystallisation from hot toluene gave the desired product as a white microcrystalline solid. Yield 7.4 g, 54%

^{1}H NMR (400 MHz, $CDCl_3$) δ_H ppm 7.3-7.1 (m, 5 H, Ar-H), 3.97 (dd, J = 8.3, 3.9 Hz, 1 H, CH), 3.66 (dd, J = 10.8, 4.4, 1 H, CH_2), 3.48 (dd, J = 10.7, 8.3, 3 H, CH_2), 2.00 (bs, 3 H).

^{13}C {^{1}H} NMR (100 MHz, $CDCl_3$) δ_C ppm 142.7, 128.7, 127.5, 126.5 (Ph), 68.0 (CH_2), 57.4 (CH).

MS (ESI) 138.3 $[M+H]^+$, 160.2 $[M+Na]^+$.

IR ν cm^{-1}: 2835 (m), 1604 (m), 1497 (m), 1453 (m), 1361 (w), 1197 (w), 1077 (m), 1047 (m), 978 (m), 882 (m), 755 (s), 700 (s).

Melting Point 76-78°C (Lit. mp 76-79°C).[16]

Elemental Analysis found (Calculated for $C_8H_{11}NO$) % C 69.79 (70.04), H 8.08 (8.08), N 10.18 (10.21).

Optical Rotation = -25.99° (Lit = -25.8°).[17]

The *S* enantiomer was synthesised in an identical manner but starting from (S)-phenylglycine. Yield 7.2 g, 53%. Optical Rotation = +25.97°

5.3.1.6 (*S*)-2-(2,2'-bipyridin-5-ylmethoxy)-1-phenylethanamine.

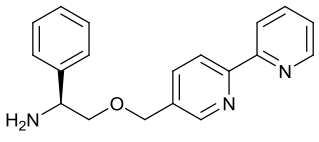

S-Phenylglycinol (1.00 g, 7.3 mmol) was dissolved in dry THF (20 ml) and was added dropwise to a stirred suspension of sodium hydride (0.36 g, 15.0 mmol) in dry THF (10 ml). The solution was stirred for 1 h at room temperature. A solution of 5-(bromomethyl)-2,2'-bipyridine (1.82 g, 7.3 mmol) in dry THF (20 ml) was added dropwise and the solution was stirred for 1 h at room temperature before being heated to reflux (65˚C) for a further 2 h. The mixture was cooled to ambient temperature and brine (40 ml) was adde. The product was extracted with diethyl ether (4 × 60 ml), dried over sodium sulphate and the solvent was removed to leave a dark yellow oil. This crude product was purified by Kugelrohr distillation to give a yellow oil that solidifies on standing. Yield = 1.25, 56 %.

^{1}H NMR (300 MHz, $CDCl_3$) δ_H ppm 8.61-8.59 (m, 1 H, Ar-H), 8.56 (d, J_{HH} 2.1 Hz, 1 H, Ar-H), 8.33-8.29 (m, 2 H, Ar-H), 7.76-7.67 (m, 2 H, Ar-H), 7.33-7.16 (m, 6 H, Ar-H), 4.54 (s, 2 H, *OCH*$_2$), 4.19 (dd, $^{2}J_{HH}$ = 4, $^{3}J_{HH}$ = 9.0, 1 H, C*H*), 3.58 (dd, $^{2}J_{HH}$ = 4, $^{3}J_{HH}$ = 8.9, 1 H, C*H*$_2$), 3.44 (t, $^{3}J_{HH}$ = 8.7, 1 H, C*H*$_2$).

^{13}C {^{1}H} NMR (75 MHz, $CDCl_3$) δ_C ppm 156.0, 155.7, 149.3, 148.6, 142.3, 137.0, 136.4, 133.7, 128.5, 127.6, 126.9, 123.8, 121.1, 120.9 (Ar), 76.9 (CH_2), 70.7 (CH_2), 55.6 (CH).

MS (ESI) 306.2 $[M+H]^+$.

IR ν cm^{-1}: 3361 (w), 3296 (w), 3055 (w), 3027 (w), 2902 (w), 2860 (w), 1589 (w), 1574 (w), 1558 (w), 1490 (w), 1459 (m), 1434 (w), 1414 (w), 1387 (w), 1349 (w), 1257 (m), 1098 (m), 1038 (w), 1022 (m), 991 (w), 936 (w).

Elemental Analysis found (Calculated for $C_8H_{11}NO$) % C 74.75 (74.73), H 6.13 (6.27), N 13.67 (13.76).

Optical Rotation = +15.41° (Recorded at 578 nm, 1.65 g/100 ml, methanol, 25 ˚C)

The *S* enotomer was synthesis in an identical manner but starting from (R)-phenylglycine. Yield 1.34 g, 60 %.

5.3.1.7 5-(benzyloxy)picolinaldehyde

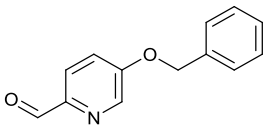

Potassium carbonate (0.59 g, 4.26 mmol, 1.05 eq.) was added to a solution of 5-(hydroxy)picolinaldehyde (0.50 g, 4.06 mmol, 1.0 eq.) in acetonitrile (40 ml). Benzyl bromide (0.73 g, 0.5 ml, 4.26 mmol, 1.05 eq.) was added to the reaction. The solution refluxed overnight before cooling to room temperature. The reaction mixture was then passed down a short column of silica, eluting with acetonitrile until the product was fully removed (monitored *via* TLC - a brown impurity remains at the top of the silica column). The solvent was then removed and the crude product was disolved in DCM, filtered through fluted filter paper, and the solvent removed from the filtrate under reduced pressure to leave a dark

orange oil, which was dried overnight *in vacuo*. Yield = 0.67 g, 3.14 mmol, 77 %.

^{1}H NMR (300 MHz, $CDCl_3$) δ_H ppm 9.99 (1H, s, COCH), 8.52 (1H, d, $^{2}J_{HH}$ = 2.7, Py), 7.96 (1H, d, $^{3}J_{HH}$ = 8.63, Py), 7.43 (6H, m, Py/Ph), 5.21 (2H, s, CH_2).

^{13}C {^{1}H} NMR (75 MHz, $CDCl_3$) δ_C ppm 192.1 (CO), 158.2, 139.2, 135.2, 129.0, 128.8, 127.7, 127.1, 123.5, 121.1 (Ph/Py), 70.78 (CH_2).

MS (ESI) m/z 236.1 $[M+Na]^+$

IR cm^{-1} 2836 (w), 1698 (s), 1571 (s), 1501 (w), 1477 (w), 1462 (w), 1452 (m), 1387 (m), 1370 (w), 1310 (s), 1262 (m), 1209 (s), 1130 (m), 1045 (w), 1032 (w), 1012 (w), 996 (w), 912 (w), 872 (w), 835 (m), 790 (w), 740 (s), 696 (s).

Elemental analysis found (Calculated for $C_{13}H_{11}NO_2$) % C 72.67 (73.23), H 5.38 (5.20), N 6.36 (6.57).

5.3.1.8 1-(azidomethyl)-4-fluorobenzene.

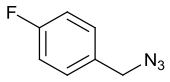

Benzyl bromide (2.0 ml, 16.84 mmol, 1.0 eq.) was dissolved in DMSO (40 ml). Sodium azide (1.64 g, 25.26 mmol, 1.5 eq.) was added as a solid and the reaction was stirred overnight at room temperature. The reaction was quenched with water (75 ml) and extracted with diethyl ether (3 × 150 ml). The combined diethyl ether layers were washed with brine (2 × 150 ml), dried over sodium sulfate and the solvent was removed to leave a clear oil. Yield = 1.63 g, 12.24 mmol, 73%.

^{1}H NMR (300 MHz, 298 K, $CDCl_3$) δ_H ppm 7.32-7.25 (2H, m, Ar), 7.10-7.00 (2H, m, Ar), 4.39 (2H, s, C*H*$_2$).

$^{13}C\{^{1}H\}$ NMR (75 MHz, 298K, $CDCl_3$) δ_C ppm 164.3 (Ph), 161 (Ph), 130.0 (d, $J_{C\text{-}C\text{-}C\text{-}F}$ 8.8 Hz, Ph), 115.9 (d, $J_{C\text{-}C\text{-}F}$ 20.8 Hz, Ph) 54.0 (CH_2)

Mass $[M+Li]^+$ 157.0

Ir 2935 (w), 2092 (s), 1894 (w), 1601 (m), 1509 (s), 1448 (w), 1417 (w), 1343 (m), 1221 (s), 1157 (s), 1098 (m), 1060 (m), 1015 (m), 946 (w), 880 (m), 850 (m), 820 (s).

5.3.1.9 Methyl pyrazine-2-carboxylate.[18]

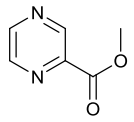

Thionyl chloride (13 ml, 21.41 g, 0.18 mol, 1.1 eq.) was added *via* syringe over 10 min under argon to dry methanol (250 ml) at 0°C. After stirring at 0°C for 15 min, 2-pyrazinecarboxylic acid (20.00 g, 0.16 mol, 1eq.) was added slowly as a solid. The reaction was then heated to 60°C for 2 h under dinitrogen. After cooling to room temperature, a solution of sodium hydrogen carbonate (29 g, 0.35 mol) in water (280 ml) was added. The solution was transferred to a round bottomed flask and the methanol (but not the water) was removed using a rotary evaporator with a water bath held at 45°C. The aqueous layer was extracted using DCM (3 × 100 ml) and the combined DCM layers were dried over sodium sulfate, filtered, and the solvent removed to leave a white solid. Mass = 19.06 g, 0.138 mol, 86 %.

^{1}H NMR (400 MHz, 298 K, $CDCl_3$) δ_H ppm 9.20 (1H, d, $^{4}J_{HH}$ = 1.35 Hz), 8.68 (1H, d, $^{3}J_{HH}$ = 2.41 Hz), 8.62 (1H, m, Py), 3.93 (3H, s, OMe)

$^{13}C\{^{1}H\}$ NMR (100 MHz, 298K, $CDCl_3$) δ_C ppm164.3 (C=O), 147.7, 146.2, 144.3, 143.2 (Ph), 53.0 (CH_3).

Mass (ESI) m/z 161.0 $[M+Na]^+$

Ir 3431 (w), 3090 (w), 3064 (w), 3017 (w), 2960 (w), 1718 (s), 1582 (m), 1526 (w), 1475 (m), 1442 (m), 1407 (m), 1313 (s), 1193 (m), 1167 (m), 1131 (s), 1051 (s), 1020 (s), 954 (m), 881 (m), 842 (m).

5.3.1.10 Pyrazine-2-carboxaldehyde.[18]

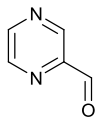

Methyl pyrazine-2-carboxylate (10.00 g, 72.40 mmol, 1 eq.) was dissolved in dry THF (200 ml) and cooled to -78°C then a suspension of lithium aluminium hydride (1.41 g, 37.23 mmol, 0.51 eq.) in dry THF (~75 ml) was added dropwise over a period of 30 min. The reaction was stirred at -78°C for a further 15 min before the reaction was quenched with glacial acetic acid (10 ml). The solvent was then removed under reduced pressure and the remaining residue was dissolved in a mixture of HCl aq. (2 M, 90 ml) and chloroform (40 ml). The organic phase was separated and the aqueous layer was extracted with chloroform (2 × 100 ml). Sodium bicarbonate (10 g) in water (20 ml) was added to the combined chloroform layers and the mixture was stirred until fizzing stopped. The layers were separated and the chloroform layer was dried over

Na_2SO_4, filtered and the solvent removed to leave an orange liquid, which was purified by Kugelrohr distillation (70 ˚C under high vaccum), to give a white solid. Mass = 4.01 g, 34.97 mmol, 51%.

^{1}H NMR (400 MHz, 298 K, $CDCl_3$) δ_H ppm 10.14 (1H, s, HC=O), 9.15 (1H, d, $^4J_{HH}$ = 1.4, Py), 8.79 (1H, d, $^3J_{HH}$ = 2.4 Hz, Py), 8.75 (1H, m, Py).

$^{13}C\{^1H\}$ NMR (100 MHz, 298 K, $CDCl_3$) δ_C ppm 192.6 (C=O), 148.6, 147.0, 145.0, 143.6 (Py).

Mass (ESI) m/z 131.0 $[M+Na]^+$

IR cm^{-1} 3039 (w), 2848 (w), 1714 (s), 1618 (w), 1575 (s), 1526 (m), 1470 (m), 1405 (s), 1367 (w), 1305 (m), 1237 (s), 1164 (s),1047 (s), 1015 (s), 838 (s).

5.3.2 Complexes

5.3.2.1 General procedure for the synthesis of complexes R_C,Δ_{Zn},HHT-$[Zn_2\mathbf{L}^{n}_3][ClO_4]_4$ (n = 12, 15-19).

$Zn(ClO_4)_2{\cdot}6H_2O$ (0.21 g, 0.56 mmol) was added to a stirred solution of the desired substituted aldehyde (0.85 mmol) and (R)-2-(2,2'-bipyridin-5-ylmethoxy)-1-phenylethanamine (0.26 g, 0.85 mmol) in acetonitrile (20 ml) at ambient temperature and stirred for 4 h. The resulting yellow solution yielded the desired product as a yellow crystalline solid on the addition of ethyl acetate.

5.3.2.2 R_C,Δ_{Zn},HHT-$[Zn_2\mathbf{L}^{12}{}_3][ClO_4]_4$

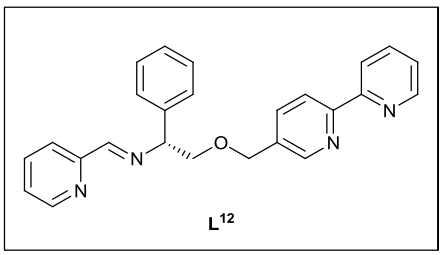

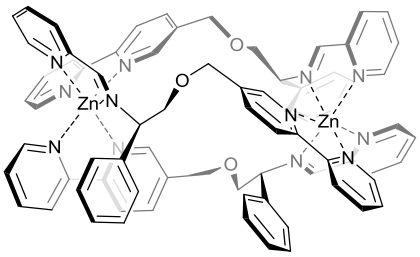

Yield 0.73 g, 76 %.

^{1}H NMR (300 MHz, 298 K, CD_3CN) δ_H ppm 9.34(1H, s,), 9.32(1H, s, HC=N), 9.22 (1H, s,), 9.17 (1H, s, Py), 9.12 (1H, s, HC=N), 8.86-7.37 (31H, m, Py), 7.16,-6.83 (7H, m), 6.68 (2H, t, $^3J_{HH}$ = 8.0 Hz), 6.53 (2H, t, $^3J_{HH}$ = 8.0 Hz), 6.07 (2H, d, $^3J_{HH}$ = 7.2 Hz), 5.95 (2H, d, $^3J_{HH}$ = 7.2 Hz, Ph), 5.47 (1H, dd, $^3J_{HH}$ = 11.4 $^4J_{HH}$ = 3.4 Hz, CH), 5.22- 5.09 (3H, m, CH_2), 4.96 (1H, dd, $^3J_{HH}$ = 11.4 $^4J_{HH}$ = 2.5 Hz) 4.85 (1H, dd, $^3J_{HH}$ = 10.6 $^4J_{HH}$ = 2.8 Hz, CH), 4.56-4.41 (3H, m, CH_2), 4.29 (1H, t $^3J_{HH}$ = 11.1 Hz), 4.17 (1H, t, $^3J_{HH}$ = 10.7 Hz), 4.09 (1H, t, $^3J_{HH}$ = 10.9 Hz, CH_2), 3.60 (1H, dd, $^3J_{HH}$ = 10.5 $^4J_{HH}$ = 3.7 Hz), 3.52-3.42 (2H, m, CH_2).

^{13}C {^{1}H} NMR (126 MHz, 298 K, CD_3CN) δ_C 164.7, 164.6, 163.9 (C=N), 151.3, 151.2, 150.4, 150.1, 149.9, 149.9, 149.6, 149.5, 149.5, 149.4, 149.1, 149.0, 148.9, 148.7, 148.6, 147.8, 147.8, 147.6, 142.0, 143.7, 143.6, 142.9, 142.8, 142.8, 142.6, 142.5, 142.8, 138.4, 138.0, 137.8, 135.3, 134.6, 134.1, 131.9, 131.5, 130.9, 130.8, 130.6, 130.1, 129.8, 129.7, 129.6, 129.5, 129.3, 128.3, 128.3, 128.1, 127.8, 127.1, 127.0, 124.6, 124.3, 124.2, 124.1, 123.6, 123.4 (Py/Ph), 70.6, 70.5, 70.4, 70.1, 70.0, 69.8 (CH_2), 69.5, 69.4, 68.4 (CH).

MS (ESI) m/z 328.5575 $[Zn_2\mathbf{L}^{12}{}_3]^{4+}$, 471.227 $[Zn_2\mathbf{L}^{12}{}_3][ClO_4]^{3+}$, 756.1427 $[Zn_2\mathbf{L}^{12}{}_3][ClO_4]_2^{2+}$.

IR ν cm^{-1} 3066 (w), 1728 (w), 1647 (w), 1599 (m), 1570 (w), 1495 (w), 1475 (m), 1440 (m), 1406 (w), 1317 (w), 1246 (w), 1078 (s), 1015 (m), 931 (m), 841 (w).

Elemental Analysis found (Calculated for $C_{75}H_{66}C_{l4}Zn_2N_{12}O_{19}\cdot 4H_2O$) % C 50.13 (50.49), H 3.80 (4.18), N 9.11 (9.42).

Crystallography

R_C,Δ_{Zn},HHT-$[Zn_2\mathbf{L}^{12}{}_3][ClO_4]_2$, M = 1920.69, monoclinic, space group C2 (no. 5), a = 36.032(8) Å, b = 13.162(3) Å, c = 18.767(4) Å, β = 99.699(7)°, V = 8773(3) $Å^3$, Z = 4, T = 100.15 K, μ(CuKα) = 2.478 mm^{-1}, *Dcalc* = 1.454 g/mm^3, 45035 reflections measured (4.776 ≤ 2Θ ≤ 133.182), 15293 unique (R_{int} = 0.0651) which were used in all calculations. The final R_1 was 0.0733 (I > 2σ(I)) and wR_2 = 0.2066 (all data). GooF 1.050, Flack 0.045(8)

5.3.2.3 R_C,Δ_{Zn},HHT-$[Zn_2\mathbf{L}^{15}{}_3][ClO_4]_4$

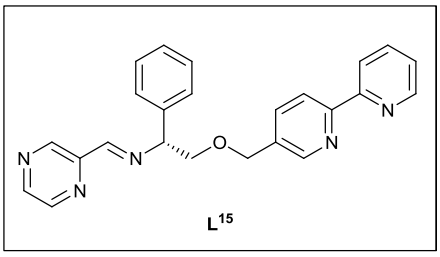

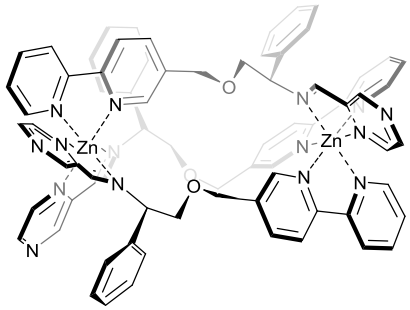

Yield 0.68 g, 71 %.

^{1}H NMR (500 MHz, 298 K, CD_3CN) δ_H ppm 9.51, 9.44 (2H, s, bpy), 9.38 (1H, s, HC=N), 9.15 (1H, s, Ph/Py), 9.10, (1H, s, Ph/Py), 9.03 (1H, s, HC=N), 8.9 4(1H,

d, 3JHH = 3.2 Hz, Ph/Py), 8.84 (2H, t, $^{3}J_{HH}$ = 3.1 Hz, Ph/Py), 8.70 (1H, s, HC=N), 8.54 (1H, d, $^{3}J_{HH}$ = 8.2 Hz, Ph/Py), 8.49 (1H, d, $^{3}J_{HH}$ = 8.7 Hz, Ph/Py), 8.40 (1H, s, Ph/Py), 8.30-7.76 (17H, m, Ph/Py), 7.58-7.48 (5H, m, Ph/Py), 7.19 (1H, t, $^{3}J_{HH}$ = 7.6 Hz, Ph), 7.09 (2H, t, $^{3}J_{HH}$ = 7.6 Hz, Ph), 7.02 (1H, t, $^{3}J_{HH}$ = 7.6 Hz, Ph), 6.98 (2H, d, 3JHH = 7.6 Hz, Ph), 6.91 (1H, t, $^{3}J_{HH}$ = 7.6 Hz, Ph), 6.72 (2H, t, $^{3}J_{HH}$ = 7.6 Hz, Ph), 6.58 (2H, t, $^{3}J_{HH}$ = 7.6 Hz, Ph), 6.12 (2H, d, $^{3}J_{HH}$ = 7.6 Hz, Ph), 6.00 (2H, d, $^{3}J_{HH}$ = 7.6 Hz, Ph), 5.49 (1H, dd, $^{3}J_{HH}$ = 11.1 Hz, $^{4}J_{HH}$ = 2.8, CH), 5.27-5.15 (3H, m, CH_2), 5.01 (1H, dd, $^{3}J_{HH}$ = 11.1 Hz, $^{4}J_{HH}$ = 2.8, CH), 4.89 (1H, dd, $^{3}J_{HH}$ = 11.1 Hz, $^{4}J_{HH}$ = 2.8, CH), 4.60-4.49 (3H, m, CH_2), 4.33 (1H, t, $^{3}J_{HH}$ = 11.3 Hz, CHCH_2), 4.21 (1H, t, $^{3}J_{HH}$ = 11.3 Hz, CHCH_2), 4.14 (1H, t, $^{3}J_{HH}$ = 11.3 Hz, CHCH_2), 3.68 (1H, dd, $^{3}J_{HH}$ = 11.0 Hz, $^{4}J_{HH}$ = 3.2, CHCH_2), 3.56 (1H, dd, $^{3}J_{HH}$ = 11.0 Hz, $^{4}J_{HH}$ = 3.2, CHCH_2), 3.52 (1H, dd, 3JHH = 11.0 Hz, $^{4}J_{HH}$ = 3.2, CHCH_2).

^{13}C NMR (126 MHz, 298 K, CD_3CN) δ 163.7, 163.0, 162.6 (HC=N), 152.7, 152.6, 152.1, 151.9, 151.7, 151.3, 151.3, 150.9, 150.4, 150.00, 149.8, 149.3, 149.2, 149.1, 149.0, 148.4, 144.3, 144.0, 143.8, 143.7, 143.5, 143.4, 143.0, 142.7, 142.1, 141.9, 141.7, 138.5, 138.1, 138.1, 134.9, 133.9, 133.8, 130.2, 130.0, 130.0, 129.9, 129.9, 129.8, 129.6, 128.6, 128.4, 128.3, 128.2, 127.9, 127.2, 127.1, 124.6, 124.5, 124.3, 124.2, 123.8, 123.7 (Ph/Py), 71.1, 70.7 (CH), 70.6, 69.8, 69.7, 69.5, 69.5 (CH_2), 69.1 (CH).

MS (ESI) m/z 395.1922 $[Zn_2\mathbf{L}^{x}_3]^{4+}$, 471.1206 $[Zn_2\mathbf{L}^{x}_3][ClO_4]_2^{2+}$.

IR ν cm^{-1} 3521 (br), 1644 (w), 1603 (w), 1495 (w), 1475 (m), 1441 (m), 1406 (w), 1318 (w), 1249 (w), 1177 (w), 1078 (s) 931 (m), 844 (m).

Elemental Analysis found (Calculated for $C_{72}H_{63}Cl_4Zn_2N_{15}O_{19}\cdot 4H_2O$) % C 48.26 (48.39), H 3.66 (4.00), N 11.65 (11.76).

5.3.2.4 R_C,Δ_{Zn},HHT-$[Zn_2L^{16}{}_3][ClO_4]_4$

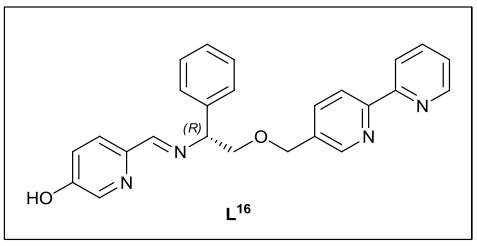

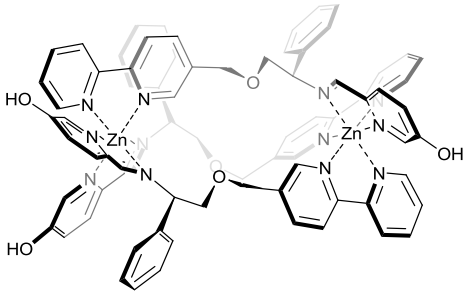

Yield 0.70 g, 71 %.

^{1}H NMR (400 MHz, 298 K, CD_3CN) δ_H ppm 9.25 (1H, d, $^4J_{HH}$ = 1.4 Hz, Py), 9.23 (1H, s, HC=N), 9.19 (1H, d, $^4J_{HH}$ = 1.5 Hz, Py), 9.14 (1H, s), 8.77 (1H, s, HC=N), 8.60-7.28 (31H, m, Py) 7.22-6.95 (6H, m), 6.92 (1H, t, $^3J_{HH}$ = 7.9 HZ), 6.72(2H, t, $^3J_{HH}$ = 7.7 Hz), 6.58 (2H, t, $^3J_{HH}$ = 8.17 Hz), 6.12 (2H, d, $^3J_{HH}$ = 7.9 Hz), 6.00 (2H, d, $^3J_{HH}$ = 7.8 Hz, Ph), 5.50 (1H, dd, $^3J_{HH}$ = 11.5 $^4J_{HH}$ = 3.4 Hz, CH), 5.26- 5.11 (3H, m, CH_2), 4.98 (1H, dd, $^3J_{HH}$ = 11.8 $^4J_{HH}$ = 3.2 Hz), 4.85 (1H, dd, $^3J_{HH}$ = 11.0 $^4J_{HH}$ = 3.6 Hz, CH), 4.60-4.44 (3H, m, CH_2), 4.31 (1H, t, $^3J_{HH}$ = 11.2 Hz), 4.23 (1H, t, $^3J_{HH}$ = 11.1 Hz), 4.05 (1H, t $^3J_{HH}$ = 11.1 Hz, CHC*H*$_2$), 3.66 (1H, dd, $^3J_{HH}$ = 10.5 $^4J_{HH}$ = 3.6 Hz), 3.56 (1H, dd, $^3J_{HH}$ = 11.1 $^4J_{HH}$ = 3.4 Hz), 3.49 (1H, dd, $^3J_{HH}$ = 11.0 $^4J_{HH}$ = 3.7 Hz, CHC*H*$_2$) 2.39 (3H, bs, OH).

^{13}C {^{1}H} NMR (126 MHz, CD_3CN) δ_C ppm 163.6, 163.4, 162.8, 159.6, 159.2, 158.8, 151.3, 151.1, 150.3, 150.1, 140.0, 149.9, 149.5, 149.1, 149.0, 149.0, 148.7, 148.6, 143.9, 143.6, 143. 6, 142.8, 142.4, 142.2, 140.3, 140.2, 138.7, 138.7, 138.5, 138.4, 138.0, 137.7, 135.9, 135.0, 134.6, 133.1, 132.8, 132.0,

129.7, 129.6, 129.5, 129.4, 128.3, 128.2, 128.0, 127.8, 127.1, 127.0, 126.7, 124.6, 124.3, 124.2, 124.1, 123.6, 123.4 (Ph/Py), 70.6, 70.6, 70.0 (CH_2), 69.9 (CH), 69.8(CH_2), 69.7 (CH), 69.6, 69.4(CH_2), 67.9 (CH).

MS (ESI) m/z 780.56 $[Zn_2\mathbf{L}^{\mathbf{16}}{}_3][ClO_4]_2{}^{2+}$.

IR ν cm^{-1} 3166 (br), 1644 (w), 1592 (w), 1572 (m), 1495 (w), 1475 (m), 1439 (m), 1405 (w), 1317 (w), 1280 (w), 1248 (w), 1212 (w), 1076 (s), 1040 (s), 929 (M), 840 (m).

Elemental Analysis found (Calculated for $C_{75}H_{66}Cl_4Zn_2N_{12}O_{22}\cdot 3H_2O$) % C 49.37 (49.66), H 3.78 (4.00), N 8.83 (9.27).

Crystallography

R_C,Δ_{Zn},HHT-$[Zn_2\mathbf{L}^{\boldsymbol{12}}{}_3][ClO_4]_2\cdot$(0.5MeCN)(MeOH)(EtOAC), M = 1900.61, monoclinic, space group C2 (no. 5), a = 37.539(3) Å, b = 13.3807(9) Å, c = 18.4948(13) Å, β = 100.782(3)°, V = 9125.9(12) $Å^3$, Z = 4, T = 100.15 K, μ(MoKα) = 0.722 mm^{-1}, *Dcalc* = 1.383 g/mm^3, 31933 reflections measured (5.9 ≤ 2Θ ≤ 50.054), 14520 unique (R_{int} = 0.1091) which were used in all calculations. The final R_1 was 0.1027 (I > 2σ(I)) and wR_2 was 0.2698 (all data). GooF 1.080, Flack 0.051(14).

5.3.2.5 R_C,Δ_{Zn},HHT-$[Zn_2L^{17}{}_3][ClO_4]_4$.

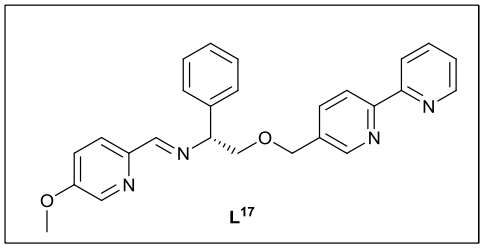

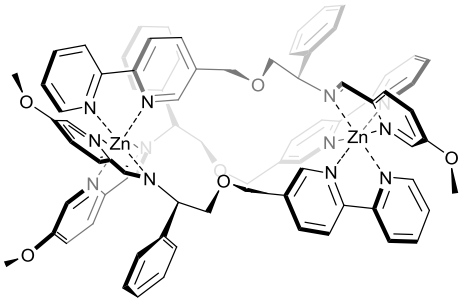

Yield 0.81 g, 81 %.

^{1}H NMR (400 MHz, CD_3CN) δ_H ppm 9.26 (1H, s, HC=N), 9.25 (1H, s), 9.19 (1H, s, Py), 9.17 (1H, s), 8.81 (1H, s, HC=N), 8.57-7.32 (31H, m, Py), 7.19 (1H, t, $^3J_{HH}$ = 7.0 Hz), 7.15-7.07 (3H, m), 7.03 (1H, t, $^3J_{HH}$ = 7.6 Hz), 6.99 (2H, d, $^3J_{HH}$ = 7.6 Hz) 6.92 (1H, t, $^3J_{HH}$ = 7.4 Hz), 6.72 (2H, t, $^3J_{HH}$ = 7.7 Hz), 6.58 (2H, t, 7.8 Hz), 6.12 (2H, d, $^3J_{HH}$ = 7.6 Hz), 6.00 (2H, d, $^3J_{HH}$ = 7.4 Hz, Ph), 5.49 (1H, dd, $^3J_{HH}$ = 11.6 $^4J_{HH}$ = 3.35 Hz, CH), 5.28-5.12 (3H, m, CH_2), 4.98 (1H, dd, $^3J_{HH}$ = 11.3 $^4J_{HH}$ = 2.7 Hz), 4.84 (1H, dd, $^3J_{HH}$ = 10.6 $^4J_{HH}$ = 3.0 Hz, CH), 4.59-4.46(3H, m, CH_2), 4.32 (1H, t, $^3J_{HH}$ = 11.0 Hz), 4.19 (1H, t, $^3J_{HH}$ = 11.0 Hz), 4.13 (1H, t, $^3J_{HH}$ = 11.1 Hz, CHC*H*$_2$), 3.92 (3H, s), 3.89 (3H, s), 3.79 (3H, s, OMe), 3.67 (1H, dd, $^3J_{HH}$ = 10.0 $^4J_{HH}$ = 4.0 Hz), 3.55 (1H, dd, $^3J_{HH}$ = 11.2 $^4J_{HH}$ = 3.0 Hz), 3.49 (1H, dd, $^3J_{HH}$ = 11.0 $^4J_{HH}$ = 4.0 Hz, CHC*H*$_2$).

$^{13}C\{^1H\}$ NMR (126 MHz, CD_3CN) δ_C ppm 163.8, 163.5, 163.0, 161.5, 161.2, 160.8, 151.3, 151.1, 150.3, 150.1, 140.0, 149.9, 149.5, 149.1, 149.1, 149.0, 148.8, 148.6, 143.9, 143.6, 143.6, 142.8, 142.4, 142.2, 140.5, 140.5, 139.4, 139.3, 139.1, 138.4, 138.0, 137.7, 135.9, 134.9, 134.5, 133.1, 132.8, 132.1, 129.8, 129.7, 129.6, 129.5, 129.5, 129.4, 128.3, 128.2, 128.0, 127.9, 127.1, 127.0, 124.6, 124.3, 124.2, 124.2, 124.1, 123.8, 123.6, 123.5 (Ph/Py), 70.6, 70.6,

70.00 (CH_2), 70.00 (CH), 69.9 (CH_2), 69.8 (CH), 69.6, 69.5 (CH_2), 66.0 (CH), 57.6, 57.5, 57.3 (Me).

MS (ESI) m/z 351.075 $[Zn_2\mathbf{L}^{\mathbf{17}}{}_3]^{4+}$, 501.25 $[Zn_2\mathbf{L}^{\mathbf{17}}{}_3][ClO_4]^{3+}$, 801.66 $[Zn_2\mathbf{L}^{\mathbf{17}}{}_3][ClO_4]_2{}^{2+}$.

IR ν cm^{-1} 3251 (br), 1643 (w), 1601 (w), 1571 (m), 1495 (w), 1475 (w), 1440 (w), 1405 (w), 1316 (m), 1280 (w), 1225 (w), 1176 (w) 1075 (s), 1014 (s), 932 (m) 843 (m).

Elemental Analysis found (Calculated for $C_{78}H_{72}Cl_4Zn_2N_{12}O_{22}\cdot 4H_2O$) % C 49.66 (49.94), H 3.93 (4.30), N 8.70 (8.97).

5.3.2.6 R_C,Δ_{Zn},HHT-$[Zn_2\mathbf{L}^{\boldsymbol{18}}{}_3][ClO_4]_4$.

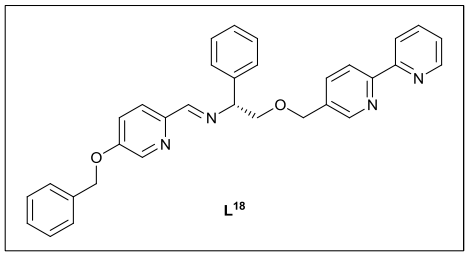

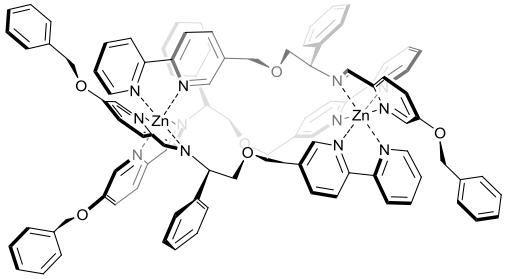

Yield 0.83 g, 73 %.

^{1}H NMR (500 MHz, 298 K, CD_3CN) δ_H ppm 9.22 (1H, s, HC=N), 9.18 (1H, d, $^4J_{HH}$ = 1.7 Hz, bpy), 9.10 (1H, d, $^4J_{HH}$ = 1.7 Hz, bpy), 9.07 (1H, s, HC=N), 8.73 (1H, s, HC=N), 8.49-8.43 (2H, m, Ph/Py), 8.33 (1H, d, $^4J_{HH}$ = 1.7 Hz, bpy), 8.33-7.17 (53H, m, Py/Ph), 6.68 (2H, t, $^3J_{HH}$ = 7.7 Hz, Ph), 6.54 (2H, t, $^3J_{HH}$ = 7.7 Hz, Ph), 6.07 (2H, d, $^3J_{HH}$ = 7.8 Hz, Ph), 5.93 (2H, d, $^3J_{HH}$ = 7.7 Hz, Ph), 5.40 (1H, dd, $^3J_{HH}$ = 10.5 $^4J_{HH}$ = 3.3 Hz, CH), 5.24-5.09 (9H, m, CH_2) , 4.91 (1H, dd, $^3J_{HH}$ =

11.1 $^{4}J_{HH}$ = 3.1 Hz, CH), 4.77 (1H, dd, $^{3}J_{HH}$ = 10.2 $^{4}J_{HH}$ = 3.8 Hz, CH), 4.55-4.44 (3H, m, CH_2), 4.29 (1H, t, $^{3}J_{HH}$ = 11.2, CHC*H*$_2$), 4.15 (1H, t, $^{3}J_{HH}$ = 11.2, CHC*H*$_2$), 4.07 (1H, t, $^{3}J_{HH}$ = 11.2, CHC*H*$_2$), 3.56 (1H, dd, $^{3}J_{HH}$ = 10.4 $^{4}J_{HH}$ = 3.7 Hz, CHC*H*$_2$), 3.49 (1H, dd, $^{3}J_{HH}$ = 11.4 $^{4}J_{HH}$ = 3.2 Hz, CHC*H*$_2$), 3.43 (1H, dd, $^{3}J_{HH}$ = 11.2 $^{4}J_{HH}$ = 3.7 Hz, CHC*H*$_2$).

^{13}C {^{1}H} NMR (126 MHz, 298 K, CD_3CN) δ_C ppm 163.7, 163.5, 162.9, 160.3, 160.0, 159.5, 159.0, 151.3, 151.0, 150.3, 150.0, 149.9, 149.8, 149.4, 149.1, 149.0, 149.0, 148.7, 148.5, 143.9, 143.6, 143.5, 142.8, 142.4, 142.2, 140.7, 140.7, 140.6, 140.4, 139.2, 139.1, 138.6, 138.3, 138.0, 137.7, 136.3, 136.1, 136.1, 135.7, 134.9, 134.5, 133.0, 132. 8, 131.9, 129.9, 129.8, 129.7, 129.6, 129.6, 129.5, 129.4, 129.0, 128.7, 128.7, 128.7, 128.3, 128.2, 128.0, 127.7, 127.5, 127.7, 127.0, 126.4, 125.9, 125.4, 124.7, 124.4, 124.2, 124.2, 123.6, 123.5 (Ph/Py), 71.9, 71.8, 71.7, 70.6, 70.5 (CH_2), 70.0 (CH), 69.9, 69.8 (CH_2), 69.8 (CH), 69.5, 69.4 (CH_2), 68.0 (CH).

MS (ESI) m/z 408.1475 $[Zn_2\mathbf{L}^{\mathbf{18}}{}_3]^{4+}$, 577.35 $[Zn_2\mathbf{L}^{\mathbf{18}}{}_3][ClO_4]^{3+}$, 915.745 $[Zn_2\mathbf{L}^{\mathbf{18}}{}_3][ClO_4]_2{}^{2+}$.

IR *v* cm^{-1} 3510 (br), 3059 (br), 2933 (w), 2873 (w), 1605 (m), 1517 (w), 1496 (w), 1468 (m), 1442 (m), 1419 (w), 1408 (w), 1364 (w), 1319 (w), 1176 (m), 1070 (s), 959 (w), 932 (m).

Elemental Analysis found (Calculated for $C_{96}H_{84}Cl_4Zn_2N_{12}O_{22}\cdot 4H_2O$) % C 54.74 (54.84), H 3.99 (4.41), N 7.89 (7.99).

5.3.2.7 R_C,Δ_{Zn},HHT-$[Zn_2L^{19}_3][ClO_4]_4$.

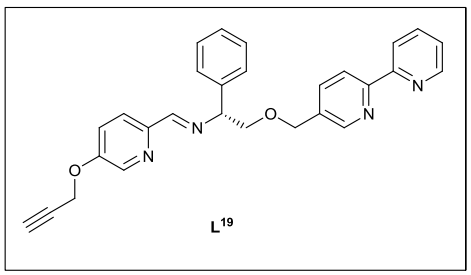

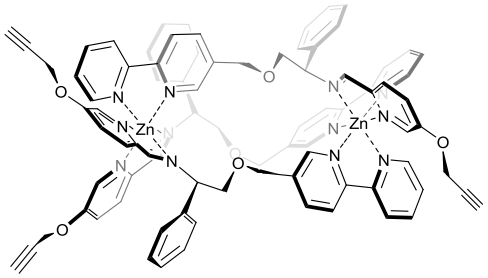

Yield 0.76 g, 72 %.

^{1}H NMR (500 MHz, CD_3CN) δ_H ppm 9.26 (1H, s, HC=N), 9.21 (1H, s, HC=N), 9.17(1H, s, bpy), 9.16(1H, s, bpy), 8.81 (1H, s, HC=N), 8.53 (1H, d, $^3J_{HH}$ = 8.3 Hz, Py), 8.48 (1H, d, $^3J_{HH}$ = 8.3 Hz, Ph/Py), 8.38 (1H, s, bpy), 8.30 (1H, d, $^3J_{HH}$ = 8.3 Hz, Py), 8.27-8.16 (3H, m, Py), 8.10-7.89 (8H, m, Py), 7.87-7.78 (4H, m, Py), 7.68 (1H, dd, $^3J_{HH}$ = 9.1 Hz $^4J_{HH}$ = 2.0 Hz, Py), 7.56-7.42 (6H, m, Py), 7.19 (1H, d, $^3J_{HH}$ = 3.4 Hz, Ph), 7.15 (1H, t, $^3J_{HH}$ = 8.2 Hz, Ph), 7.09 (2H, t, $^3J_{HH}$ = 8.2 Hz, Ph), 6.99 (1H, t, $^3J_{HH}$ = 8.2 Hz, Ph), 6.96 (2H, d, $^3J_{HH}$ = 8.2 Hz, Ph), 6.89 (1H, t, $^3J_{HH}$ = 8.2 Hz, Ph), 6.69 (2H, t, $^3J_{HH}$ = 8.2 Hz, Ph), 6.55 (2H, t, $^3J_{HH}$ = 8.2 Hz, Ph), 6.10 (2H, d, $^3J_{HH}$ = 8.2 Hz, Ph), 5.98 (2H, d, $^3J_{HH}$ = 8.2 Hz, Ph), 5.47 (1H, dd, $^3J_{HH}$ = 11.2 Hz, $^4J_{HH}$ = 3.5 Hz, CH), 5.25-5.11 (3H, m, OCH_2), 4.96 (1H, dd, $^3J_{HH}$ = 11.2 Hz, $^4J_{HH}$ = 3.5 Hz, CH), 4.86 (2H, d, $^4J_{HH}$ = 2.8 Hz, C*H*$_2$CH), 4.84-4.78 (3H, m, C*H*$_2$CH overlapping with CH), 4.73 (2H, d, $^4J_{HH}$ = 2.8 Hz, C*H*$_2$CH), 4.57-4.45 (3H, m, OCH_2), 4.30 (1H, t, $^3J_{HH}$ = 11.2 Hz, CH_2), 4.17 (1H, t, $^3J_{HH}$ = 11.2 Hz, CH_2), 4.10 (1H, t, $^3J_{HH}$ = 11.2 Hz, CH_2), 3.63 (1H, dd, $^3J_{HH}$ = 10.7 Hz, $^4J_{HH}$ = 3.5 Hz, CH_2), 3.52 (1H, dd, $^3J_{HH}$ = 10.7 Hz, $^4J_{HH}$ = 3.5 Hz, CH_2), 3.47 (1H, dd, $^3J_{HH}$ = 10.7 Hz, $^4J_{HH}$ = 3.5 Hz, CH), 3.00 (1H, t, $^4J_{HH}$ = 2.0 Hz, CH_2C*H*), 2.90 (1H, t, $^4J_{HH}$ = 2.0 Hz, CH_2C*H*), 2.80 (1H, t, $^4J_{HH}$ = 2.0 Hz, CH_2C*H*).

^{13}C {^{1}H} NMR (126 MHz, CD_3CN) δ_C ppm 163.78, 163.46, 162.92 (H*C*=N), 159.12, 158.80, 158.35, 151.31, 151.15, 150.33, 150.07, 149.95, 149.89, 149.49, 149.15, 149.10, 149.05, 148.86, 148.58, 143.96, 143.71, 143.62, 142.84, 142.44, 142.31, 141.30, 141.28, 141.25, 138.79, 138.71, 138.40, 138.01, 137.80, 135.66, 134.80, 134.41, 132.88, 132.60, 131.82, 129.78, 129.71, 129.67, 129.59, 129.53, 129.43, 128.33, 128.22, 128.00, 127.81, 127.65, 127.11, 127.04, 126.28, 126.20, 125.98, 124.67, 124.39, 124.21, 124.14, 123.60, 123.48 (Ph/Py), 79.04, 78.88, 77.73 (*C*H_2CH), 77.51, 77.47, 70.63 (CH_2*C*H), 70.58 (CH_2), 70.13 (CH), 69.96 (CH_2), 69.92 (CH), 69.85, 69.60, 69.46 (CH_2), 68.12 (CH), 57.87, 57.75, 57.71 (CH_2*C*H).

MS (ESI) m/z 523.79 $[Zn_2\mathbf{L^{19}}_3][ClO_4]_2^{2+}$, 835.165 $[Zn_2\mathbf{L^{19}}_3][ClO_4]_3^{+}$.

Elemental Analysis found (Calculated for $C_{105}H_{90}Cl_4CuF_3IN_{21}O_{22}Zn_2$) % C 52.37 (53.66), H 3.55 (4.18), N 8.63 (8.94).

5.3.2.8 R_C,Δ_{Zn},HHT-$[Zn_2L^{20}{}_3][ClO_4]_4$.

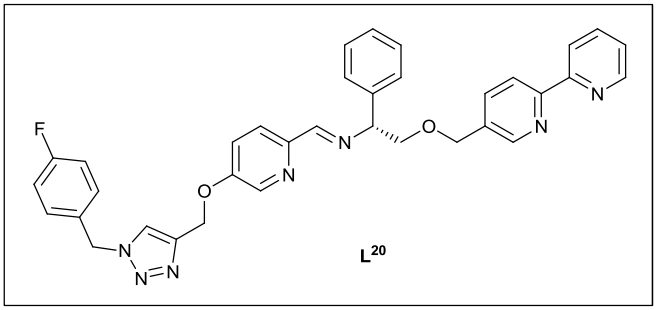

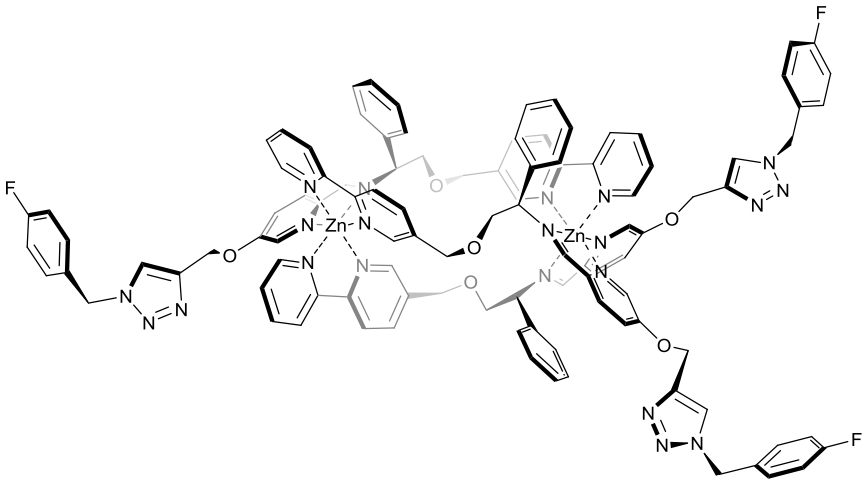

R_C,Δ_{Zn},HHT-$[Zn_2L^{19}{}_3][ClO_4]_4$ (0.50 g, 0.27 mmol) was dissolved in dry acetonitrile (30 ml) in a Schlenk vessel. Dry triethylamine (0.08 ml, 0.79 mmol) was added, followed by 1-(azidomethyl)-4-fluorobenzene (0.12 g, 0.79 mmol) in dry acetonitrile (10 ml). Finally, copper(I) iodide (0.12 g, 0.79 mmol) was added as a solid. The solution remained yellow in colour and was stirred for 24 h under argon at room temperature. The solvent was removed under reduced pressure and the resulting solid was recrystallised from acetonitrile and ethyl acetate.

Yield 0.41 g, 66 %.

^{1}H NMR (500 MHz, 298 K, CD_3CN) δ_H ppm 9.24 (1H, s, HC=N), 9.19 (1H, s, HC=N), 9.13 (1H, s, bpy), 9.10 (1H, s, bpy), 8.74 (1H, s, HC=N), 8.50, 8.34 (1H, s, bpy), 8.28 (1H, d, $^3J_{HH}$ = 9.7 Hz (Ph/Py), 8.23-8.14 (4H, m, Ph/Py), 8.08-7.69 (22H m, Ph/Py/Imz), 7.59-6.81 (38H, m, Ph/Py), 6.78 (2H, d, $^3J_{HH}$ = 7.8 Hz, Ph),

6.68 (2H, t, $^{3}J_{HH}$ = 7.8 Hz, Ph), 6.54 (2H, t, $^{3}J_{HH}$ = 7.8 Hz, Ph), 6.08 (2H, d, $^{3}J_{HH}$ = 7.8 Hz, Ph), 5.95 (2H, d, $^{3}J_{HH}$ = 7.8 Hz, Ph), 5.71-5.36 (12H, m, CH2), 5.31-5.03 (12H, m, CH_2), 4.93 (1H, dd, $^{3}J_{HH}$ = 11.2 Hz $^{4}J_{HH}$ = 2.8, CH), 4.79 (1H, dd, $^{3}J_{HH}$ = 11.2 Hz $^{4}J_{HH}$ = 2.8, CH), 4.53 (2H, d, $^{3}J_{HH}$ = 13.6 Hz), 4.46 (1H, d, $^{3}J_{HH}$ = 12.8 Hz), 4.29 (1H, dd, $^{3}J_{HH}$ = 11.2 Hz CH_2), 4.14 (1H, dd, $^{3}J_{HH}$ = 11.2 Hz, CH_2), 4.06 (1H, dd, $^{3}J_{HH}$ = 11.2 Hz, CH_2), 3.59 (1H, dd, $^{3}J_{HH}$ = 11.2 Hz $^{4}J_{HH}$ = 2.8, CH_2), 3.51 (1H, dd, $^{3}J_{HH}$ = 11.2 Hz $^{4}J_{HH}$ = 2.8, CH_2), 3.44 (1H, dd, $^{3}J_{HH}$ = 11.2 Hz $^{4}J_{HH}$ = 2.8, CH_2).

^{13}C {^{1}H} NMR (126 MHz, 298 K, CD_3CN) δ_C ppm 164.54, 163.73, 163.42, 162.78, 162.59, 159.98, 159.69, 159.07, 151.21, 150.99, 150.27, 150.07, 150.03, 149.84, 149.56, 149.07, 149.03, 148.73, 148.55, 143.88, 143.54, 143.48, 142.76, 142.68, 142.37, 142.10, 140.80, 140.75, 139.33, 139.09, 138.73, 138.27, 137.94, 137.64, 135.64, 134.84, 134.44, 132.90, 132.77, 132.72, 131.74, 131.63, 131.57, 131.37, 131.30, 131.23, 129.73, 129.63, 129.52, 129.48, 129.39, 129.31, 128.23, 127.88, 127.63, 127.05, 126.96, 126.58, 125.84, 125.71, 125.42, 124.74, 124.42, 124.22, 124.16, 123.55, 123.51, 116.77, 116.74, 116.69, 116.59, 116.56, 116.52 (Ph/Py/ImZ), 70.63, 70.57, 70.01 (CH_2), 69.98 (CH), 69.84 (CH_2), 69.80 (CH), 69.49, 69.45 (CH_2), 67.92 (CH), 63.24, 63.06, 63.04, 60.96, 53.84, 53.75, 53.66 (CH_2).

IR ν cm^{-1} 3075 (w), 1644 (w), 1603 (w), 1571 (m), 1510 (w), 1475 (m), 1453 (m), 1440 (m), 1404 (m), 1316 (m), 1262 (s), 1219 (s), 1080 (s), 1051 (w), 1014 (m), 935 (m), 4841 (m).

Elemental Analysis found (Calculated for $C_{105}H_{90}Cl_4CuF_3IN_{21}O_{22}Zn_2$) % C 49.71 (50.08), H 3.33 (4.56), N 11.49 (11.68).

5.4 **Experimental for chapter 4**

5.4.1 General synthesis of HHT-[$Fe_2\mathbf{L}^{n}$]Cl_4 (where *n* =12,16-18).

$FeCl_2$ (0.14 g, 1.1 mmol) was added to a stirred solution of the desired substituted aldehyde (1.64 mmol) and (R)-2-(2,2'-bipyridin-5-ylmethoxy)-1-phenylethanamine (0.5 g, 1.64 mmol) in methanol (20 ml) at ambient temperature to give a purple solution that was then refluxed for 24 h. The reaction was cooled to room temperature, filtered though a celite plug prior to the solvents being removed *in vaccuo* to yield the desired product as a purple solid.

5.4.1.1 R_c,Δ_{Fe},HHT-[$Fe_2\mathbf{L}^{12}$]Cl_4

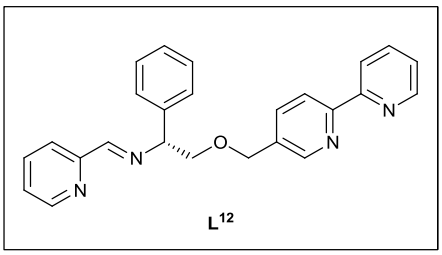

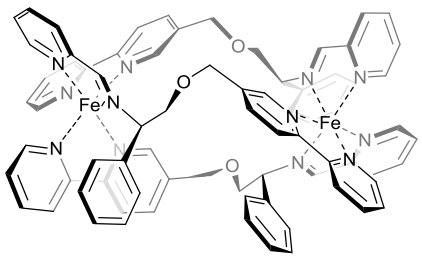

Yield 0.68 g, 87 %

^{13}C {^{1}H} NMR (126 MHz, MeOH) δ_C ppm 174.7, 174.6, 174.0 (HC=O), 161.0, 160.4, 160.3, 160.0, 159.9, 159.9, 159.5, 159.3, 158.9, 158.7, 156.4, 155.7, 155.4, 154.8, 154.4, 154.2, 141.6, 141.4, 140.5, 140.0, 139.8, 138.8, 138.6, 138.3, 135.3, 133.8, 133.5, 132.7, 132.0, 131.4, 130.6, 130.3, 130.2, 130.1, 129.9, 129.7, 129.6, 129.2, 129.0, 128.9, 128.7, 127.0, 125.8, 125.1, 125.1, 124.2, 123.6 (Ar), 74.5, 74.4, 72.6 (CH), 70.9, 70.8, 70.5, 69.9 (CH_2).

MS (ESI) m/z 323.7 [$Fe_2\mathbf{L}^{12}{}_3$]$^{4+}$

IR ν cm^{-1} 3331 (br), 3023 (w), 1604 (m), 1493 (m), 1438 (m), 1403 (w), 1360 (w), 1318 (w), 1242 (m), 1102 (m), 1073 (s), 1010 (w), 936 (m), 866 (w), 836 (w).

Elemental analysis found (calculated for $C_{75}H_{66}Cl_4Fe_2N_{12}O_3 \cdot 9H_2O$) % C 56.52 (56.33), H 5.31 (5. 92), N 10.68 (10.51)

S_c,Λ_{Fe},HHT-[Fe_2**L**^{12}]Cl_4

Yield 0.64 g, 82 %

MS (ESI) m/z 323.7 [Fe_2**L**$^{12}{}_3$]$^{4+}$

Elemental analysis found (calculated for $C_{75}H_{66}Cl_4Fe_2N_{12}O_3 \cdot 9H_2O$) % C 56.02 (56.33), H 5.22 (5.29), N 10.34 (10.51)

5.4.1.2 R_c,Δ_{Fe},HHT-[Fe_2**L**^{15}]Cl_4

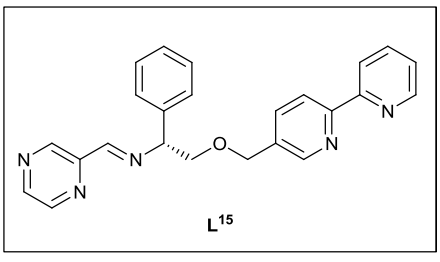

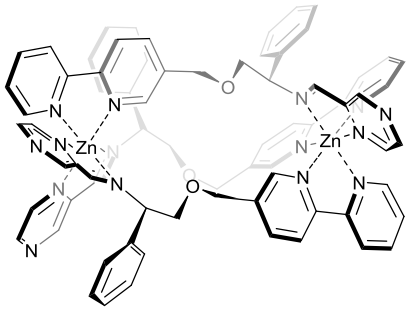

Yield 0.6 g, 75 %

^{13}C {^1H} NMR (126 MHz, 298 K, MeOH) δ_C ppm 173.8, 173.3, 172.5 (HC=O), 160.5, 159.6, 159.6, 159.2, 158.9, 158.8, 158.7, 157.6, 157.0, 156.3, 156.1, 155.6, 154.9, 154.4, 152.0, 151.3, 151.0, 150.7, 150.2, 149.9, 148.9, 148.3,

142.2, 142.1, 141.9, 140.9, 140.8, 140.5, 140.1, 139.3, 139.2, 138.5, 134.8, 133.4, 133.3, 130.7, 130.5, 130.5, 130.3, 130.2, 130.2, 130.1, 129.2, 128.6, 128.4, 127.0, 125.9, 125.4, 125.3, 125.0, 124.3, 124.0 (Ar), 74.9, 74.7, 73.1 (CH), 70.7, 70.6, 70.4, 70.2, 70.1, 69.9 (CH_2).

MS (ESI) m/z 324.4 $[Fe_2\mathbf{L^{12}}_3]^{4+}$

IR ν cm^{-1} 3364 (br), 3062 (w), 1603 (m), 1572 (w), 1494 (w), 1464 (m), 1464 (m), 1440 (w), 1404 (w), 1366 (m), 1318 (w), 1288 (w), 1241 (w), 1172 (s), 1142 (w), 1109 (m), 1073 (s), 1007 (m), 937 (m), 840 (m).

605 0.7841

Elemental analysis found (calculated for $C_{72}H_{63}Cl_4Fe_2N_{15}O_3 \cdot 10H_2O$) % C 53.61 (53.38), H 5.03 (5.16), N 12.49 (12.97).

S_c,Λ_{Fe},HHT-$[Fe_2\mathbf{L^{12}}]Cl_4$

Yield 0.67 g 83 %

MS (ESI) m/z 324.4 $[Fe_2\mathbf{L^{12}}_3]^{4+}$

Elemental analysis found (calculated for $C_{72}H_{63}Cl_4Fe_2N_{15}O_3 \cdot 10H_2O$) % C 53.55 (53.38), H 5.05 (5.16), N 12.92 (12.97).

5.4.1.3 R_c,Δ_{Fe},HHT-[Fe_2**L**^{16}]Cl_4

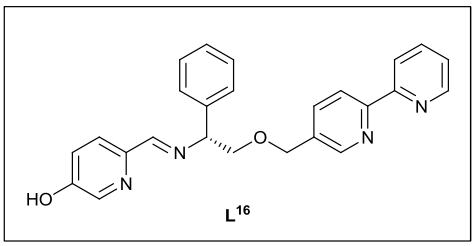

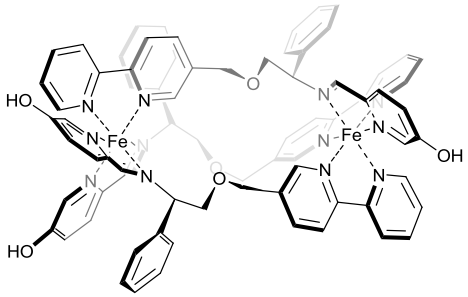

Yield 0.59 g 74 %

MS (ESI) m/z 335.7 [Fe_2**L**$^{16}{}_3$]$^{+4}$

IR ν cm^{-1} 3313 (br), 2922 (br), 1552 (s), 1490 (m), 1466 (s), 1439 (s), 1403 (w), 1362 (w), 1283 (s), 1221 (s), 1108 (m), 1074 (s), 1026 (m), 936 (m), 837 (m).

Elemental analysis found (calculated for $C_{75}H_{76}Cl_4Fe_2N_{12}O_{11}\cdot 9H_2O$) % C 54.88 (54.96), H 4.78 (5.14), N 10.22 (10.02).

S_c,Λ_{Fe},HHT-[Fe_2**L**^{16}]Cl_4

Yield 0.64 g 80 %

5.4.1.4 R_c,Δ_{Fe},HHT-[Fe_2**L**^{17}]Cl_4

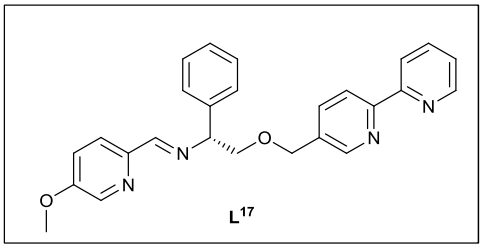

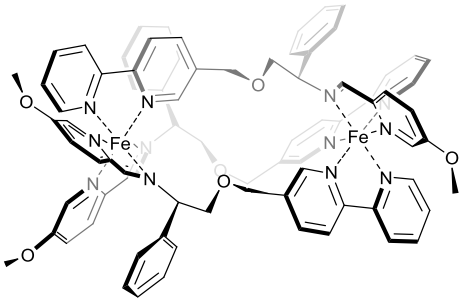

Yield 0.64 g 76 %

^{1}H NMR (500 MHz, MeOH) δ 9.92 (1H, s, HC=N), 9.79 (1H, s, HC=N), 9.40 (1H, s, HC=N), 9.35 (1H, s, Ar), 8.77-8.65 (1H, d, $^3J_{HH}$ = 8.7), 8.59-8.51 (1H, m), 8.21 (2H, m), 8.21-8.13 (3H, m), 8.12-8.04 (3H, m), 7.96-7.82 (6H, m), 7.81-7.77 (1H, m), 7.73 (1H, d, $^3J_{HH}$ = 9.3), 7.53-7.32 (7H, m), 7.23-7.12 (4H, m), 7.08-6.92 (7H, m), 6.79-6.70 (3H, m), 6.63 (2H, t, $^3J_{HH}$ = 7.5), 6.30 (1H, s), 6.07-5.79 (2H, Br s, Ar), 5.47 (1H, dd, $^3J_{HH}$ = 11.4, $^4J_{HH}$ = 3.0), 5.32 (1H, dd, $^3J_{HH}$ = 12.1 $^4J_{HH}$ = 3.0, CH), 5.13 (1H, d $^3J_{HH}$ = 12.1), 4.75-4.50 (9H, m), 4.43 (1H, t, $^3J_{HH}$ = 10.1, CHC*H*$_2$), 3.96, 3.87, 3.85, 3.75, 3.58, 3.42, 3.29.

^{13}C {^{1}H} NMR (126 MHz, 298 K, MeOH) δ_C ppm 172.5, 172.4, 171.8 (HC=N), 161.2, 160.5, 160.4, 160.3, 160.2, 160.1, 160.0, 159.7, 159.1, 158.8, 156.4, 155.4, 155.0, 154.4, 152.8, 152.5, 152.5, 145.2, 144.6, 143.7, 141.4, 141.3, 141.1, 140.4, 140.0, 139.7, 138.8, 138.5, 138.3, 136.0, 134.3, 134.1, 133.4, 132.7, 132.3, 130.3, 130.2, 130.1, 130.0, 129.8, 128.9, 128.8, 128.5, 128.4, 126.9, 125.4, 125.0, 124.7, 124.0, 123.5, 122.4, 122.2, 122.1, 120.0 (Ar), 73.8, 73.7, 71.7 (*C*H), 70.6, 70.5, 70.3, 70.2, 70.0, 69.8 (CH*C*H$_2$/O*C*H$_2$), 57.1, 57.0 (OMe).

MS (ESI) m/z 346.2 $[Fe_2\mathbf{L^{17}}_3]^{4+}$

IR ν cm^{-1} 3379 (br), 2932 (br), 1591 (m), 1557 (s), 1493 (m) 1466 (m), 1435 (m), 1439, (m), 1403 (m), 1363 (m), 1304 (m), 1277 (m), 1237 (s), 1185 (w), 1136 (w), 1110 (m), 1074 (s), 1008 (m), 962 (w), 937 (m), 824 (m).

Elemental analysis found (calculated for $C_{78}H_{72}Cl_4Fe_2N_{12}O_6 \cdot 9H_2O$) % C 55.52 (55.46), H 5.19 (5.37), N 10.17 (9.95).

S_c,Λ_{Fe},HHT-$[Fe_2\mathbf{L^{17}}]Cl_4$

Yield 0.67 g 80 %

Elemental analysis found (calculated for $C_{78}H_{72}Cl_4Fe_2N_{12}O_6 \cdot 8H_2O$) % C 55.7 (55.46), H 5.24 (5.37), N 9.92 (9.95).

5.4.1.4.1 R_c,Δ_{Fe},HHT-$[Fe_2\mathbf{L^{18}}]Cl_4$

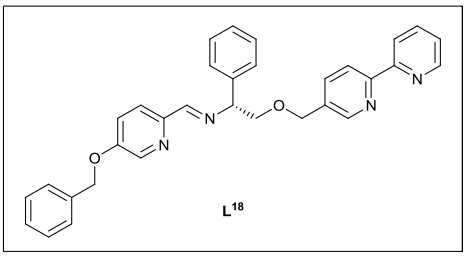

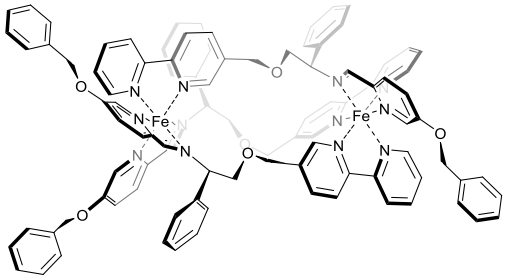

Yield 0.71 g 74 %

^{13}C {^{1}H} NMR (126 MHz, 298 K, MeOH) δ_C ppm 172.6, 172.5, 171.7 (HC=O), 161.1, 160.3, 159.9, 159.6, 159.4, 159.2, 159.0, 158.8, 158.6, 156.3, 155.3, 154.8, 154.2, 153.1, 152.9, 152.7, 144.0, 143.8, 143.4, 141.3, 141.1, 140.3, 139.9, 139.7, 138.8, 138.5, 138.2, 136.4, 136.1, 136.0, 135.9, 134.2, 134.0, 133.2, 132.7, 132.0, 130.2, 130.1, 130.0, 129.9, 129.8, 129.7, 129.6, 128.8, 128.7, 128.6, 128.5, 126.8, 125.5, 125.0, 124.8, 124.7, 124.6, 124.3, 124.0, 123.5 (Ar), 73.8, 73.7 (CH), 72.2, 72.0, 71.9 (O*C*H_2Bn), 71.7(CH), 70.6, 70.5, 70.3, 69.9, 69.7 (CH*C*H_2/O*C*H_2).

Ms (ESI) m/z 403.3 $[Fe_2\mathbf{L}^{\mathbf{18}}{}_3]^{4+}$

IR ν cm^{-1} 3294 (br), 3027 (br), 2932 (br), 1591 (m) 1556 (s), 1493 (m), 1467 (m),1453 (m), 1402 (w), 1372 (w), 1275 (m), 1229 (s), 1109 (w), 1075 (s), 1003 (m), 938 (w), 842 (m).

Elemental analysis found (calculated for $C_{96}H_{84}Cl_4Fe_2N_{12}O_6{\cdot}7H_2O$) % C 61.79 (61.29), H 5.04 (5.25), N 9.02 (8.93).

S_c,Λ_{Fe},HHT-$[Fe_2\mathbf{L}^{\mathbf{18}}]Cl_4$

Yield 0.73 g 76 %

Ms (ESI) m/z 403.3 $[Fe_2\mathbf{L}^{\mathbf{18}}{}_3]^{4+}$

Elemental analysis found (calculated for $C_{96}H_{84}Cl_4Fe_2N_{12}O_6{\cdot}7H_2O$) % C 61.18 (61.29), H 5.17 (5.25), N 9.02 (8.93).

5.4.2 Biological experimental

5.4.2.1 Chemosensitivity (MTT assay)

MDA-MB-468 (human breast adenocarcinoma) and HCT116 wild type p53 (human colon carcinoma) cells were incubated in 96-well plates at a cell concentration of 2.0×10^4 cells/ml. Complete cell media containing RPMI-1640, supplemented with 10% foetal calf serum, sodium pyruvate (1 mM) and L-glutamine (2 mM), was used to prepare the desired cell concentration and reference wells. Plates containing cells were incubated for 24 h at 37°C in an atmosphere of 5% CO_2, prior to drug exposure. All compounds were dissolved in complete RPMI-1640 cell media to give an initial concentration of 100 mM and diluted further with cell media to obtain concentrations ranging from 100 μM – 5 nM. Cell media (200 μl) was added to the reference cells and differing concentrations of drug solution (200 μl) were added to the remaining wells. The plates were incubated for a further 96 h at 37°C in an atmosphere of 5% CO_2. 3-(4,5-Dimethylthiazol-1-yl)-2,5-diphenyltetrazolium bromide (MTT) solution (0.5 mg/ml) was added to each well and incubated for a further 4 h at 37°C in an atmosphere of 5% CO_2. Upon completion all solutions were removed from the wells and dimethyl sulfoxide (150 μl) was added to each well to dissolve the purple formazan crystals. A Thermo Scientific Multiskan EX microplate photometer was used to measure the absorbance at 540 nm. Lanes containing 100% cell media and untreated cells were used as a blank and 100% cell survival respectively. Cell survival was determined as the absorbance of treated cells minus the blank cell media, divided by the absorbance of the untreated control; this value was expressed as a percentage. The IC_{50} values were determined from

a plot of percentage cell survival against drug concentration (μM). All assays were conducted in triplicate and the mean IC_{50} ± standard deviation was determined.

5.4.2.2 FACS Assays (H2AX and Cell Cycle)[19]

5.4.2.2.1 Cell Preparation

HCT116 wild type p53 cells (5×10^5 cells/flask, 10 ml complete RPMI medium) were incubated for 18 h at 37°C in 5% CO_2, then treated with 10 μM triplex metallohelix (10 ml in complete RPMI medium) for 24 h. The supernatant, containing any dead cells, was collected and the cells were harvested by trypsinisation. This single cell suspension in trypsin was added to the supernatant and centrifuged at 1500 rpm (300 g) for 5 min. The cells were washed twice with PBS (phosphate buffered saline), re-suspended in ice-cold methanol in PBS (90:10) and incubated in ice for 30 min, then stored at -20°C until required for analysis.

5.4.2.2.2 H2AX Assay

The pre-treated cells were washed twice in incubation buffer (PBS containing 0.5 BSA) then re-suspended in 100 μl incubation buffer for 10 min at room temperature. 2 μl of primary rabbit anti-human phosphor Histon H2AX (Ser 139) antibody (final 1:50 concentration, cell signalling Technology) was added and incubated at RT and incubated for a further 1 h. This was then washed twice with

incubation buffer, re-suspended in 100 µl incubation buffer containing Alexa Fluor conjugated antirabbit IgG secondary antibody (final 1:1000 concentration, cell signalling Technology) and incubated in the absence of light at room temperature for 30 min then the cells were stored at 0 °C until analysis using the FACS.

5.4.2.2.3 Cell Cycle Assay

300 µl PBS containing Propidium Iodide (40 µg/ml) and RNAse A (200µg/ml) was added to the pre-treated cells and they were incubated in the absence of light at room temperature for 30 min. 200µl ice-cold PBS was added (final volume of 600 µl) and the cells were placed on ice until analysis using the FACS. The cell cycle assay was repeated four times with each compound and the mean % cells in each phase ± standard deviation was determined. Red fluorescence was observed at 488nm excitation by flow cytometry and data analysed using WinMDI2.9 and Cylchred software. As can be seen in table S3, treatment with either compound both increased the population of cell in the sub G_1 and G_2/M phases and decreased the population of the S phase of the cell cycle a statistically significant amount when compared to the untreated control cells.

5.4.2.3 Single Cell Gel Electrophoresis Assay[20]

The induction of single strand breaks (SSB) and cross linking in HCT116 (wild type p53) cells was determined *via* single cell gel electrophoresis. Cells seeded at 3×10^5 cells/well in 6-plates in complete RPMI-1640 medium and incubated for 18 h at 37°C in an atmosphere of 5% CO_2, following treatment with each

compound (2 ml of 10 µM in complete RPMI-1640 medium) the cells were washed twice with HBSS and harvested by trypsinisation and embedded in 0.5% low-melting point agarose and transferred to agarose coated glass slides. these slides were immersed in freshly prepared ice-cold lysis buffer (2.5 M NaCl, 100 mM Na_2EDTA, 10 mM Trisma base, 1% sodium hydroxide, pH 10.0) 1% Triton X-100 and 10% dimethyl sulfoxide. The slides were then submerged in electrophoresis buffer (300 mM sodium hydroxide, 1 mM Na_2EDTA, pH > 13.0) for 30 min in a horizontal gel electrophoresis, and then subjected to electrophoresis at 0.6 Vcm^{-1} for 25 min. Following electrophoresis, the slides were neutralised (3 × drop wise addition of 0.4 M Trisma buffer, pH 7.5) rinsed with water and fixed with 100% ice-cold ethanol and dried in air for 18 h. To detect cross links drug treated cells were further treated with 100 µM of hydrogen peroxide for 20 minutes prior to gel electrophoresis. Immediately before analysis the slides were stained with SYBR™ Gold solution (Molecular probes Inc.) and viewed with an epifluorescent microscope (Nikon Eclipse E800, Japan). The tail moment was measured on 50 randomly selected comets using Comet assay III software (Perceptive Instruments, UK) and each assay was performed in triplicate.

5.4.3 Antimicrobial Experiments

5.4.3.1 Preparation of bacterial stocks[21]

Verified stocks of MRSA [USA300] and *E. coli* [TOP10] were grown to 10^8 cfu/ml (cfu = colony forming units) respectively in sterile Luria-Bertani (LB) medium, as measured by OD_{600} (optical density measured at wavelength: 600

nm) and confirmed by hemocytometer measurement. These were used to diluted of 10^6 cfu/ml in sterile Mueller-Hinton (MH) broth (15% w/v glycerol) and flash-frozen in liquid N_2 to store use.

5.4.3.2 Minimum Inhibitory Concentration[21, 22]

In order to assess the potency of the triplex metallohelices minimum inhibitory concentrations (MICs) were established using the standardised macrobroth dilution method in cation-adjusted MH broth. 200µl aliquots (128 µg/ml triplex metallohelix in sterilized MH broth, diluted 2^n µg/ml × 5) were added to 96-well plates in duplicate. This was inoculated with each bacterial strain (bacterial density of 10^3 cfu/ml, ~200 cells per well) and sealed. After mixing at 720 strokes/min for 10 seconds, growth was monitored over 20 h at 37 °C by recording OD_{600} every 10 mins with an iEMS 96-well plate reader. The lowest concentration to inhibit growth across each repeat is classified as the MIC. Positive (medium and untreated bacteria) and negative (medium only) controls were run with each plate. The antimicrobial properties of our recently reported flexicate systems were reproduced as a positive control alongside ampicillin.

5.4.3.3 Minimum Bactericidal Concentration[23]

10 µl of the bacteria/compound mix (128 µg/ml) was recovered from the MIC 96-well plate and diluted 1:20 in sterile phosphate buffered saline, spread onto a sterile LB/agar plate and incubated for 18 h at 37 °C (in duplicate). The MBC was determined to be the lowest concentration at which this dilution/plating experiment showed no visible growth across both plates to within a 5% error.

5.5 **References**

1. A. Damianoglou, E. J. Crust, M. R. Hicks, S. E. Howson, A. E. Knight, J. Ravi, P. Scott and A. Rodger, *Chirality*, 2008, **20**, 1029-1038.
2. S. J. Coles and P. A. Gale, *Chemical Science*, 2012, **3**, 683-689.
3. G. M. Sheldrick, *Acta Crystallographica Section A*, 1990, **46**, 467-473.
4. G. M. Sheldrick, *Acta Crystallographica Section A*, 2008, **64**, 112-122.
5. S. Grimme, S. Ehrlich and L. Goerigk, *J. Comput. Chem.*, 2011, **32**, 1456-1465.
6. A. A. Granovsky, *Firefly version 8.0*, *http://classic.chem.msu.su/gran/firefly/index.html*.
7. M. W. Schmidt, K. K. Baldridge, J. A. Boatz, S. T. Elbert, M. S. Gordon, J. H. Jensen, S. Koseki, N. Matsunaga, K. A. Nguyen, S. Su, T. L. Windus, M. Dupuis and J. A. Montgomery, *J. Comput. Chem.*, 1993, **14**, 1347-1363.
8. R. J. Deeth, A. Anastasi, C. Diedrich and K. Randell, *Coord. Chem. Rev.*, 2009, **253**, 795-816.
9. R. J. Deeth, N. Fey and B. Williams–Hubbard, *J. Comput. Chem.*, 2005, **26**, 123-130.
10. M. Seredyuk, A. B. Gaspar, V. Ksenofontov, Y. Galyametdinov, J. Kusz and P. Gütlich, *J. Am. Chem. Soc.*, 2008, **130**, 1431-1439.
11. E. J. O'Neil, K. M. DiVittorio and B. D. Smith, *Org. Lett.*, 2006, **9**, 199-202.
12. P. Das, A. Ghosh, M. K. Kesharwani, V. Ramu, B. Ganguly and A. Das, *Eur. J. Inorg. Chem.*, 2011, **2011**, 3050-3058.
13. R. Ballardini, V. Balzani, M. Clemente-Leon, A. Credi, M. T. Gandolfi, E. Ishow, J. Perkins, J. F. Stoddart, H. R. Tseng and S. Wenger, *J. Am. Chem. Soc.*, 2002, **124**, 12786-12795.
14. C. Dallaire, I. Kolber and M. Gingras, *Org. Synth.*, 2002, **78**, 82.
15. Y. Hsiao and L. S. Hegedus, *J. Org. Chem.*, 1997, **62**, 3586-3591.
16. J. M. Janey, T. Iwama, S. A. Kozmin and V. H. Rawal, *J. Org. Chem.*, 2000, **65**, 9059-9068.
17. K. Sutowardoyo, M. Emziane and D. Sinou, *Tetrahedron Lett.*, 1989, **30**, 4673-4676.
18. O. Branytska, L. J. W. Shimon and R. Neumann, *Chem. Commun.*, 2007, 3957-3959.
19. S. J. Allison, M. Jiang and J. Milner, *Aging-Us*, 2009, **1**, 316-327.
20. R. M. Phillips and T. H. Ward, *Anticancer research*, 2001, **21**, 1795-1801.
21. *J. Antimicrob. Chemother.*, 1991, **27**, 22-30.
22. J. M. Andrews, *J. Antimicrob. Chemother.*, 2001, **48**, 5-16.
23. *Antibiotics in laboratory medicine*, Williams & Wilkins, 1991.

Appendix 1

TGA Data showing water loss of complexes $[Fe_2\mathbf{L}^{n}_3]Cl_4$ (where n = 12, 15-18).

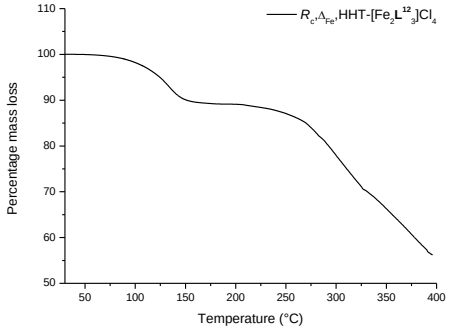

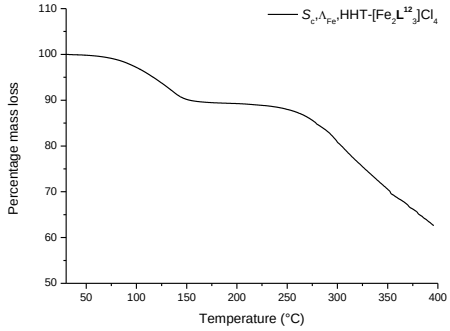

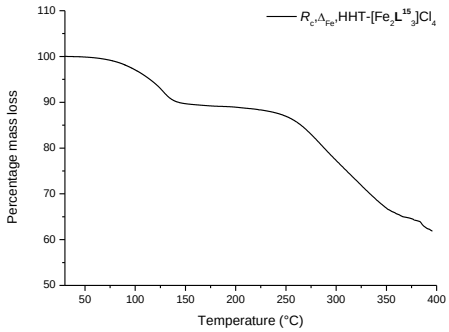

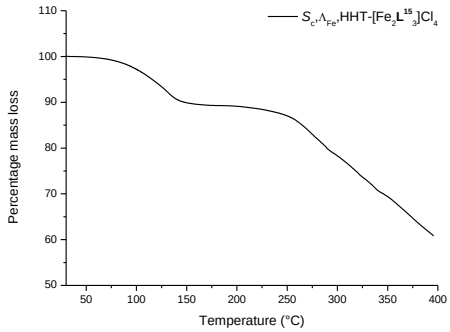

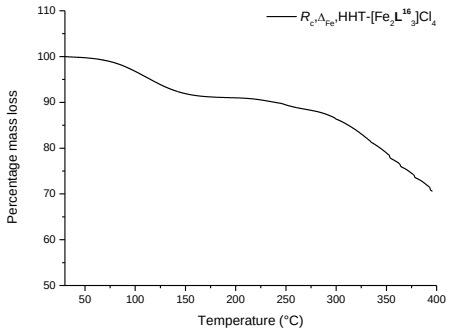

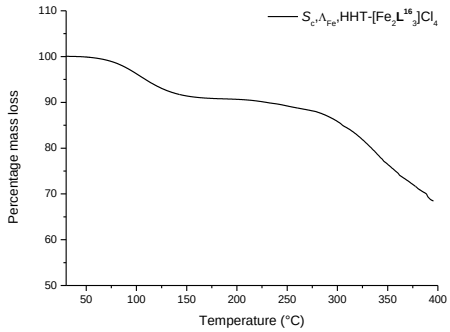

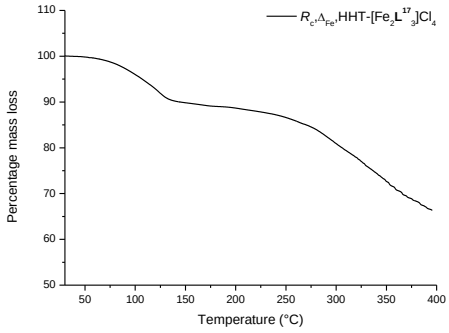
R_{c^1},Δ_{Fe^1}-HHT-[Fe_2**L**$^{17}_3$]Cl_4
Percentage mass loss
Temperature (°C)

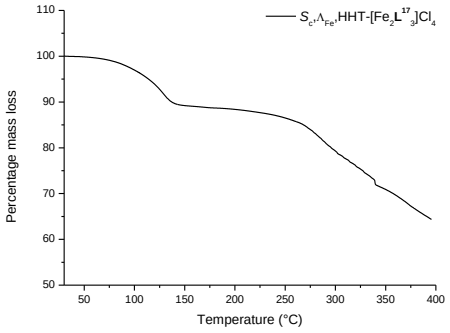
S_{c^1},Λ_{Fe^1}-HHT-[Fe_2**L**$^{17}_3$]Cl_4
Percentage mass loss
Temperature (°C)

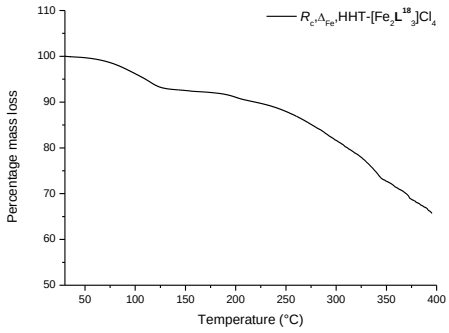
R_{c^1},Δ_{Fe^1}-HHT-[Fe_2**L**$^{18}_3$]Cl_4
Percentage mass loss
Temperature (°C)

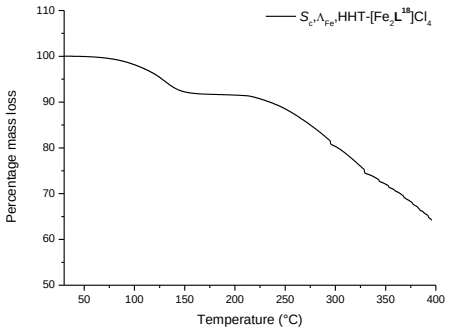
S_{c^1},Λ_{Fe^1}-HHT-[Fe_2**L**^{18}]Cl_4
Percentage mass loss
Temperature (°C)

Appendix 2

CD data of complexes $[Fe_2\mathbf{L}^{n}{}_3]Cl_4$ (where n =15-18).

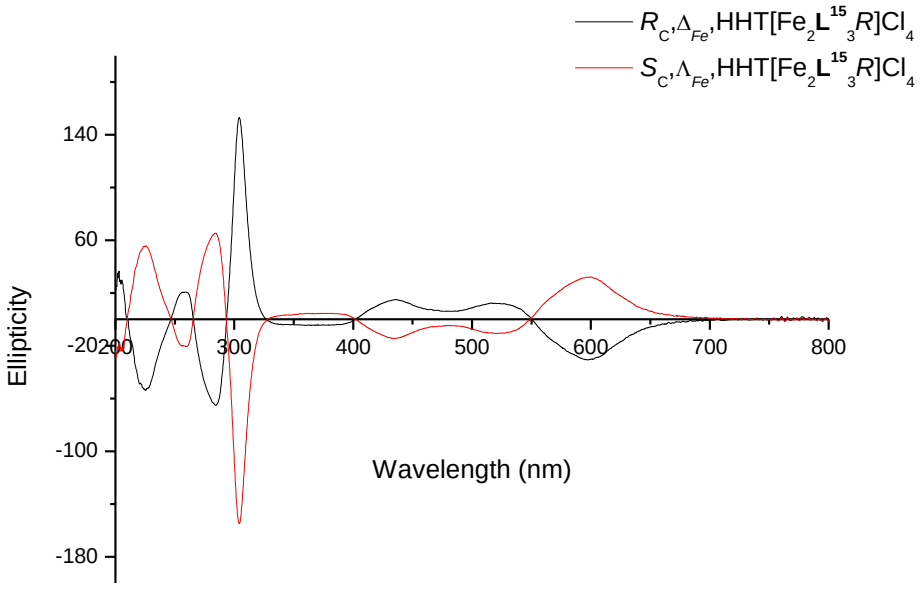

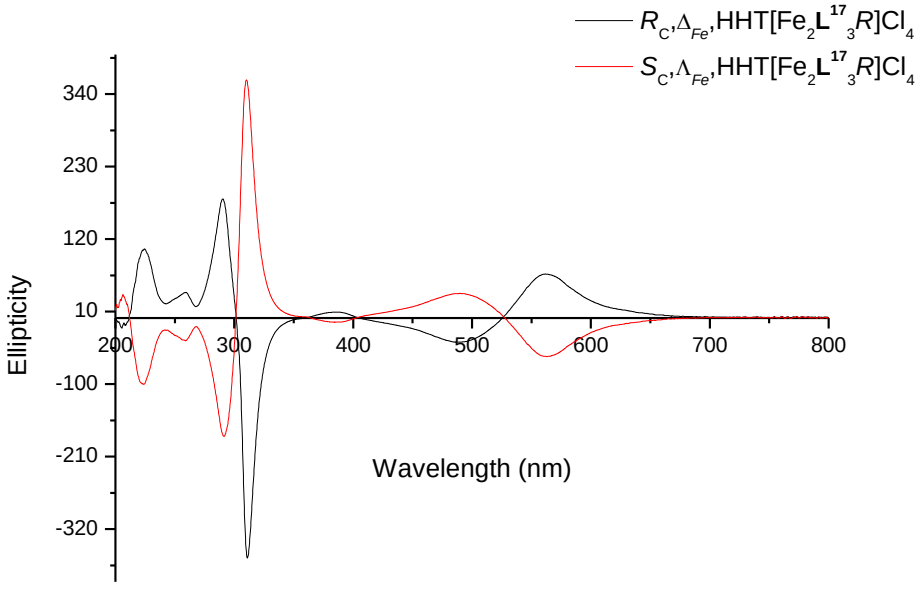

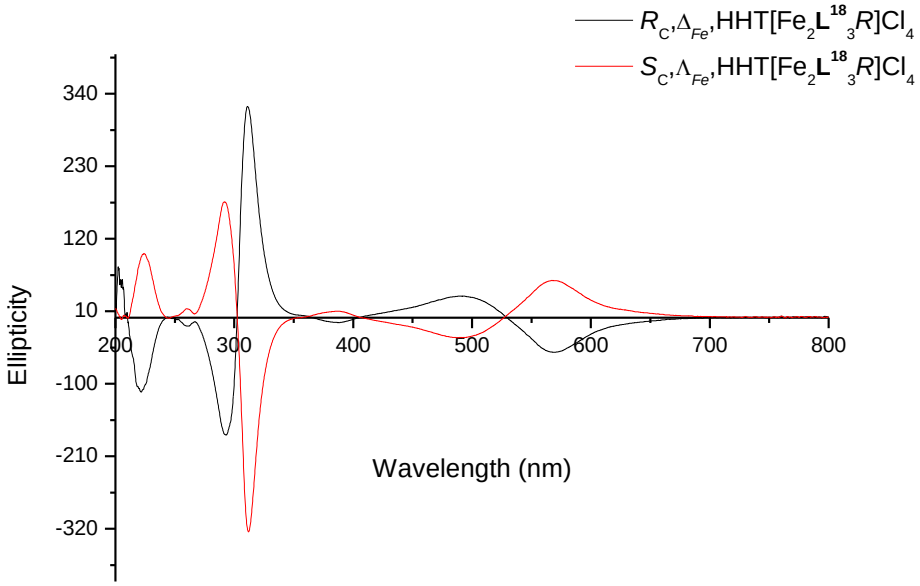
R_C,Δ_{Fe},HHT[Fe$_2$**L**^{18}$_3$$R$]Cl$_4$
S_C,Λ_{Fe},HHT[Fe$_2$**L**^{18}$_3$$R$]Cl$_4$
Ellipticity
340
230
120
10
-100
-210
-320
200
300
400
500
600
700
800
Wavelength (nm)